A STUDY OF INGESTION AND DISPERSION
OF ENGINE EXHAUST PRODUCTS IN
TRAILING VORTEX SYSTEMS

by

Jack N. Nielsen, Stephen S. Stahara,
and James P. Woolley

NEAR TR 54

November 1973

SUMMARY

Detailed analysis has been made of the ingestion and dispersion of engine exhaust products into the trailing vortex system of supersonic aircraft flying in the stratosphere. The rate of mixing between the supersonic jet and the co-flowing supersonic stream was found to be an order of magnitude less than would be expected on the basis of subsonic eddy-viscosity results. The length of the potential core was 66 nozzle exit radii so that the exhaust gases remain at elevated temperatures and concentrations over much longer distances than previously estimated. Ingestion started at the end of the potential core and all hot gas from the engine was ingested into the trailing vortex within two core lengths. The vortex inhibits entrainment and thermally insulates the hot gases in the core from the stratosphere. The final buoyancy phase started only ten seconds after leaving the trailing edge. The temperature rise in the wake of the supersonic aircraft is much greater than that for a subsonic transport since temperature rise was found to vary directly as speed squared and inversely as aspect ratio. The buoyancy theory incorporates an entrainment coefficient which is a function of local turbulence conditions. Comparison between the buoyancy calculations for the supersonic case with nondimensionalized subsonic aircraft contrail data on wake spreading showed good agreement. Velocity and temperature profiles have been specified at various stages of the wake, and the analysis in this report can be used to predict variations of concentrations of species such as NO under conditions of chemical reaction.

TABLE OF CONTENTS

A STUDY OF INGESTION AND DISPERSION OF ENGINE
EXHAUST PRODUCTS IN TRAILING VORTEX SYSTEMS

By Jack N. Nielsen, Stephen S. Stahara,
and James P. Woolley
Nielsen Engineering & Research, Inc.

1.0 INTRODUCTION

This document represents the final report on an analytical study of
the ingestion and dispersion of engine exhaust products in trailing vortex
systems under Contract NAS2-7337. The emphasis of the work is on super-
sonic flight in the stratosphere although the analytical methods developed
herein are for the most part not limited to those conditions.

The problem of what influences the exhaust gas products of supersonic
aircraft will have on the chemical balance of the stratosphere is a subject
of great current interest and controversy. Specifically what long term
influences the nitrogen oxides of the exhaust will have on the ozone
balance of the stratosphere has been discussed by Johnson and Whitten
(ref. 1-1) and by Goldsmith, Tuck, Foot, Simmons and Newson (ref. 1-2)
who have reached opposite conclusions. One of the questions which bears
on the general problem is how the exhaust gases from the engines are in-
gested into the trailing vortices of the aircraft and how they are
ultimately dispersed. For instance, at supersonic speeds the engine
can have long potential cores which are uniformly at the exit conditions,
and these hot cores may influence the chemical concentration of the final
exhaust products. Also, trailing vortices can be very long for super-
sonic flight in the atmosphere, and if the exhaust products are entrained
by these vortices the concentrations can remain relatively high compared
to what they might otherwise be. Also, a knowledge of the entrainment
of the exhaust gas by the trailing vortices is important if flight testing
is to be conducted to obtain concentration measurements.

In this report a physical description will be given of the ingestion
and dispersion of the engine air by the trailing vortices including a
breakdown of the process into several phases. The analysis of the several
phases is then carried out in detail. Primarily the analytical methods
are applied to the case of a supersonic two-engine aircraft flying in the
stratosphere.

The report contains distinct theories for the pure jet stage, the hot gas ingestion stage, the equilibrium vortex stage, and the asymptotic buoyancy stage. These theories are contained in sections 4 to 8. For the reader who is not concerned with theoretical details, it is recommended that he read section 3 which describes the ingestion and dispersion processes, and then go to section 9 which contains the calculative example.

2.0 SYMBOLS

Because this report contains a number of distinct theories, the symbol list is extensive. In the following list, the symbols are separated in accordance with the sections in which they appear. If the same quantity is used in more than one section, it is listed under each section. In a few cases the same symbol has been used in different sections to designate different physical quantities where no confusion should result.

Section 4.0

A, B	constants in modified Crocco law
A', B'	constants in Crocco law
b	b^*/r_n^*
b^*	mixing region characteristic length, $r_e^* - r_i^*$
c	mass fraction of exhaust gases
c_p	c_p^*/c_{pj}^*
c_j^2	jet Crocco number, $\dfrac{U_j^{*2}}{2H_j^*} = \dfrac{\gamma - 1}{2} M_j^2 \Big/ (1 + \dfrac{\gamma - 1}{2} M_j^2)$
c_p^*	specific heat at constant pressure
D	constant having a value of either 0 or 1
E_m	$E_m^*/2\pi \dot{m}_j^* H_j^*$
E_z	$E_z^*/2\pi \dot{m}_j^* H_j^*$

2

E_m^*	downstream energy flux through any normal cross section of the mixing zone
E_z^*	energy flux into mixing zone across upstream boundaries of zone
H	H^*/H_j^*
H^*	stagnation enthalpy
H_j^*	jet stagnation enthalpy
H_∞^*	free-stream stagnation enthalpy
K	constant in eddy viscosity equation
K_o	eddy viscosity constant given by equation (4-50)
ℓ_p	ℓ_p^*/r_n^*
ℓ_p^*	length of potential core
$\dot{m}_a$	$\dot{m}_a^*/\dot{m}_j^*$
$\dot{m}_a^*$	$1/2\pi$ times mass flow rate per second entrained by jet up to a given axial position
$\dot{m}_j^*$	$1/2\pi$ times mass flow rate at jet exit
M_c	Mach number on jet centerline
M_d	Mach number on streamtube containing jet exit flow
M_j	Mach number of jet in potential core region
M_∞	free-stream Mach number
$(q^*)^2$	average mean squared velocity taking into account turbulent fluctuations
r	r^*/r_n^*
r_d	r_d^*/r_n^*
r_e	r_e^*/r_n^*
r_i	r_i^*/r_n^*
r_s	r_s^*/r_n^*

3

r^*	radial distance from jet centerline
r_d^*	radius of streamtube containing jet exit mass flow
r_e^*	radius of entire jet
r_i^*	radius of potential core
r_n^*	exit radius of nozzle
r_s^*	radius of "s" streamtube
T	T^*/T_j^*
T_a	T_a^*/T_j^*
T_{ave}	T_{ave}^*/T_j^*
T_c	T_c^*/T_j^*
T_j	$T_j^*/T_j^* = 1$
T_o	$T_o^*/T_{o_j}^*$
$\bar{T}_o$	time average of T_o
T_{o_c}	$T_{o_c}^*/T_{o_j}^*$
T_{o_d}	$T_{o_d}^*/T_{o_j}^*$
T_{o_j}	$T_{o_j}^*/T_{o_j}^* = 1$
T_{o_∞}	$T_{o_\infty}^*/T_{o_j}^*$
T_∞	T_∞^*/T_j^*
T^*	static temperature
T_{ave}^*	mass average static temperature over jet cross section
T_c^*	static temperature on nozzle centerline
T_d^*	temperature of streamtube comtaining jet exit flow
T_j^*	static temperature in potential core

4

T_{o}^{*}	stagnation temperature
$T_{o_c}^{*}$	stagnation temperature on jet centerline
$T_{o_d}^{*}$	stagnation temperature on streamtube containing jet exit flow
$T_{o_j}^{*}$	stagnation temperature of potential core
$T_{o_\infty}^{*}$	free-stream stagnation temperature
T_{∞}^{*}	static temperature in free stream
$\overline{u'^{2*}}$	time average mean square axial turbulent velocity fluctuation
U	U^{*}/U_{j}^{*}
$\overline{U}$	$(U - U_{\infty})/(U_c - U_{\infty})$, normalized velocity
U_{ave}	U_{ave}^{*}/U_{j}^{*}
U_c	U_{c}^{*}/U_{j}^{*}
U_d	U_{d}^{*}/U_{j}^{*}
U_j	$U_{j}^{*}/U_{j}^{*} = 1$
U_{max}	U_{max}^{*}/U_{j}^{*}
U_{min}	U_{min}^{*}/U_{j}^{*}
U_{∞}	U_{∞}^{*}/U_{j}^{*}
U^{*}	axial velocity component
U_{ave}^{*}	mass average axial velocity over jet cross section
U_{c}^{*}	axial velocity on jet centerline
U_{d}^{*}	axial velocity on streamtube containing jet exit flow
U_{j}^{*}	axial velocity of potential core

5

U_{max}^*	maximum axial velocity at given jet cross section
U_{min}^*	minimum axial velocity at given jet cross section
U_∞^*	free-stream axial velocity
$\overline{v'^{2*}}$	time average mean square radial turbulent velocity fluctuation
V	radial velocity divided by U_j^*
W	W^*/W_j^*
W^*	molecular weight
W_j^*	molecular weight of exhaust gases
W_∞^*	molecular weight of free stream
z	z^*/r_n^*
z^*	axial distance behind nozzle exit
Δz	increment in z
α	$\rho_\infty T_{O_\infty} \lambda$
γ	ratio of specific heats
ϵ_d	$\epsilon_d^*/U_c^* b^*$
ϵ^*	turbulent eddy viscosity $= \epsilon_u^*$
ϵ_d^*	value of ϵ^* on streamtube containing jet exit flow
ϵ_h^*	eddy thermal conductivity coefficient
ϵ_m^*	eddy diffusion coefficient
ϵ_s^*	value of ϵ^* on streamtube "s"
ϵ_u^*	eddy momentum diffusivity (viscosity) $= \epsilon^*$
η	$(r - r_i)/(r_o - r_i)$
λ	$(1 + U_\infty)/(1 - U_\infty)$

6

ρ	ρ^*/ρ_j^*
ρ^*	density
ρ_c^*	density on jet centerline
ρ_d^*	density on streamtube containing initial jet exit flow
ρ_j^*	density in potential region
ρ_s^*	density on streamtube "s"
ρ_∞^*	free-stream density
τ^*	turbulent shearing stress associated with radial gradient of axial velocity
τ_d^*	value of τ^* on streamtube initially containing jet exit flow

Sections 5.0 and 6.0 ; Additional Symbols

b	wing span
c_D	crossflow drag coefficient per unit length
$(\hat{e}_x, \hat{e}_y, \hat{e}_z)$	unit vectors in (x^*, y^*, z^*) direction
F_{BY}	nondimensional net buoyant force per unit length, normalized by $\dot{m}_j^* U_j^*/r_n^*$
F_{Dx}	nondimensional drag force per unit length in x^* direction, normalized by $\dot{m}_j^* U_j^*/r_n^*$
F_{Dy}	nondimensional drag force per unit length in y^* direction, normalized by $\dot{m}_j^* U_j^*/r_n^*$
F_{vx}	nondimensional vortex force per unit length in x^* direction, normalized by $\dot{m}_j^* U_j^*/r_n^*$
F_{vy}	nondimensional vortex force per unit length in y^* direction, normalized by $\dot{m}_j^* U_j^*/r_n^*$
g	acceleration due to gravity
K_o	total trailing vortex strength, $\Gamma_o/2\pi$

K_k nondimensional circulation of kth vortex $= \Gamma_k/2\pi$, normalized by $U_j^* r_n^*$

$\dot{m}_a$ nondimensional mass flow rate of ambient air ingested by jet up to a given axial location, normalized by $\dot{m}_j^*$

$\dot{m}_t$ nondimensional total jet mass flow rate up to a given axial location, normalized by $\dot{m}_j^*$

$\dot{m}_j^*$ initial jet mass flow rate

N number of external vortex pairs

p nondimensional pressure, normalized by $\rho_j^* U_j^{*2}$

p_∞ nondimensional free-stream pressure, normalized by $\rho_j^* U_j^{*2}$

r_e nondimensional radius of jet outer boundary normalized by r_n^*

r_{vk} nondimensional radial distance from jet centerline to k^{th} vortex, normalized by r_n^*

r_{vmk} nondimensional radial distance from jet centerline to symmetric image of kth vortex, normalized by r_n^*

r_{vmo} nondimensional radial distance from jet centerline to left wing panel vortex centroid, normalized by r_n^*

r_{vo} nondimensional radial distance from jet centerline to right wing panel vortex centroid, normalized by r_n^*

t nondimensional time, normalized by r_n^*/U_j^*

$\overline{T}_j$ nondimensional mass-averaged jet temperature, normalized by T_j^*

T_∞ nondimensional free-stream temperature, normalized by T_j^*

$\overline{U}_j$ nondimensional mass-averaged jet velocity, normalized by U_j^*

U_∞ nondimensional free-stream velocity, normalized by U_j^*

v nondimensional lateral velocity in x direction relative to moving jet centerline, normalized by U_j^*

8

V_r nondimensional radial flow velocity at outer boundary of jet, normalized by U_j^*

V_{vx} nondimensional velocity in x direction induced by external vortices, normalized by U_j^*

V_{vy} nondimensional velocity in y direction induced by external vortices, normalized by U_j^*

$\vec{V}_i$ nondimensional combination of free-stream and vortex-induced velocities normal to jet centerline, normalized by U_j^*

w nondimensional velocity in y direction relative to moving jet centerline, normalized by U_j^*

W nondimensional complex velocity potential, normalized by $U_j^* r_n^*$

(x,y,z) nondimensional aircraft-fixed inertial Cartesian coordinate system with z axis directed rearward, x axis directed to the right facing forward, and y axis directed vertically upward; normalized by r_n^*

(x_1,y_1) nondimensional crossflow coordinate system fixed to moving jet centerline; normalized by r_n^*

(x_c,y_c) nondimensional location of jet centerline in inertial (x,y) coordinates, normalized by r_n^*

(x_{vk},y_{vk}) nondimensional location of kth right wing-panel vortex in inertial (x,y) coordinates, normalized by r_n^*

(x_{vmk},y_{vmk}) nondimensional location of left wing-panel image of kth vortex in inertial (x,y) coordinates, normalized by r_n^*

(x_{vmo},y_{vmo}) nondimensional location of left wing-panel vortex centroid in inertial (x,y) coordinates, normalized by r_n^*

(x_{vo},y_{vo}) nondimensional location of right wing-panel vortex centroid in inertial (x,y) coordinates, normalized by r_n^*

(x_{vo}^*,y_{vo}^*) location of vortex centroid in dimensional inertial coordinates

z_1 nondimensional complex variable in crossflow plane, $z_1 = x_1 + iy_1$

z_{vk} nondimensional complex coordinates in crossflow plane of right wing panel image of kth vortex, $z_{vk} = x_{vk} + iy_{vk}$

9

z_{vmk} nondimensional complex coordinates in crossflow plane of left wing panel image of kth vortex, $z_{vmk} = x_{vmk} + iy_{vmk}$

z_{vo} nondimensional complex coordinates in crossflow plane of right wing-panel vortex centroid, $z_{vo} = x_{vo} + iy_{vo}$

Γ_o trailing vortex circulation

θ polar angle in crossflow plane

θ_{xz} angle of jet centerline with (y,z) plane

θ_{yz} angle of jet centerline with (x,z) plane

$\bar{\rho}_j$ nondimensional mass-averaged jet density, normalized by ρ_j^*

ρ_∞ nondimensional free-stream density, normalized by ρ_j^*

ϕ real part of complex velocity potential W

Section 7.0

c_p specific heat at constant pressure

$C_1, C_2 \ldots$ constants of integration

I_o time average stagnation enthalpy

I_o' turbulent fluctuation in stagnation enthalpy

k laminar thermal conductivity

k_t turbulent thermal conductivity

K $\Gamma/2\pi$

K_o $\Gamma_o/2\pi$

K_1 value of K at position of maximum tangential velocity

p static pressure

q_t heat transfer rate due to turbulent fluctuations

r radial distance

r_1 radial distance to maximum tangential velocity

r_i outer radius of part of vortex in solid body rotation

10

r_j	radius at outer edge of logarithmic region
r_o	radius where $\Gamma/\Gamma_o = 0.99$
R	gas constant for air
t	time
T	static temperature
T_i	value of T at r_i
T'	turbulent fluctuation in T
T_∞^*	free-stream static temperature
u	radial velocity
u'	turbulent fluctuation in radial velocity
v	tangential velocity
v'	turbulent fluctuation in tangential velocity
v_1	value of v at r_1
w	axial velocity
z	axial distance
γ	ratio of specific heat at constant pressure to that at constant volume
Γ	circulation, $2\pi r v$
Γ_o	total circulation of vortex
μ	laminar viscosity
μ_t	turbulent viscosity
ν	μ/ρ
ν_t	turbulent eddy viscosity
ρ	mass density
σ	laminar Prandtl number
σ_t	turbulent Prandtl number
τ_t	turbulent shearing stress, Reynolds stress
Ω	angular velocity of vortex eye

11

Section 8.0

c_p	specific heat at constant pressure
C	constant of integration
d_b	buoyant length given by equation (8-4)
D	$m/\pi\Delta x$
F	function defined by equation (8-33)
F_B	buoyant force
g	acceleration of gravity
G	function defined by equation (8-34)
h	upward distance with $h = 0$ at $t = t_i$
H	heat energy added to wake per unit time
ℓ	reference length given by equation (8-5)
ℓ_b	$gH/\pi\rho_\infty c_p T_\infty^* (U_\infty^*)^3$
L	airplane lift
m	total mass of recirculating flow
$\dot{m}_e$	mass rate of entrainment
p_∞	atmospheric static pressure
R	average radius of plume or wake cross section
R_g	gas constant for air
S	$U_\infty^*/\ell_b \omega$
t	time
T_∞^*	static temperature of atmosphere
$\overline{T}$	average temperature of air in wake
u	axial velocity of air in plume
U_∞^*	free-stream velocity
v	horizontal wind velocity
w	vertical upward velocity of wake

x	distance behind aircraft
Δx	thickness of wake cross-sectional slab measured in axial direction
α	entrainment coefficient, equations (8-1) and (8-8)
β	entrainment coefficient, equation (8-1)
γ	ratio of specific heats
Γ	vortex circulation
ϵ	rate of entrainment of ambient air
θ	inclination of plume axis to horizontal
ξ	$gh/R_g T_\infty^*$
$\bar{\rho}$	mass average density of recirculating flow
ρ_∞	atmospheric mass density
ω	Brunt-Väisällä frequency, equation (8-3)

Subscript

i	initial value of a quantity

Section 9.0

AR	wing aspect ratio
b	wing span
c	mass fraction of jet exhaust gases
c_{ave}	mass weighted average of c across jet cross section
c_p	specific heat at constant pressure for air
C_D	airplane drag coefficient
C_L	airplane lift coefficient
E_m	see equation (4-65)

E_z	see equation (4-65)
h	increase in height during buoyant phase
K	vr
K_o	circulation parameter, $\Gamma_o/2\pi$
K_1	$v_1 r_1$
L	airplane lift
$\dot{m}_a$	ratio of mass of entrained air to mass of exhaust gases
M_c	Mach number on jet centerline
M_j	Mach number in jet exit
M_∞	free-stream Mach number
r	radial distance from center of trailing vortex
r_d	r_d^*/r_n^*
r_e	r_e^*/r_n^*
r_i	r_i^*/r_n^*
r_o	radius of center to the 99-percent circulation position
r_e^*	jet outer radius
r_d^*	radius of streamtube originating at jet exit
r_i^*	radius of potential core
r_n^*	radius of jet exit
r_1^*	radius to point of vortex maximum tangential velocity
R	equivalent radius of recirculation region during buoyant phase
R_i	initial equivalent radius of recirculation region at beginning of buoyant phase
t	time after airplane passage
t_c	characteristic time, equation (9-2)

14

Δt	average wake temperature rise due to engine heat
T	static temperature in trailing vortex
T_{ave}	T^*_{ave}/T^*_j
T_c	T^*_c/T^*_j
T_{O_∞}	$T^*_{O_\infty}/T^*_{O_j}$
T_∞	T^*_∞/T^*_j
T^*_{ave}	mass average temperature in jet
T^*_c	jet centerline temperature
T^*_j	jet exit temperature
T^*_∞	free-stream temperature
T^*_O	free-stream total temperature
$T^*_{O_j}$	total temperature at jet exit
U_{ave}	U^*_{ave}/U^*_j
U_c	U^*_c/U^*_j
U_∞	U^*_∞/U^*_j
U^*_{ave}	mass average axial velocity in jet
U^*_c	jet centerline velocity
U^*_j	velocity in jet exit
U^*_∞	velocity at edge of jet
v	tangential velocity in trailing vortex
v_1	vortex maximum tangential velocity
V_∞	airplane speed (numerically equal to U^*_∞)

x, y	lateral and vertical coordinates, respectively, with the origin at the trailing-edge location on the vertical plane of symmetry of the airplane
x_v, y_v	lateral and vertical coordinates with origin at centerline of trailing vortex
z	z^*/r_n^*
z_i	value of z for start of jet break-up
z^*	axial distance behind wing trailing edge
α	entrainment coefficient
Γ_o	trailing vortex strength
η_I	efficiency of conversion of engine heat into propulsion work
ρ_∞	free-stream air mass density
ρ_{∞_i}	initial value of ρ_∞ at beginning of buoyant phase
$\bar{\rho}$	average mass density of fluid in recirculation region
$\bar{\rho}_i$	initial value of $\bar{\rho}$ at beginning of buoyant phase

3.0 PHYSICAL DESCRIPTION AND MODELS OF INGESTION AND DISPERSION PROCESSES

3.1 Preliminary Considerations

The exhaust products of an engine contain many components including water, nitrogen oxides, and particulate matter. Wake concentrations at the exhaust of high altitude aircraft are expected (ref. 3-1) to be 90,000 ppm H_2O vapor, 500-5000 ppm CO, 50-200 ppm NO and 1-10 ppm SO_2. Ambient levels at 20 kilometers are of the order of 3 ppm H_2O vapor, 0.01-0.20 ppm CO, 0.001-0.003 ppm NO, 0.0001-0.001 ppm SO_2 and 2 ppm O_3. In the analysis of the problem we will neglect the particulate matter. It is generally sufficiently small that it will follow the streamlines, and in any event presents such a minor mass fraction that it should not influence the gas flow significantly.

16

Another assumption that we will generally use is that the temperature and concentration profiles in the jets are similar. Low speed theory and experiment show that the transfer of heat and mass are similar but both differ from the transfer of momentum. The radial spread of temperature and concentration is slightly faster than that of velocity.

Wilder and Hindersinn (ref. 3-2) have shown by measurement that the spread of a CO_2 jet exhausting into a supersonic airstream was in good agreement with jet spread data determined on the basis of total temperature measurements. They also showed that gas dynamic expansions and compressions within the jet caused no essential change in the nature of the jet spread due to turbulent mixing. The rate of spread due to mixing was found to be small. Data on free jets generally show similar concentration and temperature profiles (ref. 3-3, pp. 98-102). If the transfer of heat and mass is dominated by turbulent diffusion and the various gas components of the engine exhaust remain in the same relative proportions, it is reasonable to take all concentration profiles similar to the temperature profiles as a first approximation. Accordingly, we are faced with determining the temperature field of the flow.

Consider the overall flow process to consist of a number of stages. The first stage is the jet stage in which the jet issues from the engine and is relatively unaffected by the presence of the wing vortex wake for a distance downstream of the aircraft. In the next stage the trailing vortices have sufficient influence to break up the jets and entrain some or all of the engine exhaust. We will designate this stage as the hot gas ingestion stage. After the ingestion stage there exists the equilibrium vortex stage in which the vortex pair act together and move with a regime of recirculating flow which is closely elliptical in cross section. In the final asymptotic stage the buoyancy force acting on the recirculating flow together with turbulent entrainment of atmospheric air combine to produce the asymptotic stage of the motion.

3.2 Jet Stage

The initial conditions for the study are taken at the point where the engine exhaust exits to the atmosphere. For the example calculations it is assumed that the jet pressure is equal to the atmospheric pressure

17

at the exit. This is achieved by means of engine flaps. If pressure equalization takes place external to the nozzle, a special calculation may be required to determine the initial conditions corresponding to atmospheric pressure. In addition to pressure equalization at the exit, we have also assumed that the velocity profile is uniform.

At the exit the flow is described in terms of a static pressure, Mach number and stagnation temperature. The jet exhausts into a mainstream at atmospheric pressure and temperature and airplane Mach number. The jet Mach number may be less than that of the free stream because of the high speed of sound in the jet.

Consider first the case where the jet axis is aligned in the flight direction. The supersonic jet in a coflowing supersonic stream now entrains free-stream air and slows down. For a certain distance behind the aircraft, the potential core exists and beyond this distance the "far field" occurs. The velocity and temperature profiles are governed by turbulent mixing between jet and free stream and on the stagnation temperature ratio of the jet and free stream. No reliable method of calculating the properties of the jet and based on data for hot supersonic jet in coflowing supersonic streams was found in the literature. Accordingly, one has been developed, as described in section 4. It turns out that the entrainment rates are much less than expected.

It is only at certain angles of attack that the jet thrust axis is aligned with the free-stream direction. For other angles of attack there is thus the additional complication of a jet obliquely inclined to the free-stream flow. The analysis of Wooler (ref. 3-4) for oblique subsonic jets has been adapted to treat this effect by means of a crossflow drag coefficient.

There is also an effect of the trailing vortices on the jet as it leaves the aircraft. One effect is that the crossflow velocity normal to the jet is reduced because of the induced downwash between the vortices so that the crossflow drag on the jet is reduced. It is also assumed that the jet before it disintegrates acts as a solid boundary for the purpose of imaging the trailing vortices. There is thus an additional component of force acting on the jet. Furthermore the motion of the vortices induced by the presence of the jets cause an additional force component acting on the jet. Finally there is the buoyant force acting

18

on the jet by virtue of its higher temperature than the surroundings. As a result of all these forces, the jet tends to straighten out parallel to the trailing vortices after a certain distance of travel behind the wing trailing edge. At some point near this position the hot gas ingestion stage commences, and the jet is allowed to disintegrate and become entrained by the trailing vortices.

3.3 Hot-Gas Ingestion Stage

No data have been found to illustrate how the jet from an engine breaks up and is entrained into a trailing vortex. In order to obtain some insight into the question, a test was made in the 40- by 80-Foot Wind Tunnel using the 6-foot span Convair 990 wing model designed and built for a trailing-vortex investigation. A trailing vortex was made visible by placing white smoke generators near the wing tip. At about the 69-percent semispan location slightly under the wing, a yellow smoke generator was used to simulate the engine jet. Smoke was forced out of the engine location at a low tunnel speed (30 ft/sec, approximately) so that observations could be made by investigators in the wind tunnel. The yellow smoke moved downward under the vortex, and reached a point directly under the vortex at about 30 feet downstream of the wing. As it moved past this point, it rapidly broke up and became ingested by the trailing vortex. The engine smoke thus maintained its identity for about five wing spans.

In calculating the jet break-up and its ingestion into the trailing vortex we have considered the jet no longer to be under the influence of crossflow drag nor to contain an image vortex system. In fact, the various regions of the jet are now considered to be independent and to be acted on only by the direct effect of the trailing vortex pair and by buoyancy. The pieces of the jet considered as mass points then tend either to spiral into the vortex or escape from the recirculation region.

During this process the initial temperatures of the various pieces are obtained from the calculated temperature profiles in the jet. As they are ingested, it is assumed that their temperature time history is the same as if the jet had continued to develop. The turbulent mixing processes in the two cases are probably different, so that the assumption is only approximate. However, if the hot gas is rapidly ingested, then

19

this assumption should be sufficiently accurate since the gas will not cool much during ingestion.

The above calculation should show how much of the exhaust gas is ingested. The amount of exhaust gas can be much greater than the amount of air in the core of the undisturbed vortex. Accordingly, hot gas ingestion will change the structure of the trailing vortex. All the hot air tends to be concentrated in the center of the vortex. Some effect of hot air_ingestion on vortex stability might be expected.

3.4 Equilibrium Vortex Stage

In the equilibrium vortex stage the ingested exhaust gases become part of the recirculating flow around the vortices. The general flow picture is shown in the following sketch as taken from reference 3-5.
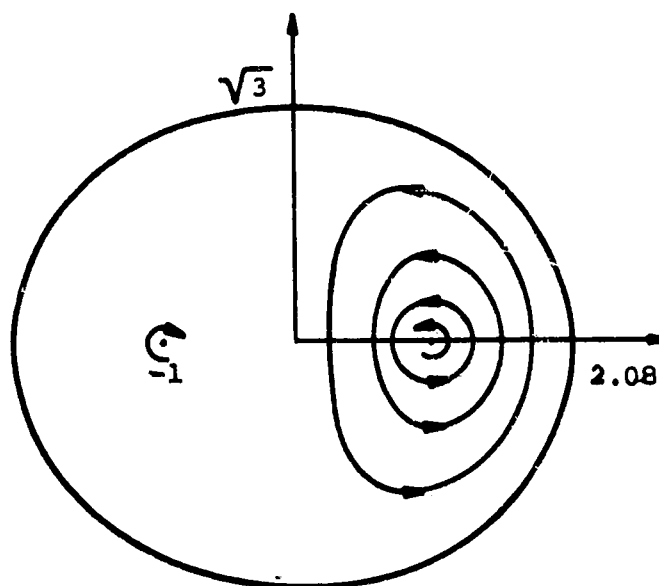
The recirculating flow near the vortices will be very similar to that for a single trailing vortex since the interference of one vortex on the other is small under these conditions. The whole recirculation region mass moves upward or downward in the atmosphere as a whole. The calculation of reference 3-5 of the rate at which vorticity diffuses from the recirculation region into a surrounding quiescent atmosphere or is annihilated along the vertical axis of symmetry shows a decrease

20

in the vortex strength in the ratio of 1/e in about 80 minutes. While
this case is for a subsonic transport, it should also give a good order
of magnitude estimate for a supersonic aircraft.

In the case of mass diffusion of the exhaust gases from the
recirculation region, mass can be detrained from the recirculation region
only across its outer boundary whereas in the case of the diffusion of
vorticity across the vertical plane of symmetry, vorticity of opposite
sign can annihilate each other. Considering now the analogy between
the diffusion of vorticity and mass, we would expect the exhaust gases
to be detrained from the recirculation region even more slowly than the
above calculation indicates for vorticity since a means of annihilating
vorticity was present along the vertical plane of symmetry where no such
means is available to annihilate mass.

The rate of escape of exhaust gases from the vortex is small during
the equilibrium vortex stage. The vortex tends to retain vorticity and
fluid within its confines. The vortex core is highly stable with a
tendency to damp out turbulence resulting in very low rates of diffusion.
The exhaust gases will concentrate in annulii surrounding the core at
radial distances according to the relative density between the species
and the environment. The vortex will act as a centrifuge in which gases
will be stratified according to the radial variation in density.

3.5 Asymptotic Buoyant Stage

In the asymptotic stage the recirculation region is influenced
chiefly by buoyancy. Accordingly it will tend to rise. At the same
time its vertical motion will cause entrainment of stratospheric air.
A detailed analysis of the asymptotic motion of the wake in a quiescient
stratosphere is made in Section 8.

An approximate analysis of the asymptotic stage of the wake motion
has been made by Conti, et al. (refs. 3-6 and 3-7) considering a number
of separate nonlinear effects.

These authors suggested that, in addition to the buoyant rise and
wake-induced turbulent growth, further dispersion occurs because of
wake collapse and horizontal wind shear. According to their analysis,
buoyant rise is the least influential of the mechanisms giving rise to
horizontal wake growth.

The towing tank experiments of Fay and Overcamp (ref. 3-8) modeled an atmosphere without wind shear, wind generated turbulence, and stratification. The experimental results confirm the predicted growth due to buoyancy in the absence of these atmospheric effects. Although wake collapse has been observed in the case of wakes in a stratified medium, it has not been observed in experiments on buoyant plumes. When buoyant plumes level off, they become internally stratified to the same extent as the surrounding fluid and no further turbulent mixing occurs. It is still not clear whether wake collapse will play a significant role in the asymptotic stage, but is seems probable that buoyant forces play a more significant role for supersonic aircraft than for subsonic aircraft because of greater wake heating.

The ultimate dispersion, on time scales of months or longer, of exhaust products will be determined by the rates of natural stratospheric dispersion which are governed by horizontal wind shear and stratification. The present study is mainly concerned with establishing the initial conditions for the dispersion by considering the movements and rates of dilution of the exhaust products from the engine exhaust through the aircraft wake.

4.0 ANALYSIS OF HOT SUPERSONIC JET CHARACTERISTICS

4.1 Introduction

A method of determining the hot jet characteristics for a supersonic jet in a coflowing supersonic stream verified by experiment for the range of interest was not found in the literature. Since the details of the jet flow must be known to determine whether it is entrained by the trailing vortices, it was necessary to develop a theory for the jet characteristics. Only one set of data was found (ref. 4-1) for supersonic jets in supersonic coflowing streams with heating, and these data have been used to determine the eddy viscosity values which are the basic empirical inputs into most if not all jet theories.

In the theory which follows constant pressure turbulent mixing has been assumed. For our example case the jet exit pressure and atmospheric pressure are closely matched. We have assumed that the velocity, concentration and temperature profiles at the jet exit are uniform. In the case of pressure equalization external to the nozzle some departure from the conditions of uniformity is to be expected.

22

In the ensuing analysis most of the work is carried out in terms of nondimensional quantities. Such quantities as density, temperature, velocity, and stagnation temperature have been nondimensionalized by the values of these quantities at the jet exit. All distances have been non-dimensionalized by the jet exit radius. Asterisks have been used to designate dimensional quantities and nondimensional quantities carry no asterisk.

4.2 Basic Equations of the Jet

The problem to be analyzed is the turbulent mixing of an initially uniform axisymmetric jet exhausting into a uniform coflowing stream under the condition of a uniform static pressure throughout the flow field external to the jet nozzle. The general features of the flow field as well as the nomenclature are depicted in figure 4-1. The axisymmetric flow field is described in terms of a radial and an axial coordinate, r^* and z^*, and the jet nozzle radius, r_n^*. The local thermodynamic and gas-dynamic parameters are designated as follows: the density, ρ^*; the stagnation temperature, T_o^*; the Mach number, M; and the velocity, U^*. The free-stream properties are denoted by the subscript, ∞, while those of the initial uniform jet are denoted by the subscript j. The properties evaluated along the axis ($r^* = 0$) are denoted by the subscript, c, those evaluated on the streamtube containing the original jet mass flow are denoted by the subscript, d, and a general streamtube by the subscript s. The outer boundary of the mixing region is designated by the radius r_e^*.

The jet is considered in two parts. For some distance downstream of the nozzle exit a potential core exists, as shown in figure 4-1, in which the velocity and thermodynamic properties are uniform at the values at the nozzle exit. The local radius of the potential core is designated r_i^*. The axial distance over which the potential core exists will also be termed the near field. Downstream of the potential core the velocity on the jet centerline U_c^* progressively decreases. This region of the jet is termed the far field.

The integral form of the governing equations for conservation of mass and momentum along a streamtube, s, are:

Mass

$$\frac{d}{dz^*} \int_0^{r_s^*} \rho^* U^* r^* dr^* = 0 \qquad (4-1)$$

Momentum

$$\frac{d}{dz^*} \int_0^{r_s^*} \rho^* (U^*)^2 r^* dr^* = r_s^*(z^*) \tau^*(z^*, r_s^*) \qquad (4-2)$$

where

$r_s^*(z^*)$ is the radius of a given streamtube, s, at any axial position, z^*.

$\tau^*(z^*, r_s^*)$ is the shear stress on the streamtube, s, at the axial position, z^*.

$$= \rho_s^* \epsilon_s^* \left. \frac{\partial U^*}{\partial r^*} \right|_{r_s^*} \qquad \text{for turbulent flow}$$

ϵ_s^* is the eddy viscosity in the flow field evaluated at the streamtube, s.

Integration of equation (4-1) along the streamtube beginning at the lip of the jet nozzle results in

$$\int_0^{r_d^*(z^*)} \rho^* U^* r^* dr^* = \rho_j^* U_j^* \frac{r_n^{*2}}{2} = \dot{m}_j^* \qquad (4-3)$$

where $\dot{m}_j^*$ is $1/2\pi$ times the mass efflux from the jet nozzle.

The total jet mass flow per unit time is proportional to the quantity

$$\int_0^{r_e^*(z^*)} \rho^* U^* r^* dr^* = \int_0^{r_d^*(z^*)} \rho^* U^* r^* dr^* + \int_{r_d^*}^{r_e^*(z^*)} \rho^* U^* r^* dz^* = \dot{m}_j^* + \dot{m}_a^*(z^*) \qquad (4-4)$$

24

where $\dot{m}_a^*(z^*)$ is $1/2\pi$ times the mass flux of free-stream fluid entrained in the mixing region up to the station z^*.

At the outer edge of the mixing region, $r_e^*(z^*)$ the shear stress, $\tau^*(r_e^*(z^*))$, vanishes. The total jet momentum is thus proportional to the quantity

$$\int_0^{r_e^*(z^*)} \rho^* U^{*2} r^* dr^* = \dot{m}_j^* U_j^* + \dot{m}_a^*(z^*) U_\infty^* \qquad (4-5)$$

which indicates that the momentum inside r_e^* at any axial station is equal to the original jet momentum,

$$2\pi \dot{m}_j^* U_j^* = \pi \rho_j^* (U_j^*)^2 r_n^{*2}$$

plus the momentum ingested into the mixing region from the free stream, $2\pi \dot{m}_a^* U_\infty^*$.

If we replace $\dot{m}_a^*$ using equation (4-4)

$$\dot{m}_a^* = \int_0^{r_e^*} \rho^* U^* r^* dr^* - \dot{m}_j^* \qquad (4-6)$$

Equation (4-5) may be put into the form

$$\int_0^{r_e^*} \rho^* U^* (U^* - U_\infty^*) r^* dr^* = \dot{m}_j^* (U_j^* - U_\infty^*) \qquad (4-7)$$

for future reference.

A similar treatment of the energy equation yields

$$\int_0^{r_e^*} \rho^* U^* H^* r^* dr^* = \dot{m}_j^* H_j^* + \dot{m}_a^* H_\infty^* \qquad (4-8)$$

where H^* is the stagnation enthalpy of the fluid. By substitution of equation (4-6) into equation (4-8) one obtains

$$\int_0^{r_e^*} \rho^* U^* (H^* - H_\infty^*) r^* dr^* = \dot{m}_j^* (H_j^* - H_\infty^*) \qquad (4-9)$$

We note that it is unnecessary up to this point to presume that the diffusion of momentum and energy have proceeded to the same outer boundary. The above relations merely require that r_e^* encompass the more extensive of the two, so that there is no contribution to either integral of equations (4-7) or (4-9) for $r^* > r_e^*$.

It will be convenient to normalize all quantities with respect to their values in the initial uniform jet since all such quantities will always be nonzero which may not be the case for the free stream. The resulting quantities will be simply those previously defined, but with the asterisk removed.

$$\rho = \frac{\rho^*}{\rho_j^*} \qquad (4-10a)$$

$$= \frac{T_j^*}{T^*} = \frac{1}{T} \qquad \text{for a perfect gas of uniform molecular weight in a constant pressure field} \qquad (4-10b)$$

$$U = \frac{U^*}{U_j^*} \qquad (4-10c)$$

$$H = \frac{H^*}{H_j^*} = \frac{T_o^*}{T_{o_j}^*} = T_o , \quad \text{for a perfect gas of uniform specific heat} \qquad (4-10d)$$

$$r = \frac{r^*}{r_n^*} \qquad (4-10e)$$

$$z = \frac{z^*}{r_n^*} \qquad (4-10f)$$

With the assumptions of uniform molecular weight W and specific heat c_p and using these normalizations, we can write using the ratio of specific heats $\gamma = c_p/c_c$,

$$T_\infty = T_{O_\infty} (1 + \frac{\gamma - 1}{2} M_j^2) / (1 + \frac{\gamma - 1}{2} M_\infty^2) \qquad (4\text{-}11)$$

$$U_\infty = \sqrt{T_\infty} \, M_\infty / M_j \qquad (4\text{-}12)$$

We also normalize the entrained mass flux,

$$\dot{m}_a = \dot{m}_a^* / \dot{m}_j^* \qquad (4\text{-}13)$$

The governing equations may now be rewritten in nondimensional form

Mass

$$2 \int_0^{r_d(z)} \frac{U}{T} r \, dr = 1 \qquad (4\text{-}14)$$

and

$$\dot{m}_a(z) = 2 \int_0^{r_e(z)} \frac{U}{T} r \, dr - 1 \qquad (4\text{-}15)$$

Momentum

$$2 \int_0^{r_e(z)} \frac{U}{T} (U - U_\infty) r \, dr = 1 - U_\infty \qquad (4\text{-}16)$$

and

$$\frac{d}{dz} \int_0^{r_d(z)} \frac{U^2}{T} r \, dr = \frac{r_d}{T_d} \left(\frac{\epsilon_d^*}{r_n^* U_j^*} \right) \frac{\partial U}{\partial r} \Big|_{r_d} \qquad (4\text{-}17)$$

For a thermally perfect gas with $W \equiv 1$ the energy equation may be written as

Energy

$$2 \int_0^{r_e(z)} \frac{U}{T} (H - H_\infty) r \, dr = 1 - H_\infty \qquad (4\text{-}18)$$

27

and for a calorically perfect gas with uniform specific heat (i.e., $c_p = 1$)

$$2 \int_0^{r_e(z)} \frac{U}{T} (T_O - T_{O_\infty}) r \, dr = 1 - T_{O_\infty} \qquad (4\text{-}19)$$

In order to complete the formulation of the problem, it is necessary to introduce further information on U, T and ϵ_d^*. The former two appear in integrated form only and reasonable approximations to their functional dependence on r and z should yield a reasonably good solution. The axial coordinate enters the problem explicitly only through equation (4-17). It is thus seen that the eddy viscosity determines the axial scale of the solution.

4.3 Temperature-Velocity Relationship

Equations (4-14), (4-15), (4-16), (4-17), and (4-19) can be evaluated if nondimensional similarity profiles for velocity and temperature are introduced into the integrals. Another approach would be to utilize a nondimensional similarity profile for either temperature or velocity, and relate these variables through a Crocco-type relationship. If the latter course is chosen, then equation (4-19) is superfluous. To the extent the Crocco-type relationship obeys the law of the conservation of energy, equation (4-19) will be fulfilled. In our analysis we have chosen to use a Crocco-type relationship between temperature and velocity and to make a check of equation (4-19) with the resulting solution. Assuming unity Prandtl number, approximate relationships between temperature and velocity have been given by Crocco (ref. 4-2) and Woolley (ref. 4-3) for laminar or turbulent flows.

The Crocco relation indicates that the stagnation temperature of a thermally and calorically perfect gas having Pr = 1 and a constant and uniform specific heat is a linear function of velocity.

$$T_O^* = A' + B'U^* \qquad (4\text{-}20)$$

The coefficients A' and B' may be suitably defined to satisfy the boundary conditions on T_O^* and U^*.

28

This relation has been well confirmed for low speed laminar flows. For high Mach number flows, however, it has been found to be at considerable variance with the measured temperature-velocity distributions. In particular, in the so-called hypersonic limit the stagnation temperature has been found to vary with the square rather than as a linear function of the velocity.

Woolley (ref. 4-3) has shown that for turbulent flows in particular, the time mean <u>static</u> temperature for a perfect gas with constant and uniform specific heat should be a linear function of the time mean velocity

$$T^* = A + BU^* \tag{4-21}$$

for unity turbulent Prandtl number with the turbulent processes dominating the molecular ones. Both T^* and U^* are time average quantities and the coefficients A and B are evaluated for the particular boundary conditions. It is noted that this relation will approach the observed stagnation temperature-velocity relation for high Mach number flows; i.e.,

$$\overline{T_o^*} = A + BU^* + \frac{q^{2*}}{2c_p^*} \tag{4-22}$$

where $(q^2)^* = U^{2*} + \overline{(u'^2)}^* + \overline{(v'^2)}^* \rightarrow (U^2)^*$ assuming $(U^2)^* \gg \overline{(u'^2)}^*$ + $\overline{(v'^2)}^*$ where $\overline{(u'^2)}^*$ and $\overline{(v'^2)}^*$ are the mean square of the longitudinal and transverse components of the fluctuating velocity field, respectively.

This modified Crocco relation, equation (4-22), was shown by Woolley to satisfy the time mean energy equation appropriate to turbulent flows with unity Prandtl number.

Both the Crocco and the modified Crocco relation can be expressed in a single form valid for the entire jet for the following boundary conditions at the jet exit and at the free-stream boundaries.

Jet Exit: $T_{o_j} = T_j = U_j = 1$

Free-Stream Boundaries: Given T_{o_∞}, T_∞, U_∞, of

which 2 are independent.

The stagnation temperature is of the form

$$\frac{T_o - T_{o_\infty}}{1 - T_{o_\infty}} = \left[\frac{U_c - U_\infty}{1 - U_\infty} - \frac{DC_j^2}{1 - T_{o_\infty}} (U_c - U_\infty)(1 - U_\infty) \right] \bar{U} + \frac{DC_j^2 (U_c - U_\infty)^2}{1 - T_{o_\infty}} \bar{U}^2 \qquad (4-23)$$

where

$$C_j^2 = \text{jet Crocco number} = \frac{U_j^{*2}}{2H_j^*} = \frac{\frac{\gamma - 1}{2} M_j^2}{1 + \frac{\gamma - 1}{2} M_j^2}$$

$$D = \begin{array}{l} 0 \text{ for Crocco relation, equation (4-20)} \\ 1 \text{ for modified Crocco relation, equation (4-22)} \end{array}$$

$$\bar{U} = \text{normalized velocity} = (U - U_\infty)/(U_c - U_\infty)$$

The static temperature form is

$$\frac{T - T_\infty}{1 - T_\infty} = \left[\frac{U_c - U_\infty}{1 - U_\infty} + (1 - D) \frac{\frac{\gamma - 1}{2} M_j^2}{1 - T_\infty} (1 - U_\infty)(U_c - U_\infty) \right] \bar{U}$$

$$- (1 - D) \frac{\frac{\gamma - 1}{2} M_j^2}{1 - T_\infty} (U_c - U_\infty)^2 \bar{U}^2 \qquad (4-24)$$

In the above expression we note that $U_c = U_j = 1.0$ in the potential core region (i.e., for $z \leq \ell_p$), but U_c is variable for $z > \ell_p$.

4.4 Reduction of Equations to Similarity Form

It has been experimentally observed that the velocity and temperature profiles in jets exhibit self-similar behaviors. That is, appropriate combinations of the radial and axial coordinates will reduce these profiles to functions of a single variable to a high degree of accuracy. The resulting mathematical advantage afforded by such a simplification is that many of the integrals in the governing equations then become independent of z, and require calculation only once. Hence we will seek to pose the problem in such a form. Since we have already expressed the temperature as a function of velocity, we are concerned only with the velocity similarity law.

Numerous theoretical and analytical investigations of turbulent mixing, Schlichting (ref. 4-4), Abramovich (ref. 4-5), Crane (ref. 4-6), Maydew

30

and Reed (ref. 4-7), have indicated that the velocity profiles for both incompressible and compressible flows are virtually indistinguishable. The functional form suggested by Abramovich for axisymmetric flows will be used:

$$\overline{U} = (1 - \eta^{3/2})^2 \ , \ 0 \le \eta \le 1 \qquad (4\text{-}25)$$

where

$\overline{U}$ = normalized velocity distribution

$$= (U - U_\infty)/(U_c - U_\infty) = (U^* - U_\infty^*)/(U_c^* - U_\infty^*) \qquad (4\text{-}26)$$

η = similarity variable

$$= (r - r_i)/(r_e - r_i) = (r - r_i)/b \qquad (4\text{-}27)$$

This definition of terms in equations (4-26) and (4-27) permits the continuous application of equation (4-25) over the entire length of the jet. In the region of the potential core, $U_c = U_j = 1$. In the far field beyond the potential core, $U_c = U_c(z)$ and $r_i = 0$ with $z \ge \ell_p$.

In reducing the jet equations to similarity form we first note that

$$r = b(\eta + r_i/b) \qquad (4\text{-}28)$$

$$\left.\frac{\partial}{\partial r}\right|_z = b \left.\frac{\partial}{\partial \eta}\right|_z \qquad (4\text{-}29)$$

$$\left.\frac{\partial}{\partial z}\right|_r = \left.\frac{\partial}{\partial z}\right|_\eta + \left.\frac{\partial \eta}{\partial z}\right|_r \left.\frac{\partial}{\partial \eta}\right|_z = \left.\frac{\partial}{\partial z}\right|_\eta - \frac{1}{b}\left(\frac{dr_i}{dz} + \eta \frac{db}{dz}\right)\left.\frac{\partial}{\partial \eta}\right|_z \qquad (4\text{-}30)$$

and

$$\int_0^r g(r)\,dr = \int_{r_i}^r g(r)\,dr + \int_0^{r_i} g(r)\,dr = \int_{r_i}^{r_e} g(r)\,dr + \frac{r_i^2}{2}$$

if $g(r) = r$ for $r \le r_i$.

31

We will now rewrite equations (4-14), (4-15), (4-16), and (4-19) in a similarity form using equations (4-25) through (4-31).

Mass

$$b^2 \int_0^{\eta_d} \frac{U}{T} \eta \; d\eta + r_i b \int_0^{\eta_d} \frac{U}{T} \; d\eta = \frac{1}{2} (1 - r_i^2) \tag{4-31}$$

and

$$\dot{m}_a(z) = 2b^2 \int_0^1 \frac{U}{T} \eta \; d\eta + 2r_i b \int_0^1 \frac{U}{T} \; d\eta - (1 - r_i^2) \tag{4-32}$$

Momentum

$$b^2 \int_0^1 \frac{U}{T} (U - U_\infty) \eta \; d\eta + r_i b \int_0^1 \frac{U}{T} (U - U_\infty) d\eta = \frac{1}{2} (1 - U_\infty)(1 - r_i^2) \tag{4-33}$$

Energy

$$b^2 \int_0^1 \frac{U}{T} (T_O - T_{O_\infty}) \eta \; d\eta + b r_i \int_0^1 \frac{U}{T} (T_O - T_{O_\infty}) d\eta = \frac{1}{2} (1 - T_{O_\infty})(1 - r_i^2) \tag{4-34}$$

The conversion of equation (4-17) to similarity form is somewhat more complicated. The left-hand side of equation (4-17) may be expanded as follows:

$$\frac{d}{dz} \int_0^{r_d(z)} \frac{U^2}{T} r \; dr = \frac{d}{dz} \left[\int_0^{r_i(z)} \frac{U^2}{T} r \; dr + \int_{r_i(z)}^{r_d(z)} \frac{U^2}{T} r \; dr \right] \tag{4-35}$$

The first term in the brackets on the right-hand side represents the axial momentum of the core.

$$\frac{d}{dz} \int_0^{r_i(z)} \frac{U^2}{T} r \; dr = \frac{d}{dz} \left[\frac{U_c^2}{T_c} \frac{r_i^2}{2} \right] = r_i \frac{dr_i}{dz} \tag{4-36}$$

32

since $r_i = 0$ when U_c and $T_c \neq 1$.

The second term on the right of equation (4-35) may be written

$$\frac{d}{dz}\int_{r_i}^{r_d(z)} \frac{U^2}{T}\, r\, dr = \frac{U_d^2}{T_d}\, r_d\, \frac{dr_d}{dz} - r_i\, \frac{dr_i}{dz} + \int_{r_i(z)}^{r_d(z)} \frac{\partial(U^2/T)}{\partial z}\bigg|_r\, r\, dr \qquad (4\text{-}37)$$

The last term in the above may be written

$$\int_{r_i(z)}^{r_d(z)} \frac{\partial(U^2/T)}{\partial z}\bigg|_r\, r\, dr = b^2 \int_0^{\eta_d(z)} \left[\frac{\partial(U^2/T)}{\partial z}\bigg|_\eta \right.$$

$$\left. - \frac{1}{b}\left(\frac{dr_i}{dz} + \eta\, \frac{db}{dz}\right)\frac{\partial(U^2/T)}{\partial\eta}\bigg|_z \right]\left(\eta + \frac{r_i}{b}\right) d\eta \qquad (4\text{-}38)$$

Noting that

$$\frac{\partial(U^2/T)}{\partial z}\bigg|_\eta = \frac{\partial(U^2/T)}{\partial U_c}\bigg|_\eta\, \frac{dU_c}{dz} \qquad \text{and} \qquad \frac{dU_c}{dz} = 0 \qquad \text{when} \qquad r_i \neq 0.$$

the first term on the right of equation (4-38) becomes

$$b^2 \int_0^{\eta_d} \frac{\partial(U^2/T)}{\partial z}\bigg|_\eta\left(\eta + \frac{r_i}{b}\right) d\eta = b^2\, \frac{dU_c}{dz}\int_0^{\eta_d(z)} \frac{\partial(U^2/T)}{\partial U_c}\bigg|_\eta\, \eta\, d\eta \qquad (4\text{-}39)$$

Integrating by parts and noting that

$$r_d = b\left(\eta_d + \frac{r_i}{b}\right)$$

and

$$\frac{d\eta_d}{dz} = \frac{1}{b}\left(\frac{dr_d}{dz} - \frac{dr_i}{dz} - \eta_d\, \frac{db}{dz}\right)$$

33

The second term on the right of equation (4-38) becomes

$$-b\int_0^{\eta_d} \frac{\partial(U^2/T)}{\partial\eta}\bigg|_z \left(\frac{dr_i}{dz} + \eta\frac{db}{dz}\right)\left(\eta + \frac{r_i}{b}\right) d\eta = \frac{U_d^2}{T_d} r_d \left(b\frac{d\eta_d}{dz} - \frac{dr_d}{dz}\right) + r_i\frac{dr_i}{dz}$$

$$+ b\int_0^{\eta_d} \frac{U^2}{T}\left[\frac{dr_i}{dz} + \frac{db}{dz}\left(2\eta + \frac{r_i}{b}\right)\right] d\eta$$

$$(4\text{-}40)$$

The right-hand side of equation (4-17) is rewritten simply as

$$\frac{r_d}{r_n^* T_d} \frac{\epsilon_d^*}{U_j^*} \frac{\partial U}{\partial r}\bigg|_{r=r_d} = \frac{r_d}{T_d} \frac{\epsilon_d^*}{U_j^* b^*} \frac{\partial U}{\partial\eta}\bigg|_{\eta=\eta_d} \qquad (4\text{-}41)$$

Collecting equations (4-35) through (4-41) we may now rewrite equation (4-17) in similarity form

$$\frac{U_d^2}{T_d} br_d \frac{d\eta_d}{dz} + r_i\frac{dr_i}{dz} + b\int_0^{\eta_d} \frac{U^2}{T}\left[\frac{dr_i}{dz} + \frac{db}{dz}\left(2\eta + \frac{r_i}{b}\right)\right] d\eta$$

$$+ b^2\frac{dU_c}{dz}\int_0^{\eta_d} \frac{\partial(U^2/T)}{\partial U_c}\bigg|_\eta \eta\, d\eta = \frac{r_d}{T_d}\epsilon_d \frac{\partial U}{\partial\eta}\bigg|_{\eta=\eta_d} \qquad (4\text{-}42)$$

where

$$\epsilon_d = \frac{\epsilon_d^*}{U_j^* b^*} \qquad (4\text{-}43)$$

In the application of equation (4-42) it is recalled that either

$$\frac{dU_c}{dz} = 0 \ , \ r_i \geq 0 \qquad \text{(near field)}$$

or

$$r_i = \frac{dr_i}{dz} = 0 \qquad \text{(far field)}$$

34

4.5 Eddy Viscosity Determination

The axial length scale through equations (4-17) or (4-42) is locally proportional to the eddy viscosity, ϵ_d. There is, unfortunately, no reliable theory and little direct information on the determination of the eddy viscosity for supersonic jets in supersonic co-flowing streams. Our approach is to correlate such data as can be found in the literature into a model for the eddy viscosity, ϵ^* and on the basis of that correlation estimate the eddy viscosity for the present circumstances.

The eddy viscosity is defined by the relation

$$\tau^* \equiv \rho^* \epsilon^* \frac{\partial U^*}{\partial r^*} \tag{4-44}$$

where

τ^* = turbulent shear stress (Reynolds stress) associated with a point in the flow field.

ρ^* = density at the point.

$\partial U^*/\partial r^*$ = radial gradient of the velocity at the point.

The form of eddy viscosity used extensively for incompressible free shear flows is

$$\epsilon^* = Kb^*(U_{max}^* - U_{min}^*) \tag{4-45}$$

where

b^* = measure of the shear layer thickness

K = nondimensional coefficient whose actual magnitude depends on the choice of b^*.

U_{max}^*, U_{min}^* = respectively, the maximum and minimum characteristic velocities of the shear flow.

In the present analysis we have adopted the general functional form of ϵ^* given in equation (4-45). We have taken b^* to be the radial width of the mixing region,

$$b^* = r_e^* - r_i^* \tag{4-46}$$

35

and

$$U^*_{max} - U^*_{min} = U^*_C - U^*_\infty \qquad (4-47)$$

For the present analysis, any effects on the eddy viscosity not fully accounted for by these two factors are contained in the parameter K. Thus,

$$\epsilon^* = Kb^*(U^*_C - U^*_\infty) \qquad (4-48)$$

Numerous investigators have noted that the eddy viscosity is dependent not only on the velocity difference across the free shear layer, but also on the velocity ratio, U_∞, (see, for example, Schlichting (ref. 4-4), Abramovich (ref. 4-5), and Sabin (4-8)). This additional dependency on velocity ratio appears to be expressible as a function of

$$\lambda = (1 + U_\infty)/(1 - U_\infty) \qquad (4-49)$$

The effects of density differences in the far field in the absence of thermal differences was investigated by Ricou and Spalding (ref. 4-9) and found to be expressible as a function of the density ratio, ρ_∞.

Investigations with heated jets, e.g., Corrsin and Uberoi (ref. 4-10) have indicated that the temperature ratio of the streams, T_∞, is a correlating parameter in this case.

Warren (ref. 4-11) found little effect of temperature on the eddy viscosity when the effect of Mach number was included in his study of single supersonic and subsonic jets in a quiescent atmosphere. It now appears that this effect is interchangeably expressed with the combined effects of the density and total temperature ratios. Similar data from Maydew and Reed (ref. 4-7) are in accord with this observation.

Wilder and Hindersinn (4-12) studied the mixing of a two-dimensional jet in a co-flowing stream. The total temperature ratio and the Mach number of both streams were varied systematically in their study. The data are the only ones of their type found in our literature search. Their results are detailed in Wilder and Hindersinn (ref. 4-1) and provide 19 data points within the following ranges: total temperature ratios,

$0.5 \leq T_{O_\infty} \leq 0.8$; jet Mach number, $0.9 < M_j < 2.8$; and free-stream Mach number, $1.25 \leq M_\infty \leq 1.6$. An eddy viscosity correlation depending solely on the ratio of the two Mach numbers (i.e., independent of T_{O_∞} and T_∞) is suggested in this study. This correlation, based on the ratio M_j/M_∞, is clearly not applicable to the condition of a quiescent free stream where $M_\infty = 0$.

With this background K is assumed to be of the form

$$K = K_o f(\rho_\infty, T_{O_\infty}, U_\infty) \tag{4-50}$$

where it is assumed that

$$f(\rho_\infty, T_{O_\infty}, U_\infty) = \rho_\infty^a T_{O_\infty}^b \lambda^c \tag{4-51}$$

$$K_o = \text{absolute constant}$$

An attempt was made to correlate all available data within this format and to evaluate K_o and the exponents $a, b,$ and c.

The eddy viscosity data used in the correlation study were put into the format indicated by the preceding equations. Because of the many definitions of ϵ^*, b^*, and the analytical approaches used in the various investigations, it was necessary to reduce the published data to the present format by the procedures given in Appendix 4A. The data were all reduced to give the effective K defined in equation (4-50) for the given experimental conditions with the definition of terms prescribed in the preceding equations. The resulting data and sources are given in Table 4-I.

The data of Table 4-I were systematically used to evaluate the exponents $a, b,$ and c of equation (4-51). These data were primarily determined from near field measurements. It was found that the coefficients $a, b,$ and c were all approximately equal within the accuracy of the given data. The values of K may thus be correlated as a function of the single parameter:

$$\alpha = \rho_\infty T_{O_\infty} \lambda \tag{4-52}$$

The correlated data are shown in figure 4-2 where it is observed that

37

$$f(\rho_\infty, T_{O_\infty}, U_\infty) = \alpha^{0.9} \tag{4-53}$$

appears to express the dependence of K on α very well. The free-jet data of Warren and the data of Wilder and Hindersinn both appear to fall along lines parallel to $\alpha^{0.9}$

The Mach number dependence noted by the preceding investigators appears to be reconciled by equation (4-53). To see that this is reasonable we note that

$$\alpha = \rho_\infty T_{O_\infty} \lambda = \frac{T_{O_\infty}}{T_\infty} \lambda = \frac{T_{O_\infty}^*}{T_{O_j}^*} \cdot \frac{T_j^*}{T_\infty^*} \lambda$$

$$\alpha = \frac{1 + \frac{\gamma - 1}{2} M_\infty^2}{1 + \frac{\gamma - 1}{2} M_j^2} \lambda \tag{4-54}$$

From equation (4-54) it is seen that for Warren's free-jet case where $M_\infty = 0$, $\lambda = 1$, the effective K was found to decrease with increasing M_j.

Further expansion of equation (4-54) shows that α is only a weak function of T_{O_∞} when expressed as a function of M_∞ and M_j. It is noted that

$$U_\infty = \frac{U_\infty^*}{U_j^*} = \frac{M_\infty}{M_j} \sqrt{\frac{T_\infty^*}{T_j^*}} = \frac{M_\infty}{M_j} \sqrt{\frac{T_{O_\infty}^* (1 + \frac{\gamma - 1}{2} M_j^2)}{T_{O_j}^* (1 + \frac{\gamma - 1}{2} M_\infty^2)}}$$

$$= \frac{M_\infty}{M_j} \sqrt{\frac{T_{O_\infty} (1 + \frac{\gamma - 1}{2} M_j^2)}{(1 + \frac{\gamma - 1}{2} M_\infty^2)}}$$

Combining this expression with equation (4-54) yields

$$\alpha = \frac{(1 + \frac{\gamma - 1}{2} M_\infty^2)}{(1 + \frac{\gamma - 1}{2} M_j^2)} \cdot \frac{1 + \sqrt{T_{O_\infty}} \cdot \frac{M_\infty}{M_j} \sqrt{\frac{(1 + \frac{\gamma - 1}{2} M_j^2)}{(1 + \frac{\gamma - 1}{2} M_\infty^2)}}}{\left| 1 - \sqrt{T_{O_\infty}} \cdot \frac{M_\infty}{M_j} \sqrt{\frac{(1 + \frac{\gamma - 1}{2} M_j^2)}{(1 + \frac{\gamma - 1}{2} M_\infty^2)}} \right|} \qquad (4\text{-}55)$$

Examination of equation (4-55) indicates that α is almost independent of T_{O_∞} for small values of M_∞/M_j and only a function of $T_{O_\infty}^{1/2}$ otherwise. Thus the correlations of eddy viscosity using Mach number will show little effect of stagnation temperature in accord with both the results of Warren and of Wilder and Hindersinn.

As can be seen from figure 4-2, the correlation of K as a function of α alone shows two distinct curves for $M_\infty = 0$ and $M_\infty > 1$. It was noted that the upper group of data (i.e., those with the higher values of K_O) were obtained with the external stream either quiescent or with the entire flow field incompressible. The lower group of data (the 19 points of Wilder and Hindersinn's data) were generally taken when both of the streams were supersonic. Three data points from Eggers and Torrence (ref. 4-13) fall between the two extremes. Two of the three points are for $M_\infty > 1$ but $M_j < 1$ while for the third point, both streams were subsonic. It thus appears that the mixing of the jet with the co-flowing stream depends strongly on whether $M_\infty = 0$ or $M_\infty > 1$. It is possible that this result is associated with the different signs of the rate of change of streamtube area with axial distance for decelerating flow at subsonic and supersonic speeds.

The range of α in the supersonic jet and supersonic free-stream data (Wilder and Hindersinn) is approximately a factor of 20, from 1.55 to 29.5. For the case of present interest α is approximately 4. It is, thus, in the range of the Wilder and Hindersinn data, whereas the free-jet data are for $\alpha \leq 1$.

The preponderance of data for conditions closest to those of present interest, even though these data are almost entirely from one investigation, suggest that the eddy viscosity coefficient, K, for mixing of two supersonic streams is best represented by

$$K = 0.0009 \, \alpha^{0.9} \tag{4-56}$$

Therefore, this is the formula employed in the analysis.

4.6 Computer Solution of Equations

The equations previously developed were programmed for computer integration in the streamwise direction to obtain the development of the flow field. It is noted that in the near field the knowledge of one local characteristic of the flow field, e.g., b, will permit the calculation of the remaining ones, e.g., r_i and r_d, through equations (4-33) and (4-31). Similarly, in the far field, if one knows, for example, U_c, the same two equations permit the computation of b and r_d. Thus, it is only necessary to obtain the variation of one characteristic with axial position to obtain all. This variation is obtained by integrating equation (4-42) in an appropriate form.

4.6.1 Near field calculations.- In the near field, $U_c = 1$ and $dU_c/dz = 0$. Thus, equation (4-42) may be written as

$$\frac{db}{dz} = \left(\frac{r_d \epsilon_d}{T_d}\right) \left.\frac{\partial U}{\partial \eta}\right|_{\eta=\eta_d} \bigg/ \left\{ \frac{br_d U_d^2}{T_d}\frac{d\eta_d}{db} + r_i\frac{dr_i}{db} + \int_0^{\eta_d} \frac{U^2}{T}\left[b\left(2\eta + \frac{dr_i}{db}\right) + r_i\right]d\eta \right\} \tag{4-57}$$

The derivatives, dr_i/db and $d\eta_d/db$ are obtained by differentiating equations (4-33) and (4-31), respectively, with respect to b .

$$\frac{dr_i}{db} = -\left[2b\int_0^1 \frac{U}{T}(U - U_\infty)\eta \, d\eta + r_i \int_0^1 \frac{U}{T}(U - U_\infty)d\eta\right]\bigg/\left[b\int_0^1 \frac{U}{T}(U - U_\infty)d\eta\right.$$

$$\left. + r_i(1 - U_\infty)\right] \tag{4-58}$$

$$\frac{d\eta_d}{db} = -\left\{\int_0^{\eta_d} \frac{U}{T}\left[b\left(2\eta + \frac{dr_i}{db}\right) + r_i\right]d\eta + r_i\frac{dr_i}{db}\right\}\bigg/\left(\frac{r_d b U_d}{T_d}\right) \tag{4-59}$$

The value of η_d is determined at each station by iteration of equation (4-31) with the values of b and r_i already computed.

40

The integration of equation (4-57) was carried out by assuming a step size Δz and determining

$$b(z + \Delta z) = b(z) + \Delta z \frac{db}{dz} \qquad (4\text{-}60)$$

The initial conditions are $b(0) = 0$, $r_i(0) = r_d(0) = 1$. We then determine r_i by

$$r_i(z + \Delta z) = r_i(z) + \Delta z \frac{db}{dz} \frac{dr_i}{db} \qquad (4\text{-}61)$$

This value of r_i was compared to that determined from equation (4-33) for $b(z + \Delta z)$. If the two values did not agree within an allowable tolerance (e.g., 0.1 percent), Δz was halved and the computations repeated until the tolerance was met. The calculation of η_d was then performed by iteration of equation (4-31). New derivatives, dr_i/db, $d\eta_d/db$ and db/dz are then computed and the cycle continued until the position $r_i = 0$ is found. This is the end of the potential core.

4.6.2 <u>Far field calculations</u>.- In the far field $r_i = dr_i/dz = 0$ and U_c is used as the primary dependent variable in the integration of equation (4-42). In a procedure identical to that for the near field the derivatives db/dU_c and $d\eta_d/dU_c$ are found from equations (4-33) and (4-31).

$$\frac{db}{dU_c} = - \int_0^1 \frac{\partial}{\partial U_c} \left[\frac{U}{T} (U - U_\infty) \right] \Big|_{\eta_1} \eta \, d\eta \bigg/ 2b \int_0^1 \frac{U}{T} (U - U_\infty) \eta \, d\eta \qquad (4\text{-}62)$$

$$\frac{d\eta_d}{dU_c} = - \left[2b \frac{db}{dU_c} \int_0^{\eta_d} \frac{U^2}{T} \eta \, d + b^2 \int_0^{\eta_d} \frac{\partial (U/T)}{\partial U_c} \Big|_{\eta_1} \eta \, d\eta \right] \bigg/ \left(\frac{b^2 U_d \eta_d}{T_d} \right) \qquad (4\text{-}63)$$

$$\frac{dU_c}{dz} = \frac{\eta_d}{T_d} \epsilon_d \frac{\partial U}{\partial \eta_1} \Big|_{\eta = \eta_d} \bigg/ \left\{ \frac{U_d^2}{T_d} r_d \frac{d\eta_d}{dU_c} + 2 \frac{db}{dz} \int_0^{\eta_d} \frac{U^2}{T} \eta \, d\eta + b \int_0^{\eta_d} \frac{\partial (U^2/T)}{\partial U_c} \Big|_{\eta_1} \eta \, d\eta \right\}$$

$$(4\text{-}64)$$

Equation (4-64) was used to evaluate ΔU_c at a selected Δz as was done with b in the near field. The initial condition $U_c(\ell_p) = 1$ is used with the remaining values coming from the near field computations.

41

A tolerance was set on b determined from Δz, equations (4-64) and (4-62) and from equation (4-33) as was done for r_i in the near field. Upon satisfaction of the tolerance, other values were calculated at the new position.

The new value of η_d is again computed from equation (4-31) for U_c and b at the new station.

In the calculative procedure the energy equation is never required. It is, however, important that the assumed velocity-temperature relation satisfies this equation. This is checked at each step (Δz) of the calculation in both the near and the far fields. Equation (4-34) is put in the form

$$E_m = E_z$$

or

$$b^2 \int_0^1 \frac{U}{T} T_o \eta \, d\eta + br_i \int_0^1 \frac{U}{T} T_o d\eta = \frac{1}{2} (1 - T_{o_\infty})(1 - r_i^2)$$

$$+ T_{o_\infty}\left[b^2 \int_0^1 \frac{U}{T} \eta \, d\eta + br_i \int_0^1 \frac{U}{T} d\eta \right] \quad (4-65)$$

Both the left and the right-hand members are calculated and printed out for comparison at each step of the calculation. It is seen that the left-hand side is related to the energy within the mixing region at a given axial station, E_m, and the right-hand side is the energy which has entered the mixing region up to that station, E_z. The two were found to agree within 3 percent or better at any point along the axis. This percentage was accepted as a sufficiently accurate balance of the energy equation by using the assumed velocity profile and temperature-velocity relation.

4.7 Concentration of Exhaust Gases

In the development of the governing equations it has been assumed that differences in the molecular weights and specific heats of the undiluted exhaust gas and air are negligible. Such differences as may exist affect the turbulent mixing process primarily because of their effect on

42

the density distribution in the constant pressure mixing region. We can show that

$$\rho = \frac{W}{T} \tag{4-66}$$

where

$$W = W*/W_j^*$$

W^* = Molecular weight of mixture at any point

W_j^* = Molecular weight of undiluted exhaust gas
(at jet exit)

In general, W will vary through the mixing region if the molecular weight of the undiluted exhaust gas and external stream differ. The local molecular weight may be expressed in terms of that of the jet, W_j^* and the free stream, W_∞^* and of the concentrations of the gases present. If we assume that there are effectively only two gases, the jet and the free-stream gases, we may represent the mass fraction of the jet gas present at any point by c. The quantity W at that point is then

$$W = c + (1 - c)W_\infty \tag{4-67}$$

where

$$W_\infty = W_\infty^*/W_j^*$$

W_∞^* = Molecular weight of the free-stream gas

Specie differences also affect the distribution of energy in the mixing region due to associated differences in the specific heats of the species. Thus the enthalpy ratios in equation (4-18) cannot be simply replaced by corresponding temperature ratios, but must incorporate the associated specific heat ratios also. Thus

$$H = c_p T_o$$

where

$$c_p = c_p^*/c_{p_j}^*$$

In exactly the same manner as for the molecular weight, the specific heat may be expressed in terms of the local concentration and the specific heats of the jet and free stream.

$$c_p = c + (1 - c)c_{p_\infty} \tag{4-68}$$

where

$$c_{p_\infty} = c_{p_\infty}^* / c_{p_j}^* = \text{ratio of } c_p^*\text{'s of the free stream and the undiluted exhaust gas.}$$

Consider now the differential equation for the concentration distribution. In a manner similar to that used for the temperature, we may associate the concentration and velocity distributions by the similarity of their governing equations. The differential equation governing momentum transport in a constant pressure, turbulent axisymmetric flow is:

Momentum

$$\rho U \frac{\partial U}{\partial z} + \rho V \frac{\partial U}{\partial r} = \frac{1}{r} \frac{\partial}{\partial r} \left(r \rho \epsilon_u \frac{\partial U}{\partial r} \right) \tag{4-69}$$

The conservation of matter leads to the following equation for the concentration

Species

$$\rho U \frac{\partial c}{\partial z} + \rho V \frac{\partial c}{\partial r} = \frac{1}{r} \frac{\partial}{\partial r} \left(r \rho \epsilon_m \frac{\partial c}{\partial r} \right) + \dot{w} \tag{4-70}$$

where

      $\dot{w}$ = the generation rate of the species associated with c by chemical means

      ϵ_m = the coefficient of turbulent diffusion for the species involved = $\epsilon_m^* / r_n^* U_j^*$

      ϵ_u = the coefficient of turbulent momentum diffusion (eddy viscosity coefficient) = $\epsilon_u^* / r_n^* U_j^*$

We observe that these two equations for U and c are of identical form if $\dot{w} = 0$. Hence, we may assume that

$$c = c(U)$$

44

and obtain from the above equations with $\dot{w} = 0$

$$\left(\rho U \frac{\partial U}{\partial z} + \rho V \frac{\partial U}{\partial r} \right) \frac{dc}{dU} = \frac{1}{r} \left[\frac{\partial}{\partial r} \left(r \rho \epsilon_m \frac{\partial U}{\partial r} \right) \frac{dc}{dU} + r \rho \epsilon_m \left(\frac{\partial U}{\partial r} \right)^2 \frac{d^2 c}{dU^2} \right] \tag{4-71}$$

Defining the Schmidt number as

$$S_c = \frac{\epsilon_m}{\epsilon_u}$$

and multiplying the momentum equation by dc/dU we may obtain

$$\frac{\partial}{\partial r} \left[r \rho \epsilon_u (S_c - 1) \frac{\partial U}{\partial r} \right] \frac{dc}{dU} + r \rho \epsilon_u S_c \left(\frac{\partial U}{\partial r} \right)^2 \frac{d^2 c}{dU^2} = 0 \tag{4-72}$$

If the Schmidt number is unity, i.e., $\epsilon_u = \epsilon_m$, we find simply that

$$c = A_c + B_c U \tag{4-73}$$

Hinze and van der Hegge Zijnen (ref. 4-20) investigated experimentally the spread of tracer gas introduced into the nozzle fluid of subsonic turbulent jets. The turbulent Schmidt number was found to vary slightly across these jets and to have an average value of about 1.36 across the jet. Such differences compared to the assumption of S_c = const. = 1 should be of little consequence in the present analysis due to its integral nature and due to the small difference between the actual Schmidt number and unity.

Using the boundary conditions

$$c = 1 \quad \text{when} \quad U = 1$$

$$c = 0 \quad \text{when} \quad U = U_\infty$$

the coefficients A_c and B_c may be evaluated to yield

$$c = \frac{U - U_\infty}{1 - U_\infty} \tag{4-74}$$

45

Introducing the similarity velocity profile

$$\bar{U} = \frac{U - U_\infty}{U_c - U_\infty} = (1 - \eta^{3/2})^2 \tag{4-75}$$

where

$U_c = U_c(z)$ the jet centerline velocity

$\eta = (r - r_i)/b$

we obtain

$$c = \frac{U_c - U_\infty}{1 - U_\infty} \bar{U} \tag{4-76}$$

or

$$c = \frac{U_c - U_\infty}{1 - U_\infty} (1 - \eta^{3/2})^2 \tag{4-77}$$

The mixing calculations provide $U_c(z)$, $r_i(z)$ and $b(z)$ such that the entire concentration distribution, $c(r,z)$, may be determined. Calculations for the present situation have been carried out under the assumption that $c_{p\infty} = W_\infty = 1$, that is, neglecting differences between specific heat at constant pressure and molecular weight between the free stream and the jet.

TABLE 4-I.- SUMMARY OF DATA FOR THE EDDY VISCOSITY COEFFICIENT K.

Source	M_j	M_∞	U_∞	T_{O_∞}	T_∞	$K = \dfrac{\epsilon^*}{b^*\left|U_c^* - U_\infty^*\right|}$	$\alpha = \rho_\infty T_{O_\infty} \lambda$
Corrsin & Uberoi (ref. 4-10)	= 0.08 = 0.08	0 0	0 0	0.650 0.950	0.650 0.950	0.00913 0.00945	1.000 1.000
Liepmann & Laufer (ref. 4-14)	= 0	0	0	1.000	1.000	0.00775	1.000
Albertson et al. (ref. 4-15)	= 0	0	0	1.000	1.000	0.00715	1.000
Pabst (ref. 4-16)	0.85	0	0	0.429	0.490	0.00836	0.875
Maydew & Reed (ref. 4-7)	0.70 0.85 0.95 1.49 1.96	0 0 0 0 0	0 0 0 0 0	1.000 1.000 1.000 1.000 1.000	1.098 1.145 1.181 1.444 1.769	0.01160 0.01140 0.01120 0.00775 0.00605	0.910 0.873 0.847 0.692 0.565
Warren (ref. 4-11)	0.69 0.69 0.97 0.97 1.51 2.60	0 0 0 0 0 0	0 0 0 0 0 0	1.000 0.700 1.000 0.700 1.000 1.000	1.095 0.766 1.188 0.892 1.452 2.345	0.00885 0.00898 0.00766 0.00788 0.00693 0.00455	0.913 0.913 0.841 0.841 0.689 0.427
Baker & Weinstein (ref. 4-17)	= 0 = 0 = 0 = 0	0 0 0 0	0.667 0.429 0.250 0.111	1.000 1.000 1.000 1.000	1.000 1.000 1.000 1.000	0.01100 0.01270 0.00964 0.00790	5.000 2.500 1.670 1.250
Eggers & Torrence (ref. 4-13)	0.942 0.813 0.470	1.302 1.268 0.580	1.360 1.540 1.210	1.000 1.000 1.000	0.881 0.857 0.980	0.01320 0.00500 0.01860	7.470 5.470 10.800

TABLE 4-I. – CONCLUDED.

Source	M_j	M_∞	U_∞	T_{o_∞}	T_∞	$K = \dfrac{\epsilon^*}{b^* \left| U_c^* - U_\infty^* \right|}$	$\alpha = \rho_\infty T_{o_\infty} \lambda$
Wilder & Hindersinn (ref. 4-1)	†0.94	1.39	1.058	0.616	0.527	0.0160	42.6
	1.58	1.60	0.9036	0.803	1.256	0.0134	20.6
	2.03	1.29	0.526	0.500	1.461	0.00156	2.36
	2.78	1.36	0.523	0.616	0.874	0.00133	1.72
	1.23	1.38	0.855	0.616	1.722	0.00824	13.65
	1.49	1.58	0.932	0.803	1.295	0.01965	29.6
	1.59	1.60	0.709	0.500	2.014	0.00352	5.91
	1.78	1.59	0.929	0.803	1.237	0.0204	27.1
	1.80	1.60	0.729	0.616	1.487	0.00400	5.84
	1.46	1.27	0.710	0.616	1.501	0.00419	5.54
	2.05	1.57	0.666	0.616	1.322	0.00332	4.08
	2.07	1.57	0.759	0.803	0.9986	0.00529	5.85
	1.77	1.27	0.626	0.616	1.314	0.00306	3.52
	2.43	1.59	0.616	0.616	1.128	0.00260	2.93
	2.45	1.58	0.699	0.803	0.8512	0.00372	3.87
	2.02	1.28	0.666	0.803	0.9052	0.00341	3.64
	2.42	1.50	0.534	0.500	1.347	0.00150	2.28
	2.20	1.25	0.625	0.803	0.827	0.00252	2.88
	2.76	1.38	0.479	0.500	1.0896	0.00111	1.55
	†1.39	0.94	0.945	1.625	1.90	0.0160	29.4

†The jet and main stream quantities were reversed for this point.
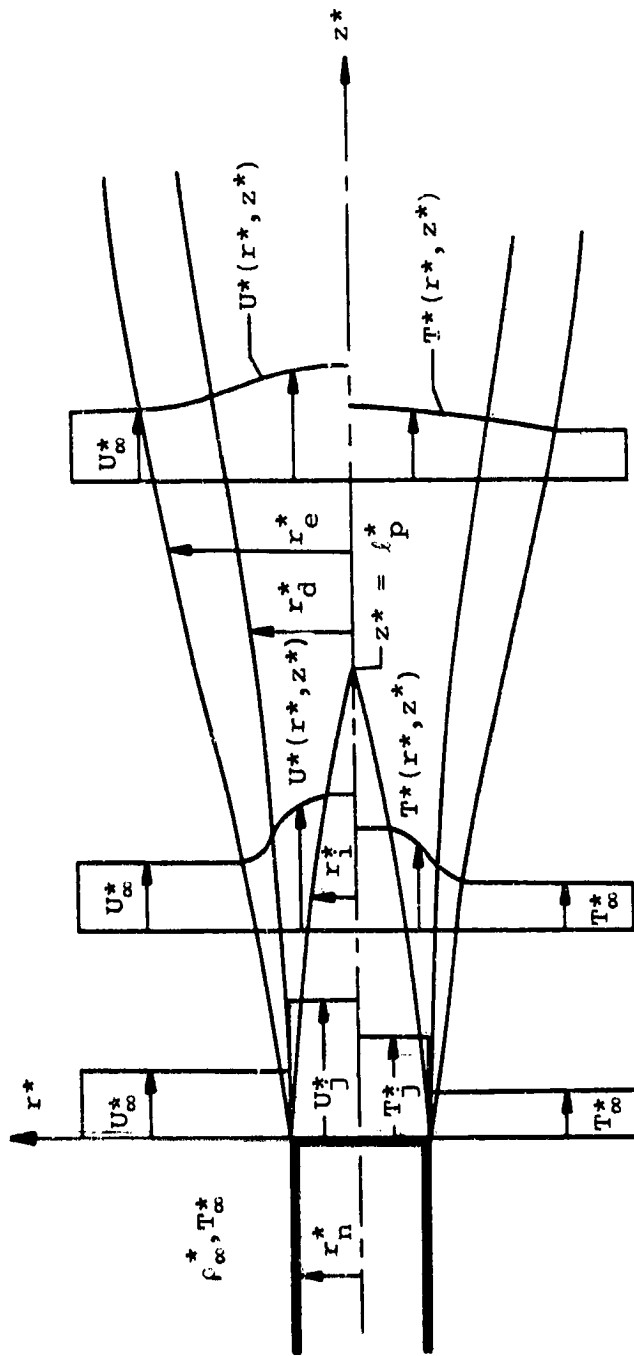
Figure 4-1.— Jet mixing configuration.

49

$$\alpha = \frac{1 + \frac{\gamma - 1}{2} M_\infty^2}{1 + \frac{\gamma - 1}{2} M_j^2} \times \frac{1 + U_\infty}{1 - U_\infty}$$

Figure 4-2.– Correlation of eddy viscosity coefficient K.

50

APPENDIX 4A

EXTRACTION OF K FROM VARIOUS DATA SOURCES

In the following the methods are shown by which the eddy viscosity
coefficient, K, defined by equation (4-48) was obtained from the published
data of various investigators: Warren, (ref. 4-11), Corrsin and Uberoi,
(ref. 4-10), and Pabst (4-16):

Warren investigated the flow field of compressible axisymmetric jets
exhausting into still air. In his investigation Warren defines the eddy
viscosity (in present notation) as

$$\epsilon^* = K_w(r^*_{1/2} - r^*_i) \frac{U^*_j}{2}$$ (4A-1)

where

$r^*_{1/2}$ = the radius at which the velocity is one-half the
centerline (jet) velocity

We may equate equation (4A-1) with the present definition, equa-
tion (4-43) since ϵ^* must be the same for both. Since $U^*_\infty = 0$ in
Warren's study, we see that

$$K = \frac{1}{2} K_w \frac{r^*_{1/2} - r^*_i}{b^*} = \frac{1}{2} K_w \eta_{1/2}$$ (4A-2)

The ratio $(r^*_{1/2} - r^*_i)/b^* = \eta_{1/2}$ and is found from the assumed
similarity velocity profile, equation (4-25), to be

$$\eta_{1/2} = 0.44$$ (4A-3)

Warren has determined values of K_w based on the definition given
in equation (4A-1) for his measurements as well as those of Corrsin and
Uberoi and of Pabst. Equations (4A-2) and (4A-3) were used to calculate
the K's presented here from those appearing in Warren's report.

Warren determined his value of K_w by obtaining the best match of
his analytically selected velocity decay rates to those measured by him.
In order to correct for differences in Warren's analysis and the present
one, we also calculated his measured potential core length for his

51

experimental conditions using the present analysis. Another value of K was obtained in this manner. It was found that the resultant K's were only slightly different from those given by Warren. The calculations are tabulated in Table 4A-I. Since these values were more directly comparable to the other data obtained, they were used in the correlation. The K's computed in this manner for the Corrsin and Uberoi data and for the Pabst data were identical to those computed using equation (4A-2).

Baker and Weinstein (ref. 4-17):

The study of low speed turbulent mixing of co-flowing dissimilar gases by Baker and Weinstein also included some measurements for air-air mixing. The definition of eddy viscosity used in this study was similar to that in the present analysis except the mixing zone width, $b_{0.05}^*$, was defined as the distance between points where $\overline{U} = 0.05$ and $\overline{U} = 0.95$. Thus,

$$K = K_{BW} b_{0.05}^* / b^*$$

$$= K_{BW} \Delta \eta_{0.05}$$

From

$$\eta = (1 - \overline{U}^{/2})^{2/3}$$

$$\Delta \eta_{0.05} = \left[1 - (0.05)^{1/2}\right]^{2/3} - \left[1 - (0.95)^{1/2}\right]^{2/3}$$

$$= 0.844 - 0.086$$

$$= 0.758$$

Thus

$$K = 0.758 \, K_{BW}$$

Maydew and Reed (ref. 4-7):

Maydew and Reed measured velocity profiles and mixing region growth in the initial (potential core) region of sub and supersonic jets issuing into still air. They compared analytical solutions for the jet velocity profiles given by Tollmien (ref. 4-18), Görtler (ref. 4-19), and Crane (ref. 4-6). These solutions are based on a similarity variable

$$\xi = \sigma y / z$$

where

y is the distance from the point where $\bar{U} = 1/2$

σ is the similarity parameter for the velocity profile chosen to indicate the spreading rate of the mixing region.

The spreading rate measured by Maydew and Reed is the spread of the two points in the velocity profile, where $U^2 = 0.9$ and $U^2 = 0.1$, and is denoted as $b_{0.1}$.

$$\frac{db}{dz} = \Delta\xi_{0.1}\,\frac{1}{\sigma}$$

$$= \Delta\eta_{0.1}\,\frac{db}{dz}$$

where

$$\Delta\xi_{0.1} = \xi_{U^2=0.9} - \xi_{U^2=0.1}$$

$$\Delta\eta_{0.1} = \eta_{U^2=0.9} - \eta_{U^2=0.1}$$

The coefficient K is related to σ and $b_{0.1}$ in the present case by

$$K = \frac{1}{2\sigma^2\,(db/dz)} = \frac{(db_{0.1}/dz)^2}{2\,(\Delta\xi_{0.1})\,(db/dz)}$$

$$K = \frac{\Delta\eta_{0.1}}{2\,(\Delta\xi_{0.1})^2}\,\frac{db}{dz} \tag{4A-4}$$

For the Crane velocity profile used by Maydew and Reed

$$\Delta\xi_{0.1} = 1.3$$

For the present velocity profile

$$\Delta\eta_{0.1} = 0.333$$

Thus, equation (4A-4) becomes

53

$$K = 0.0905 (db_{0.1}/dz) \tag{4A-5}$$

which was used to obtain K from these data.

Eggers and Torrence (ref. 4-13):

This study is concerned with the mixing of an axisymmetric jet with a co-flowing stream. The jet Mach number ranges from 0.47 to 0.94 and the free-stream Mach number ranges from 0.58 to 1.3. Both streams are air and have the same stagnation temperature.

The eddy viscosity definition used in this investigation was not based on the velocity difference between the streams but only on the jet velocity. Thus,

$$\epsilon^* = K_E b^*_{0.95} U^*_c \tag{4A-6}$$

where

$$b_{0.95} = r^*(\overline{U} = 0.5) - r^*(\overline{U} = 0.95) \tag{4A-7}$$

Comparing equations (4A-6) and (4A-7) with equations (4-49) and (4-46) respectively, it is found that

$$K = K_E \left[b^*_{0.95} U_c / b^* (U_c - U_\infty) \right]$$

and

$$b^*_{0.95}/b^* = 0.355$$

Thus,

$$K = 0.355 \, K_E U_c / (U_c - U_\infty) \tag{4A-8}$$

Equation (4A-8) was used to calculate K from the K_E of Eggers and Torrence.

Wilder and Hindersinn (ref. 4-1):

In this investigation the turbulent mixing of two-dimensional compressible air streams was comprehensively investigated. Stagnation temperature ratios, T_{O_∞}, of 0.5, 0.616 and 0.803 were studied within the

54

Mach number ranges $0.94 \leq M_j \leq 2.8$ and $1.25 \leq M_\infty \leq 1.6$. Stagnation temperature profiles were obtained for a total of 19 conditions within these ranges of Mach number and stagnation temperature ratio. The eddy viscosity was evaluated for each of these conditions based on an error function velocity profile. The Crocco relation, equation (4-20), was assumed to hold between the stagnation temperature and the velocity fields. Therefore, the error function profile was also assumed to represent the stagnation temperature profile, Thus, it was assumed that

$$\beta = \frac{1}{2} (1 + \phi(\zeta)) \tag{4A-9}$$

where

$$\phi(\zeta) = \frac{2}{\sqrt{\pi}} \int_0^\zeta e^{-t^2} \tag{4A-10}$$

$$\zeta = (r^*_{0.5} - r^*) / \sqrt{(2\epsilon_0 / U^*_\infty L)} \; \overline{z^*} \tag{4A-11}$$

$$\beta = (T^*_O - T^*_{O_\infty}) / (T^*_{O_j} - T^*_{O_\infty}) = (T_O - T_{O_\infty}) / (1 - T_{O_\infty}) \tag{4A-12}$$

$$r^*_{0.5} = \text{the radius at which } \beta = 0.5 \tag{4A-13}$$

$$\overline{z} = z + a \tag{4A-14}$$

a = a displacement of the origin to account for heat transfer between the streams prior to the jet nozzle exit.

The eddy viscosity was formulated simply as

$$\epsilon^* = \epsilon_0 \frac{\overline{z}}{L} \tag{4A-15}$$

After "a" was selected to provide axial similarity for the profiles, values of (ϵ_0/L) were determined for 19 conditions by seeking the best fit of the data to equation (4A-9). The selection of "a" appeared to be somewhat arbitrary so it was decided to eliminate $\overline{z}$ in computing K from (ϵ_0/L). The following is the calculation procedure which appeared most satisfactory although three others were used and generally yielded results within 10 to 15 percent of these.

By comparing equations (4A-15) and (4-48), it is seen that

$$K = \frac{\epsilon_o}{U_\infty^* L} \frac{\overline{z}}{b} \frac{U_\infty}{|1 - U_\infty|} \tag{4A-16}$$

We also note that matching the slope of β at its maximum (i.e., at $\beta = 0.5$, $\zeta = 0$) we obtain a good match of the β profile with the theory. It may be shown from equations (4A-9) and (4A-10) that

$$\frac{d\beta}{d\zeta}\bigg|_{\beta=0.5} = \frac{1}{\sqrt{\pi}} \tag{4A-17}$$

From equations (4A-11) and (4-27) it is seen that

$$\zeta = \frac{1}{\sqrt{\dfrac{2\epsilon_o}{U_\infty^* L}}} \frac{b}{z} (\eta_{0.5} - \eta) \tag{4A-18}$$

where $\eta_{0.5} = \eta$ at $\beta = 0.5$, from which we obtain

$$\frac{d\beta}{d\zeta} = -\sqrt{\frac{2\epsilon_o}{U_\infty^* L}} \frac{\overline{z}}{b} \frac{d\beta}{d\eta} \tag{4A-19}$$

Using (4A-17) and (4A-19) it may be shown that

$$\frac{b}{z} = \sqrt{\frac{2\pi\epsilon_o}{U_\infty^* L}} \left(- \frac{d\beta}{d\eta}\bigg|_{\eta_{0.5}}\right) \tag{4A-20}$$

Equations (4A-16) and (4A-20) are now combined to yield

$$K = \frac{U_\infty}{|1 - U_\infty|} \sqrt{\frac{\epsilon_o}{2\pi U_\infty^* L}} \bigg/ \left(- \frac{d\beta}{d\eta}\bigg|_{\eta_{0.5}}\right) \tag{4A-21}$$

After evaluating $(d\beta/d\eta_{\eta_{0.5}})$ we may use the data from Wilder and Hindersinn directly in equation (4A-21) to determine K. We now proceed to evaluate $(d\beta/d\eta)$ using the relation

$$\frac{d\beta}{d\eta} = \frac{d\beta}{d\overline{U}} \frac{d\overline{U}}{d\eta}$$

From equation (4-23) for $U_c = 1$ (all data are for near field conditions).

$$\beta = \left[1 - D\ C_j^2\ \frac{(1 - U_\infty)^2}{1 - T_{O_\infty}} \right] \overline{U} + D\ C_j^2\ \frac{(1 - U_\infty)}{1 - T_{O_\infty}}\ \overline{U}^2 \qquad (4A-22)$$

where

$$C_j^2 = (U_j^{*2}/2)/H_j^* = \frac{\gamma - 1}{2}\ M_j^2 \bigg/ \left(1 + \frac{\gamma - 1}{2}\ M_j^2 \right)$$

$$D = \begin{cases} 0 & \text{for Crocco relation} \\ 1 & \text{for modified Crocco relation} \end{cases}$$

From

$$\frac{d\beta}{d\overline{U}} = 1 + D\ C_j^2\ \frac{(1 - U_\infty)^2}{1 - T_{O_\infty}}\ (2\overline{U} - 1) \qquad (4A-23)$$

From equation (4-25)

$$\overline{U} = (1 - \eta^{3/2})^2 \qquad (4A-25)$$

we observe that

$$\frac{d\overline{U}}{d\eta} = -3\ (1 - \eta^{3/2})^{1/2}$$

or, using equation (4A-25)

$$\frac{d\overline{U}}{d\eta} = -3\ \overline{U}^{1/2}(1 - \overline{U}^{1/2})^{1/3} \qquad (4A-25)$$

Thus, combining equations (4A-24) and (4A-25)

$$\frac{d\beta}{d\eta} = -3\ \overline{U}^{1/2}(1 - \overline{U}^{1/2})^{1/3} \left[1 + D\ C_j^2\ \frac{(1 - U_\infty)^2}{1 - T_{O_\infty}}\ (2\overline{U} - 1) \right] \qquad (4A-26)$$

We see that for the Crocco relation $\beta = \overline{U}$ and $(d\beta/d\eta) = (d\overline{U}/d\eta)$

$$\left.\frac{d\beta}{d\eta}\right|_{\eta_{0.5}} = \left.\frac{d\overline{U}}{d\eta}\right|_{\eta_{0.5}} = -3(0.5)^{1/2}(1 - 0.5^{1/2})^{1/3} \qquad (4A-27)$$

$$\left.\frac{d\beta}{d\eta}\right|_{\eta_{0.5}} = -1.41 \qquad \text{for Crocco relation}$$

For the modified Crocco relation, equation (4A-22) may be solved for $\overline{U}_{0.5}$ with $D = 1$.

$$\overline{U}_{0.5} = \frac{1}{2}\left[1 - \frac{1 - T_{O_{\infty}}}{C_j^2(1 - U_{\infty})^2} + \sqrt{1 + \left(\frac{1 - T_{O_{\infty}}}{C_j^2(1 - U_{\infty})^2}\right)^2}\right] \qquad (4A-28)$$

Solution of equation (4A-28) for the particular values of M_j, $T_{O_{\infty}}$, and U_j and substitution into equation (4A-26) yield $(d\beta/d\eta_{\eta_{0.5}})$ to be used in computing K from equation (4A-21). The basic data and tabulated computations are shown in Table 4A-II.

A tabulation of all final data appearing in figure 2 may be found in Table 4A-I and Table 4A-II.

TABLE 4A-I.- CALCULATION OF K FROM

WARREN'S POTENTIAL CORE DATA.

M_j	T_{o_∞}	Experiment ℓ_p	Computed $K\ell_p$ (Present Analysis)	K	$0.22 \, K_w$
0.69	1.0	10.2	0.0904	0.00885	0.00848
0.69	0.7	9.4	0.0844	0.00898	0.00850
0.97	1.0	12.0	0.0921	0.00766	0.00791
0.97	0.7	10.7	0.0843	0.00788	0.00814
1.51	1.0	14.1	0.0977	0.00693	0.00780
2.60	1.0	25.0	0.1136	0.00455	0.00550

TABLE 4A-II.— COMPUTATION OF K FROM WILDER AND HINDERSINN'S DATA.

M_j	M_∞	T_{o_∞}	U_∞	$T_\infty = \frac{1}{\rho_\infty}$	$U_\infty^{*\dagger}$ Ft/Sec	ϵ_o/L Ft/Sec	$\frac{\epsilon_o}{U_\infty^* L} \times 10^6$	$-\frac{\partial B}{\partial \eta}\ \eta_{o.5}$	$*K$
0.94	1.39	0.616	1.05805	1.9533	1320	0.0127	9.6	1.41	0.01600
1.39	0.94	1.625	0.945	0.511			10.15	1.41	0.0155**
1.58	1.60	0.803	0.9036	1.2560	1452	0.037	25.4	1.41	0.0134
2.03	1.29	0.50	0.5257	1.4612	1251	0.047	37.6	1.445	0.00156
2.78	1.36	0.616	0.5234	0.8736	1300	0.027	20.8	1.502	0.00133
1.23	1.38	0.616	0.855	1.7219	1315	0.032	24.3	1.41	0.00824
1.49	1.58	0.803	0.932	1.2945	1442	0.037	25.6	1.41	0.01965
1.59	1.60	0.50	0.709	2.0144	1455	0.038	26.1	1.41	0.00352
1.78	1.59	0.803	0.929	1.2374	1450	0.044	30.35	1.41	0.0204
1.80	1.60	0.616	0.729	1.4868	1455	0.042	28.9	1.41	0.00400
1.46	1.27	0.616	0.710	1.5010	1239	0.045	36.3	1.41	0.00419
2.05	1.57	0.616	0.666	1.3223	1438	0.C50	34.8	1.42	0.00332
2.07	1.57	0.803	0.759	0.99856	1438	0.051	35.5	1.42	0.00529
1.77	1.27	0.616	0.626	1.3137	1239	0.052	42.0	1.42	0.00306
2.43	1.59	0.616	0.616	1.1283	1450	0.050	34.5	1.445	0.00260
2.45	1.58	0.803	0.699	0.85119	1442	0.048	33.3	1.435	0.00372
2.02	1.28	0.803	0.666	0.90525	1246	0.047	37.7	1.435	0.00341
2.42	1.50	0.500	0.534	1.3473	1392	0.046	33.1	1.453	0.00150
2.20	1.25	0.803	0.625	0.82706	1222	0.037	30.3	1.451	0.00252
2.76	1.38	0.500	0.479	1.0896	1315	0.027	20.5	1.490	0.00111

$\dagger T_{o_\infty}^* = 530°R \rightarrow U_\infty^* = 2500 \sqrt{\frac{\gamma-1}{2} M_\infty^2 \Big/ \left(1 + \frac{\gamma-1}{2} M_\infty\right)}$

$*K = \frac{U_\infty}{|1 - U_\infty|} \sqrt{\sqrt{\left(\frac{\epsilon_o}{2\pi U_\infty^2}\right)} \Big/ \left(\frac{\partial B_{o.5}}{\partial \eta}\right)^2}$

** Reciprocal quantities used such that $U_\infty < 1$.

5.0 INITIAL INTERACTION BETWEEN TRAILING VORTICES AND JETS

5.1 Description of Model

During the initial stage of the jet exhaust-trailing vortex interaction process, the hot gas jets retain their integrity and axisymmetric shape while the trailing vortex sheet wraps up into a pair of concentrated vortices. Because of aircraft angle of attack, the jets originally cant downward and tend to move away from the vortices in the crossflow plane. The component of free-stream velocity in the crossflow plane causes an upwash about the jets which, due to crossflow drag, turns the jets into the free-stream direction. The downwash on the jets caused by the trailing vortex sheet diminishes this effect somewhat.

In determining this initial interaction between the trailing vortices and the jet, it is assumed that the jet acts as a solid boundary expanding outward at a rate given by the characteristics of the turbulent jet alone and that the crossflow drag coefficient is uniform and given in accordance with the work of Wooler (ref. 5-1). It is also assumed that the jet remains axisymmetric about its curving centerline, that its other properties are the same as for no curvature, and that the jet boundary is the proper boundary to image the external vortex sheet. Both sides of the wing have been accounted for in the rolling-up calculation.

In order to illustrate the method, consider the two exhaust jets together with one pair of external vortices, as shown below.

$-K_o$ K_o

$r = r_e$

Vertical plane of symmetry

61
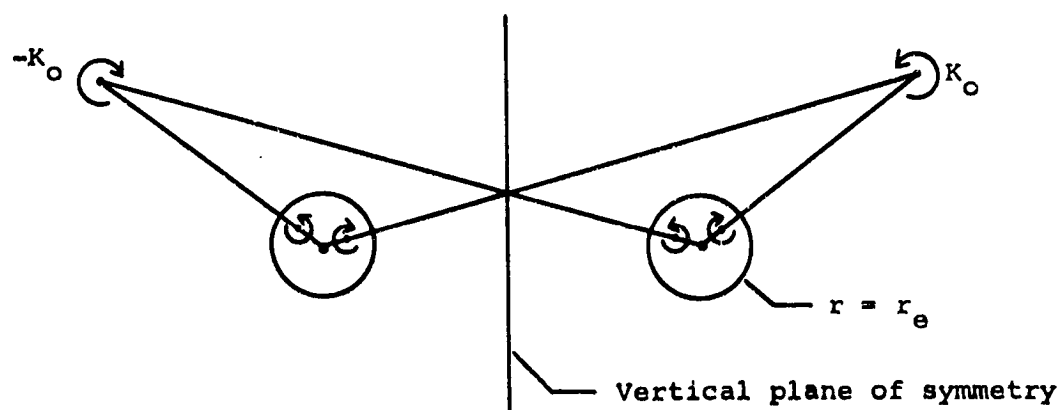
The image vortices inside each jet are included. We note that the sum of these internal image vortices is zero for each jet, so that the influence of the left jet on the right vortex and right jet can be neglected. However, the effect of the left vortex and its image in the right cylinder on the motion of the right vortex is of higher order and must be included. A total of 10 equal strength vortices on each wing panel, located to correspond to an elliptical loading at the trailing edge, have been taken to model the vortex sheet, which is constrained to have mirror symmetry. In addition to the pressure forces on the jet due to the vortices, and the crossflow drag force due to the initial downward cant of the jet, there will be a net buoyant force on the jet due to the temperature difference between the hot exhaust gases and the ambient air. The initial interaction of the jet and trailing vortices and subsequent motion is the result of all of these combined effects, and the governing differential equations for the trajectories are derived in the following section.

5.2 Differential Equations for Jet-Trailing Vortex Trajectories

The differential equations for the mutually interactive motion of the jet and trailing vortex sheet are derived by considering the momentum equations for a thin cross-sectional slice of the jet exhaust under the combined action of the pressure forces due to the vortex sheet, crossflow drag, and buoyancy. Consider the side and top views of the right-wing vortex centroid and jet as sketched below
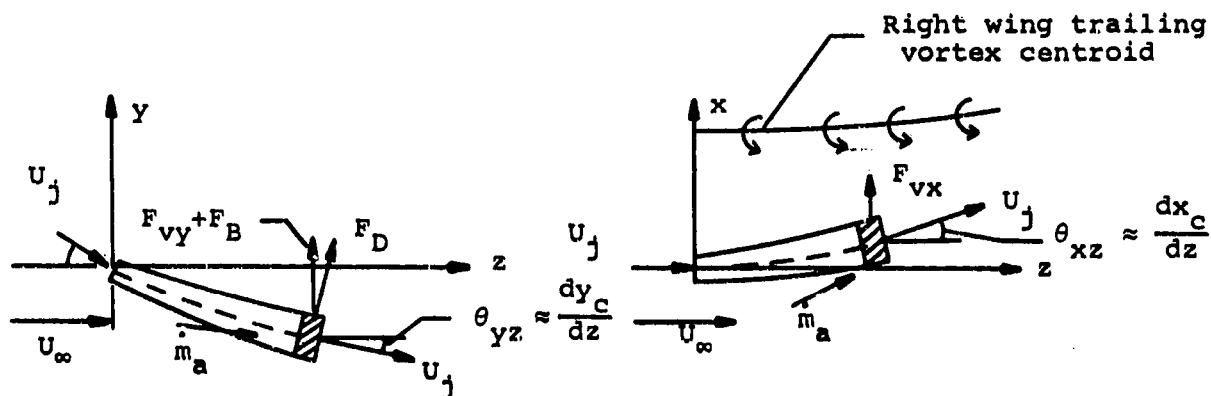
The jet is initially canted downward as viewed in the yz plane at the thrust axis inclination. As the jet proceeds downstream, it ingests free-stream air at a rate $\dot{m}_a$ given by the turbulent jet characteristics. This tends to align the jet with the free stream, as does the action of the crossflow drag force per unit length, F_D. The action of the net buoyant force F_B per unit length tends to cause the jet to rise vertically, while the influence of the trailing vortex sheet pressure forces (F_{vx}, F_{vy}) is primarily such as to cause the jet to move in and around the center of vorticity.

Thus, the nondimensional equations of motion of the thin slice of the jet are given by

$$\frac{d}{dz}\left(\dot{m}_t U_j \frac{dx_c}{dz}\right) = F_{vx} + F_{Dx} \tag{5-1}$$

$$\frac{d}{dz}\left(\dot{m}_t U_j \frac{dy_c}{dz}\right) = F_{vy} + F_{Dy} + F_B \tag{5-2}$$

5.2.1 Vortex forces.- The vortex forces per unit length (F_{vx}, F_{vy}) can be obtained by integrating the pressure in the crossflow plane, as given by the unsteady Bernoulli equation, around the boundary of the moving jet.

This unsteady surface pressure can be calculated as follows. Consider the crossflow plane view of the moving cylinder of exhaust gas and a typical pair of vortices centered with respect to the plane of symmetry of the aircraft.

63
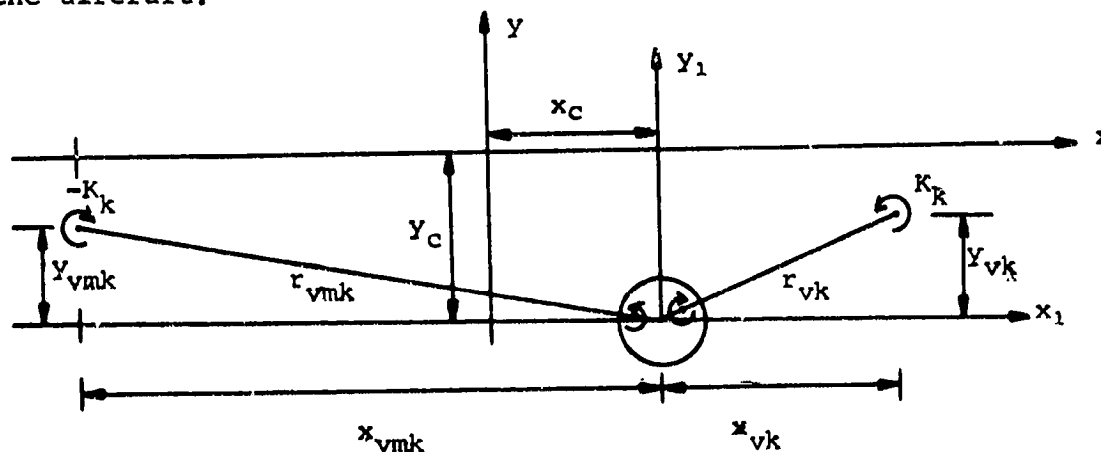
The complex velocity potential for this external vortex pair plus images with respect to the moving cylinder at (x_c, y_c) in cylinder coordinates $Z_1 = x_1 + iy_1$ is given by

$$W(Z_1) = - iK_k \ln \left[\frac{(Z_1 - Z_{vk}) \cdot (Z_1 + \frac{r_e^2}{Z_{vk} + 2x_c}) \cdot (Z_{vk} + 2x_c)}{(Z_1 - \frac{r_e^2}{\overline{Z}_{vk}}) \cdot (Z_1 + \overline{Z}_{vk} + 2x_c) \cdot \overline{Z}_{vk}} \right]$$

$$- \left[(\dot{x}_c - i\dot{y}_c)Z_1 + \frac{r_e^2 (\dot{x}_c + i\dot{y}_c)}{Z_1} \right] + r_e V_r \ln Z_1 \qquad (5\text{-}3)$$

where V_r is the radial velocity at the boundary of the jet as given by turbulent jet theory.

This is easily generalized to N vortex pairs by

$$W(Z_1) = - i \sum_{k=1}^{N} K_k \ln \left[\frac{(Z_1 - Z_{vk}) \cdot (Z_1 + \frac{r_e^2}{Z_{vk} + 2x_c}) \cdot (Z_{vk} + 2x_c)}{(Z_1 - \frac{r_e^2}{\overline{Z}_{vk}}) \cdot (Z_1 + \overline{Z}_{vk} + 2x_c) \cdot \overline{Z}_{vk}} \right]$$

$$- \left[(\dot{x}_c - i\dot{y}_c)Z_1 + \frac{r_e^2 (\dot{x}_c + i\dot{y}_c)}{Z_1} \right] + r_e V_r \ln Z_1 \qquad (5\text{-}4)$$

The pressure is determined from the unsteady Bernoulli equation, which is given in nondimensional form in the accelerating (x_1, Y_1) coordinate system by Lamb (ref. 5-2, p. 233) as

$$p = p_\infty - \rho_\infty \left[\frac{1}{2} (v^2 + w^2) + U_\infty \cdot \frac{d\phi}{dz} + U_\infty \cdot \left\{ x_1 \frac{d^2 x_c}{dz^2} + y_1 \frac{d^2 y_c}{dz^2} \right\} \right]$$

$$(5\text{-}5)$$

where time derivatives have been replaced by their equivalent longitudinal derivatives, i.e. $\partial/\partial t = U_\infty \, d/dz$ and ϕ, v, and w are determined from $W(Z_1)$ in the usual way, i.e.

$$\phi = R.P. \ W(Z_1) \tag{5-6}$$

and

$$\frac{dW}{dZ_1} = v - iw \tag{5-7}$$

Finally, the forces (F_{vx}, F_{vy}) on the cylinder due to the vortical flow field described by $W(Z_1)$ are determined by

$$F_{vx} + iF_{vy} = -\int_0^{2\pi} r_e p(r_e) e^{i\theta} \, d\theta \tag{5-8}$$

where $p(r_e)$ is the nondimensional pressure at the jet boundary $r = r_e$ as given by equation (5-5).

While the expression for the complex potential (5-4) is compact, the operations indicated by equations (5-5) through (5-8) are rather lengthy. The resulting expressions for (F_{vx}, F_{vy}) are given by

$$
F_{vx} = 2\pi r_e^2 \rho_\infty \left\{ \sum_{k=1}^N \frac{K_k}{r_{vk}^2} \times \left[\frac{K_k}{r_{vk}^2} \times \frac{x_{vk}}{1 - (\frac{r_e}{r_{vk}})^2} \right. \right.
$$

$$
\left. - U_\infty \left(\frac{dx_{vk}}{dz} + \frac{dx_c}{dz} \right) \left(\frac{2x_{vk}y_{vk}}{r_{vk}^2} \right) + U_\infty \left(\frac{dy_{vk}}{dz} + \frac{dy_c}{dz} \right) \left(\frac{x_{vk}^2 - y_{vk}^2}{r_{vk}^2} \right) \right]
$$

$$
+ \sum_{k=1}^N \frac{K_k}{r_{vmk}^2} \times \left[\frac{K_k}{r_{vmk}^2} \times \frac{x_{vmk}}{1 - (\frac{r_e}{r_{vmk}})^2} \right.
$$

65

$$- U_\infty \left(\frac{dx_{vk}}{dz} + \frac{dx_c}{dz}\right)\left(\frac{2x_{vmk}y_{vmk}}{r_{vmk}^2}\right) - U_\infty \left(\frac{dy_{vk}}{dz} + \frac{dy_c}{dz}\right)\left(\frac{x_{vmk}^2 - y_{vmk}^2}{r_{vmk}^2}\right)\Bigg]$$

$$+ R.P. \sum_{\substack{\text{all external} \\ \text{vortex} \\ \text{combinations}}} K_i K_j \left[\frac{\frac{1}{\overline{z}_{vi}^2}}{z_{vj} - \frac{r_e^2}{\overline{z}_{vi}}} + \frac{\frac{1}{\overline{z}_{vj}^2}}{z_{vi} - \frac{r_e^2}{\overline{z}_{vj}}}\right] - \frac{U_\infty^2}{2}\frac{d^2 x_c}{dz^2}\Bigg\}$$

$$(5\text{-}9)$$

$$F_{vy} = 2\pi r_e^2 \rho_\infty \Bigg\{ \sum_{k=1}^{N} \frac{K_k}{r_{vk}^2} \times \left[\frac{K_k}{r_{vk}^2} \times \frac{y_{vk}}{1 - (\frac{r_e}{r_{vk}})^2}\right.$$

$$+ U_\infty \left(\frac{dx_{vk}}{dz} + \frac{dx_c}{dz}\right)\left(\frac{x_{vk}^2 - y_{vk}^2}{r_{vk}^2}\right) + U_\infty \left(\frac{dy_{vk}}{dz} + \frac{dy_c}{dz}\right)\left(\frac{2x_{vk}y_{vk}}{r_{vk}^2}\right)\Bigg]$$

$$+ \sum_{k=1}^{N} \frac{K_k}{r_{vmk}^2} \times \left[\frac{K_k}{r_{vmk}^2} \times \frac{y_{vmk}}{1 - (\frac{r_e}{r_{vmk}})^2}\right.$$

$$+ U_\infty \left(\frac{dx_{vk}}{dz} + \frac{dx_c}{dz}\right)\left(\frac{x_{vmk}^2 - y_{vmk}^2}{r_{vmk}^2}\right) - U_\infty \left(\frac{dy_{vk}}{dz} + \frac{dy_c}{dz}\right)\left(\frac{2x_{vmk}y_{vmk}}{r_{vmk}^2}\right)\Bigg]$$

$$+ I.P. \sum_{\substack{\text{all external} \\ \text{vortex} \\ \text{combinations}}} K_i K_j \left[\frac{\frac{1}{\overline{z}_{vi}^2}}{z_{vj} - \frac{r_e^2}{\overline{z}_{vi}}} + \frac{\frac{1}{\overline{z}_{vj}^2}}{z_{vi} - \frac{r_e^2}{\overline{z}_{vj}}}\right] - \frac{U_\infty^2}{2}\frac{d^2 y_c}{dz^2}\Bigg\}$$

$$(5\text{-}10)$$

66

where the vortex motions are given by

$$U_\infty \left(\frac{dx_{vk}}{dz} + \frac{dx_c}{dz} \right) = \frac{K_k}{r_{vk}^2} \times \frac{y_{vk}}{1 - \left(\frac{r_e}{r_{vk}} \right)^2}$$

$$+ U_\infty \left(\frac{r_e}{r_{vk}} \right)^2 \times \left[\frac{dx_c}{dz} \times \left(\frac{x_{vk}^2 - y_{vk}^2}{r_{vk}^2} \right) + \frac{dy_c}{dz} \left(\frac{2x_{vk}y_{vk}}{r_{vk}^2} \right) \right]$$

$$+ V_r r_e \frac{x_{vk}}{r_{vk}^2} + I.P. \left\{ \sum_{\substack{j=1 \\ j \neq k}}^{N} K_j \left[\frac{1}{z_{vk} - z_{vj}} - \frac{1}{z_{vk} - \frac{r_e^2}{\overline{z}_{vj}}} \right] \right.$$

$$\left. - \sum_{j=1}^{N} K_j \left[\frac{1}{z_{vk} - z_{vmj}} - \frac{1}{z_{vk} - \frac{r_e^2}{\overline{z}_{vmj}}} \right] \right\} \qquad (5\text{-}11)$$

$$U_\infty \left(\frac{dy_{vk}}{dz} + \frac{dy_c}{dz} \right) = \frac{-K_k}{r_{vk}^2} \times \frac{x_{vk}}{1 - \left(\frac{r_e}{r_{vk}} \right)^2}$$

$$+ U_\infty \left(\frac{r_e}{r_{vk}} \right)^2 \times \left[\frac{dx_c}{dz} \times \left(\frac{2x_{vk}y_{vk}}{r_{vk}^2} \right) - \frac{dy_c}{dz} \left(\frac{x_{vk}^2 - y_{vk}^2}{r_{vk}^2} \right) \right]$$

$$+ V_r r_e \frac{x_{vk}}{r_{vk}^2} + R.P. \left\{ \sum_{\substack{j=1 \\ j \neq k}}^{N} K_j \left[\frac{1}{z_{vk} - z_{vj}} - \frac{1}{z_{vk} - \frac{r_e^2}{\overline{z}_{vj}}} \right] \right.$$

$$\left. - \sum_{j=1}^{N} K_j \left[\frac{1}{z_{vk} - z_{vmj}} - \frac{1}{z_{vk} - \frac{r_e^2}{\overline{z}_{vmj}}} \right] \right\} \qquad (5\text{-}12)$$

67

<u>5.2.2 Crossflow drag force</u>.- The nondimensional crossflow drag force per unit length of the jet is given by the relation

$$F_{Dx}\hat{e}_x + F_{Dy}\hat{e}_y = C_D \frac{1}{2} \rho_\infty \left|\vec{V}_1\right| \vec{V}_1 r_e \tag{5-13}$$

where C_D is the crossflow drag coefficient per unit length and is given from the work of Wooler (ref. 5-1) by $C_D = 1.8$, and $\vec{V}_1$ is the total nondimensional crossflow velocity (free stream plus vortex induced) normal to the jet centerline. For small jet inclinations to the free-stream direction, $\vec{V}_1$ is given by

$$\vec{V}_1 = \left(\sum_{\substack{\text{all external} \\ \text{vortices}}} V_{vx} - U_\infty \frac{dx_c}{dz}\right)\hat{e}_x + \left(\sum_{\substack{\text{all external} \\ \text{vortices}}} V_{vy} - U_\infty \frac{dy_c}{dz}\right)\hat{e}_y$$

$$\tag{5-14}$$

where the summations $\sum V_{vx}$ and $\sum V_{vy}$ indicate the total external vortex-induced velocities at the jet centerline in the x and y directions, respectively. For example, for a single vortex pair

$$\sum V_{vx} = K_1 \left[\frac{Y_{v1}}{r_{v1}{}^2} - \frac{Y_{vm1}}{r_{vm1}{}^2}\right] \tag{5-15}$$

$$\sum V_{vy} = K_1 \left[\frac{-x_{v1}}{r_{v1}{}^2} + \frac{x_{vm1}}{r_{vm1}{}^2}\right] - \tag{5-16}$$

<u>5.2.3 Buoyant force</u>.- The buoyant force per unit length F_B represents the net vertical force on the jet due to the temperature differential between the jet and the surrounding ambient air, and is equal to the difference in the upward force due to the atmospheric pressure gradient acting on the cylinder and the downward force due to gravitational attraction. In nondimensional form, F_B is given by

$$F_B = \pi r_e{}^2 (\rho_\infty - \overline{\rho}_j) \, g r_n^* / U_j^{*2} \tag{5-17}$$

68

5.2.4 Equations for jet and concentrated vortex pair.

5.2.4 Equations for jet and concentrated vortex pair.- Although equations (5-1) through (5-17) are somewhat lengthy for the general case of N external vortex pairs, they simplify into more reasonable forms for the case where the vortex sheet can be adequately represented by a pair of concentrated vortices. The equations of motion for the jet centerline and the vortex centroid trajectories are

$$
\frac{d}{dz}\left[\left(\dot{m}_j v_j + \frac{U_\infty^2}{T_\infty} \times r_e^2\right)\frac{dx_c}{dz}\right] =
$$

$$
\frac{2r_e^2}{T_\infty} \times \left\{ \frac{K_o}{r_{vo}^2} \times \left[\frac{K_o}{r_{vo}^2} \times \frac{x_{vo}}{1 - (\frac{r_e}{r_{vo}})^2} - U_\infty\left(\frac{dx_{vo}}{dz} + \frac{dx_c}{dz}\right)\left(\frac{2x_{vo}y_{vo}}{r_{vo}^2}\right)\right.\right.
$$

$$
\left. + U_\infty\left(\frac{dy_{vo}}{dz} + \frac{dy_c}{dz}\right)\left(\frac{x_{vo}^2 - y_{vo}^2}{r_{vo}^2}\right)\right] + \frac{K_o}{r_{vmo}^2} \times \left[\frac{K_o}{r_{vmo}^2} \frac{x_{vmo}}{1 - (\frac{r_e}{r_{vo}})^2}\right.
$$

$$
\left. - U_\infty\left(\frac{dx_{vo}}{dz} + \frac{dx_c}{dz}\right)\left(\frac{2x_{vmo}y_{vmo}}{r_{vmo}^2}\right) - U_\infty\left(\frac{dy_{vo}}{dz} + \frac{dy_c}{dz}\right)\left(\frac{x_{vmo}^2 - y_{vmo}^2}{r_{vmo}^2}\right)\right]
$$

$$
\left. - K_o^2 \; \text{R.P.} \left[\frac{\frac{1}{\bar{z}_{vo}^2}}{z_{vmo} - \frac{r_e^2}{\bar{z}_{vo}}} + \frac{\frac{1}{\bar{z}_{vmo}^2}}{z_{vo} - \frac{r_e^2}{\bar{z}_{vmo}}}\right]\right\}
$$

$$
+ \frac{r_e}{T_\infty}\left[K_o\left(\frac{y_{vo}}{r_{vo}^2} - \frac{y_{vmo}}{r_{vmo}^2}\right) - U_\infty\frac{dx_c}{dz}\right]\left[2U_\infty\frac{dr_e}{dz} + \frac{C_D}{2\pi}|\vec{V}_1|\right] + \frac{U_\infty^2}{T_\infty} r_e \frac{dr_e}{dz} \frac{dx_c}{dz}
$$

$$
(5-18)
$$

69

$$\frac{d}{dz}\left[\left(\dot{m}_j V_j + \frac{U_\infty^2}{T_\infty} \times r_e^2\right)\frac{dy_c}{dz}\right] =$$

$$\frac{2r_e^2}{T_\infty} \times \left\{\frac{K_O}{r_{vo}^2} \times \left[\frac{K_O}{r_{vo}^2} \times \frac{y_{vo}}{1-(\frac{r_e}{r_{vo}})} + U_\infty\left(\frac{dx_{vo}}{dz} + \frac{dx_c}{dz}\right)\left(\frac{x_{vo}^2 - y_{vo}^2}{r_{vo}^2}\right)\right.\right.$$

$$+ \left. U_\infty\left(\frac{dy_{vo}}{dz} + \frac{dy_c}{dz}\right)\left(\frac{2x_{vo}y_{vo}}{r_{vo}^2}\right)\right] + \frac{K_O}{r_{vmo}^2} \times \left[\frac{K_O}{r_{vmo}^2}\frac{y_{vmo}}{1-(\frac{r_e}{r_{vmo}})^2}\right.$$

$$+ U_\infty\left(\frac{dx_{vo}}{dz} + \frac{dx_c}{dz}\right)\left(\frac{x_{vmo}^2 - y_{vmo}^2}{r_{vmo}^2}\right) - U_\infty\left(\frac{dy_{vo}}{dz} + \frac{dy_c}{dz}\right)\left(\frac{2x_{vmo}y_{vmo}}{r_{vmo}^2}\right)\right]$$

$$- K_O^2 \text{ I.P.}\left[\frac{\frac{1}{\overline{z}_{vo}^2}}{z_{vmo} - \frac{r_e^2}{\overline{z}_{vo}}} + \frac{\frac{1}{\overline{z}_{vmo}^2}}{z_{vo} - \frac{r_e^2}{\overline{z}_{vmo}}}\right] + \frac{1}{2}\left(1 - \frac{T_\infty}{T_j}\right)\frac{gr_n^*}{U_j^{*2}}\right\}$$

$$+ \frac{r_e}{T_\infty}\left[K_O\left(\frac{-x_{vo}}{r_{vo}^2} + \frac{x_{vmo}}{r_{vmo}^2}\right) - U_\infty\frac{dy_c}{dz}\right]\left[2U_\infty\frac{dr_e}{dz} + \frac{C_D}{2\pi}|\vec{V}_1|\right] + \frac{U_\infty^2}{T_\infty}r_e\frac{dr_e}{dz}\frac{dy_c}{dz}$$

$$(5-19)$$

70

$$U_\infty \left(\frac{dx_{vo}}{dz} + \frac{dx_c}{dz} \right) =$$

$$\frac{K_o}{r_{vo}^2} \frac{y_{vo}}{1 - (\frac{r_e}{r_{vo}})^2} + U_\infty \left(\frac{r_e}{r_{vo}}\right)^2 \left[\frac{dx_c}{dz} \frac{(x_{vo}^2 - y_{vo}^2)}{r_{vo}^2} + \frac{dy_c}{dz} \frac{2x_{vo}y_{vo}}{r_{vo}^2} \right]$$

$$+ r_e V_r \frac{x_{vo}}{r_{vo}^2} - K_o \text{ I.P.} \left[\frac{1}{z_{vo} + \overline{z}_{vo} + 2x_c} - \frac{1}{z_{vo} + \frac{r_e^2}{\overline{z}_{vo} + 2x_c}} \right]$$

$$(5-20)$$

$$U_\infty \left(\frac{dy_{vo}}{dz} + \frac{dy_c}{dz} \right) =$$

$$\frac{K_o}{r_{vo}^2} \frac{x_{vo}}{1 - (\frac{r_e}{r_{vo}})^2} + U_\infty \left(\frac{r_e}{r_{vo}}\right)^2 \left[\frac{dx_c}{dz} \frac{2x_{vo}y_{vo}}{r_{vo}^2} + \frac{dy_c}{dz} \frac{(x_{vo}^2 - y_{vo}^2)}{r_{vo}^2} \right]$$

$$+ r_e V_r \frac{y_{vo}}{r_{vo}^2} - K_o \text{ R.P.} \left[\frac{1}{z_{vo} + \overline{z}_{vo} + 2x_c} - \frac{1}{z_{vo} + \frac{r_e^2}{\overline{z}_{vo} + 2x_c}} \right]$$

$$(5-21)$$

and where $\left| \vec{V}_1 \right|$ is found from equations (5-14) to (5-16).

5.3 Initial Interaction Calculations

The equations of motion given by equations (5-1) through (5-17) have been integrated with 10 equal strength vortices distributed on the trailing edge of each wing panel according to an elliptical loading, and for the initial conditions and physical parameters corresponding to the calculative example discussed in Section 9. Comparisons were made in the motions of the cylinder and vortex centroids for this $N = 10$ case with the analogous results obtained by concentrating the vorticity into a pair of vortices located at the center-of-gravity of vorticity (i.e. integrating eqs. (5-18) through (5-21)), and the results were virtually identical. Consequently, all the calculations of the initial jet-vortex interaction stage and also the ingestion stage were performed with the simpler concentrated vortex-pair model.

The interaction calculations were carried out according to the following criteria. The equations of motion were integrated from the aircraft trailing edge downstream to a point where the outer jet boundary (which is considered as solid during this phase) has expanded to a size sufficiently large that the image vortices inside the jet begin to interact with the near external vortex centroid in a strong and spurious manner. At that location, the initial interaction calculation is terminated since it can now be safely assumed that the external vortex has begun to tear apart and ingest at least the closest portion of the hot jet. The jet disintegration and ingestion process, described in the following section, is then initiated, using as starting conditions, the locations and crossflow velocities predicted by the initial interaction model.

6.0 INGESTION OF JETS BY TRAILING VORTICES

6.1 Description of Model

When the jet and trailing vortex begin to interact strongly, the model constructed for the initial phase of the interaction process is no longer valid and must be modified. In particular, the assumption of the outer jet boundary as being solid and impervious to the crossflow flow field must be relaxed in order to track the various jet segments as the jet disintegrates and is ingested into the vortex recirculation region.

To model the break-up and ingestion process, the technique used is to track the entire jet using the initial interaction equations of Section 5 to the point of strong jet-vortex interaction, then subdivide the jet into a number of equal area segments (5 to 10), initialize the various segments with crossflow velocities predicted by the initial jet-vortex interaction model, and subsequently track the various jet segments under the combined action of the trailing-vortex pair pressure forces plus buoyancy effects. During this process, it is assumed that the jet segments are sufficiently small that the mutual interference between segments is negligible, and also that the segments can be considered to have no internal structure (i.e., do not satisfy a no-flow boundary condition at their surfaces) so that there are no image vortices nor dipoles located inside them. In addition, since the jet is now essentially aligned longitudinally with the trailing-vortex pair, the crossflow drag can be neglected.

6.2 Differential Equations for Jet Disintegration

The differential equations governing the various segments of the jet during the break-up process can be obtained either from first principles, or as a limiting case of the initial interaction equations as both the radius and rate of change of the radius of the segments goes to zero. Also, because the mutual interaction between the segments is assumed to be small, the motion of each individual segment can be calculated independently of the others. Consequently, the equations governing the location of an arbitrary segment of the disintegrating jet are given by

73

$$\frac{d^2 x_c}{dz^2} = \left(\frac{2}{U_\infty^2 + U_j^2 \frac{T_\infty}{\overline{T}_j}}\right)\left\{\frac{K_o}{r_{vo}^2}\left[\frac{K_o}{r_{vo}^2} x_{vo} + U_\infty\left(\frac{dy_{vo}}{dz} + \frac{dy_c}{dz}\right)\left(\frac{x_{vo}^2 - y_{vo}^2}{r_{vo}^2}\right)\right]\right.$$

$$+ \frac{K_o}{r_{vmo}^2}\left[\frac{K_o}{r_{vmo}^2} x_{vmo} - U_\infty\left(\frac{dy_{vo}}{dz} + \frac{dy_c}{dz}\right)\left(\frac{x_{vmo}^2 - y_{vmo}^2}{r_{vmo}^2}\right)\right]$$

$$\left. - K_o^2 \text{ R.P.}\left[\frac{\frac{-1}{\overline{Z}_{vo}^2}}{\overline{Z}_{vo} + 2x_c} + \frac{\frac{1}{(Z_{vo} + 2x_c)^2}}{Z_{vo}}\right]\right\} \tag{6-1}$$

$$\frac{d^2 y_c}{dz^2} = \left(\frac{2}{U_\infty^2 + U_j^2 \frac{T_\infty}{\overline{T}_j}}\right)\left\{\frac{K_o}{r_{vo}^2}\left[\frac{K_o}{r_{vo}^2} y_{vo} + U_\infty\left(\frac{dy_{vo}}{dz} + \frac{dy_c}{dz}\right)\left(\frac{2x_{vo}y_{vo}}{r_{vo}^2}\right)\right]\right.$$

$$+ \frac{K_o}{r_{vmo}^2}\left[\frac{K_o}{r_{vmo}^2} y_{vmo} - U_\infty\left(\frac{dy_{vo}}{dz} + \frac{dy_c}{dz}\right)\left(\frac{2x_{vmo}y_{vmo}}{r_{vmo}^2}\right)\right]$$

$$\left. + \frac{1}{2U_\infty^2}\left(1 - \frac{T_\infty}{\overline{T}_j}\right)\frac{gr_n^*}{U_j^{*2}}\right\} \tag{6-2}$$

and the vortex pair by

$$U_\infty\left(\frac{dx_{vo}}{dz} + \frac{dx_c}{dz}\right) = 0 \tag{6-3}$$

74

$$U_\infty\left(\frac{dy_{vo}}{dz} + \frac{dy_c}{dz}\right) = \frac{-K_o}{2(x_{vo} + x_c)} \tag{6-4}$$

Equations (6-3) and (6-4) indicate that the motion of the concentrated vortex pair is strictly vertical at a downward rate equal to their mutually-induced velocity. This, of course, is expected since the assumption was made that the individual jet segments are sufficiently small so that their influence on the motion of the trailing-vortex pair is negligible.

6.3 Disintegration Calculations

The jet disintegration trajectory equations (6-1) through (6-4) were integrated according to the following criteria. At the end of the initial interaction phase, the jet is divided into a number of equal area segments (five were found to be sufficient). The locations and crossflow velocities of the jet segments predicted by the initial interaction calculated are used as starting conditions for equations (6-1) through (6-4). These equations are then integrated downstream for each segment of the jet to a point sufficiently far that it is clear that the particular segment is either captured or escapes. The criteria used for capture is that the trajectory of the segment becomes either a closed curve about the vortex or a spiral into the core.

To investigate the effect of various initial velocities of the jet segments, a series of disintegration calculations were carried out beginning at various longitudinal positions upstream of the-point where the initial interaction calculations are terminated.

It was found that for the typical parameters and conditions corresponding to the calculative example, the vortex strength is sufficiently high to capture all of the hot jet exhaust within a relatively short distance downstream. This result was relatively insensitive to the starting position of the disintegrating phase. These calculations are described in detail in Section 9.

7.0 EQUILIBRIUM VORTEX STAGE

7.1 Introduction

It has been calculated that all the exhaust products from the engines are entrained in the recirculating flow. The actual distribution of temperature in the recirculating flow is not necessarily an indication of the engine exhaust gas concentration as during the jet phase because the vortices cause radial pressure gradients which themselves cause temperature differences even when no exhaust gas products are present. It appears that the turbulent transport processes in the recirculation region will control the distribution of temperature within that region if the stage lasts sufficiently long.

Within the recirculation region the field near the vortices will be dominated by the local vortex and will take on the character of an equilibrium turbulent vortex. In the outer reaches of the recirculation region between the vortices, the effect of both vortices will be present. It is possible to obtain a good idea of the characteristics of much of the flow by considering it to be simply two isolated equilibrium turbulent vortices. This is particularly true of the core region where most of the exhaust gases tend to be entrained. Accordingly we will now consider the questions of the temperature and concentration distributions for an isolated equilibrium vortex.

7.2 Kinematics of an Equilibrium Turbulent Vortex

Before determining the temperature distribution of an equilibrium turbulent vortex, it is helpful to describe the regions of the vortex and its tangential velocity and circulation distributions. A turbulent vortex can be considered to fall into three parts as discussed by Nielsen and Schwind in reference 7-1. The center of a turbulent vortex is in solid body rotation with the tangential velocity proportional to the radius. This region merges into the central part of the vortex wherein the circulation varies logarithmically with the radius. In this region the tangential velocity reaches maximum v_1 at a radius r_1. Beyond the logarithmic region of the vortex is a "wake" region analogous to the wake region of a turbulent boundary layer. In this region the circulation decays exponentially with radius.

With this brief description, we now introduce figure 7-1 taken from reference 7-1. In this figure r_i is the radius of the "eye" of the vortex in solid body rotation, r_j is the radius of the outer edge of the logarithmic region, and r_o is the outer edge of the vortex taken where the circulation is 99 percent of the total circulation. The following empirical results taken from reference 7-1 are based on the data of Hoffman and Joubert (ref. 7-2) and give the circulation distributions in the three regions.

$$\text{Eye:} \quad 0 \leq r \leq r_i \qquad \frac{K}{K_1} = 1.47 \left(\frac{r}{r_1}\right)^2 \tag{7-1}$$

$$\genfrac{}{}{0pt}{}{\text{Logarithmic}}{\text{Region}} : \quad r_i \leq r \leq r_j \qquad \frac{K}{K_1} = 0.938 \ln\left(\frac{r}{r_1}\right) + 1 \tag{7-2}$$

$$\text{Wake:} \quad r_j \leq r \leq r_o \qquad \frac{K_o - K}{K_1} = 4.43 \ e^{-4.8(r/r_o)} \tag{7-3}$$

$$\frac{r_i}{r_j} = 0.562 \tag{7-4}$$

$$\frac{r_j}{r_o} = 0.515 \tag{7-5}$$

r_1 = core radius based on experiment

v_1 = tangential velocity at core radius

$K_1 = v_1 r_1$

The tangential velocity distribution is simply given by $v = K/r$.

7.3 Vortex Temperature Distribution

We now determine the temperature distribution through an equilibrium turbulent vortex.

7.3.1 Vortex "eye".- Consider first the "eye" of the vortex in solid body rotation. For this region it is known that rotation has a strong

influence in damping the turbulent fluctuations so that to the first approximation we will treat this region as laminar.

The governing equations as taken from Hall (ref. 7-3) are

Continuity

$$\frac{\partial \rho}{\partial t} + \frac{1}{r} \frac{\partial}{\partial r} (r\rho u) + \frac{\partial (\rho w)}{\partial z} = 0 \tag{7-6}$$

Momentum

$$\frac{\rho v^2}{r} = \frac{\partial p}{\partial r} \tag{7-7}$$

$$\rho \left(\frac{\partial v}{\partial t} + u \frac{\partial v}{\partial r} + w \frac{\partial v}{\partial z} + \frac{uv}{r} \right) = \frac{1}{r^2} \frac{\partial}{\partial r} \left[r^2 \mu \left(\frac{\partial v}{\partial r} - \frac{v}{r} \right) \right] \tag{7-8}$$

$$\rho \left(\frac{\partial w}{\partial t} + u \frac{\partial w}{\partial r} + w \frac{\partial w}{\partial z} \right) = - \frac{\partial p}{\partial z} + \frac{1}{r} \frac{\partial}{\partial r} \left(r\mu \frac{\partial w}{\partial r} \right) \tag{7-9}$$

Energy

$$\rho \left(\frac{\partial I_o}{\partial t} + u \frac{\partial I_o}{\partial r} + w \frac{\partial I_o}{\partial z} \right) - \frac{\partial p}{\partial t} = \frac{1}{r} \frac{\partial}{\partial r} \left[\frac{\mu}{\sigma} r \frac{\partial I_o}{\partial r} + \frac{\mu}{\sigma} (\sigma - 1) \left(v \frac{\partial v}{\partial r} + w \frac{\partial w}{\partial r} \right) \right.$$

$$\left. - \mu v^2 \right] \tag{7-10}$$

where the total enthalpy is

$$I_o = c_p T + \frac{1}{2} (u^2 + v^2 + w^2)$$

$$\sigma = \text{Prandtl number}$$

Assumptions in deriving these equations include

(a) Viscosity and thermal conductivity are constant

(b) Laminar flow

(c) Axial symmetry

(d) Axial time derivatives are small compared to radial time derivatives

78

We now add the following assumptions

    (e) $\sigma = 1$

    (f) Steady flow

so that equation (7-10) becomes

$$\rho u \frac{\partial I_o}{\partial r} + \rho w \frac{\partial I_o}{\partial z} = \frac{1}{r} \frac{\partial}{\partial r} \left[\frac{\mu r}{\sigma} \frac{\partial I_o}{\partial r} - \mu v^2 \right] \tag{7-11}$$

Trailing vortices in the equilibrium vortex stage are many miles long and their core diameter changes very slowly. Thus u and $\partial I_o/\partial z$ are very small. We will take them to be zero so that

$$\frac{\partial}{\partial r} \left[\frac{\mu r}{\sigma} \frac{\partial I_o}{\partial r} - \mu v^2 \right] = 0 \tag{7-12}$$

This equation simply states that the work done on the eye of the vortex by viscous shear is transferred back out as heat.

We now have

$$r \frac{\partial I_o}{\partial r} = v^2 + C_1 \tag{7-13}$$

Since

$$v = 0 \qquad \frac{\partial I_o}{\partial r} = 0 \qquad \text{at} \qquad r = 0$$

$$C_1 = 0$$

and

$$\frac{\partial I_o}{\partial r} = \frac{v^2}{r} = \Omega^2 r$$

$$I_o = \frac{\Omega^2 r^2}{2} + C_2 \tag{7-14}$$

Since $u \ll v$, $w \ll v$

$$c_p T + \frac{v^2}{2} = \frac{\Omega^2 r^2}{2} + C_2$$

Let T_i be the temperature at the outer edge of the edge of the eye of the vortex at radius r_i.

$$r = r_i \qquad T = T_i \qquad v = v_i = \Omega r_i \qquad (7\text{-}15)$$

The resulting equation is

$$T = T_i \qquad r \leq r_i \qquad (7\text{-}16)$$

For a Prandtl number different from unity, equation (7-12) yields

$$T - T_i = \left(1 - \frac{r^2}{r_i^2}\right)\frac{v_i^2}{2c_p}\,(\sigma - 1) \qquad (7\text{-}17)$$

We will use the simple $\sigma = 1$ solution with the eye of the vortex in solid body rotation at uniform static temperature.

7.3.2 Outer region.- For the outer region we will assume that all transport by laminar means is negligible compared to that by turbulent transport

$$\mu \ll \mu_t$$

$$k \ll k_t$$

We make the additional assumptions

    (a)   Steady flow

    (b) $\partial/\partial z = 0 \qquad w = 0$

    (c)   Density fluctuations are zero

    (d)   Axial symmetry

The resulting equations deduced from reference 7-3 are

$$\frac{\partial}{\partial r}\,(\rho r u) = 0 \qquad (7\text{-}18)$$

$$\frac{\rho v^2}{r} = \frac{\partial p}{\partial r} \qquad (7\text{-}19)$$

80

$$\rho u \frac{\partial v}{\partial r} + \rho \frac{uv}{r} = - \frac{1}{r^2} \frac{\partial}{\partial r} (r^2 \rho \overline{u'v'}) \tag{7-20}$$

$$\rho u \frac{\partial I_o}{\partial r} = - \frac{1}{r} \frac{\partial}{\partial r} (r\rho \overline{u'I_o'}) \tag{7-21}$$

At this point we introduce the Reynolds stress τ_t due to turbulence and the corresponding heat transfer q_t

$$\left. \begin{array}{c} \tau_t = - \rho \overline{u'v'} \\[2mm] q_t = - \rho c_p \overline{u'T'} \end{array} \right\} \tag{7-22}$$

In rotary flow the shearing stress is taken proportional to the eddy viscosity as follows

$$\frac{\tau_t}{\rho} = - \overline{u'v'} = \nu_t \left(\frac{\partial v}{\partial r} - \frac{v}{r} \right) \tag{7-23}$$

with the kinematic term zero for solid body rotation. With respect to the eddy thermal conductivity, it has been suggested (ref. 7-4) that adiabatic temperature changes associated with radial pressure gradients do not act as a driving force for heat transfer so that

$$-c_p \overline{u'T'} = \frac{k_t}{\rho} \left[\frac{\partial T}{\partial r} - \left(\frac{\partial T}{\partial p} \right)_{ad} \frac{\partial p}{\partial r} \right] \tag{7-24}$$

Now for adiabatic changes

$$\left(\frac{\partial T}{\partial p} \right)_{ad} = \frac{\gamma - 1}{\gamma} \frac{1}{\rho R} = \frac{1}{c_p \rho} \tag{7-25}$$

so that

$$-c_p \overline{u'T'} = + \frac{k_t}{\rho} \left[\frac{\partial T}{\partial r} - \frac{1}{c_p \rho} \frac{\partial p}{\partial r} \right] \tag{7-26}$$

For small fluctuations we have

$$I_o' = c_p T' + vv'$$

$$\overline{u' I_o'} = c_p \overline{u'T'} + v \overline{u'v'} \tag{7-27}$$

Incorporating this result into equation (7-21) and letting $u = 0$ yield

$$\frac{\partial}{\partial r} (r\rho \overline{u'I_o'}) = \frac{\partial}{\partial r} \left[r\rho (c_p \overline{u'T'} + v \overline{u'v'}) \right] = \frac{\partial}{\partial r} \left\{ r\rho \left[\frac{k_t}{\rho} \frac{\partial T}{\partial r} \right. \right.$$

$$\left. \left. - \frac{k_t}{c_p \rho^2} \frac{\partial p}{\partial r} + \nu_t v \frac{\partial v}{\partial r} - \nu_t \frac{v^2}{r} \right] \right\} = 0 \tag{7-28}$$

or assuming the turbulent Prandtl number is unity

$$\frac{\partial}{\partial r} \left\{ r\rho \ \nu_t \left[c_p \frac{\partial T}{\partial r} + v \frac{\partial v}{\partial r} - \frac{2v^2}{r} \right] \right\} = 0$$

and

$$r\rho \ \nu_t \left[\frac{\partial}{\partial r} \left(q_t + \frac{v^2}{2} \right) - \frac{2v^2}{r} \right] = C_3 \tag{7-29}$$

or

$$\frac{\partial}{\partial r} \left(c_p T + \frac{v^2}{2} \right) - \frac{2v^2}{r} = \frac{C_3}{r\rho \nu_t} \tag{7-30}$$

The right-hand side of the equation can be treated by use of equations (7-20) and (7-23)

$$\frac{\partial}{\partial r} (r^2 \rho \overline{u'v'}) = - \frac{\partial}{\partial r} \left[r^2 \rho \nu_t \left(\frac{\partial v}{\partial r} - \frac{v}{r} \right) \right] = 0 \tag{7-31}$$

Thus

$$\frac{1}{r\rho \nu_t} = C_4 r \left(\frac{\partial v}{\partial r} - \frac{v}{r} \right) \tag{7-32}$$

substituting into equation (7-30), we find

$$\frac{\partial}{\partial r} \left(c_p T + \frac{v^2}{2} \right) = \frac{2v^2}{r} + C_3 C_4 r \left(\frac{\partial v}{\partial r} - \frac{v}{r} \right) \tag{7-33}$$

In seeking solutions to equation (7-33) we need to specify the radial distribution of the tangential velocity, $v(r)$. Several possibilities occur. We can specify the radial distribution for an equilibrium vortex as given by equations (7-1) to (7-3). For a simple solution we might specify a variation corresponding to a potential vortex in the field external to the eye of the vortex. It is of interest to compare equation (7-33) with equation (7-14) before proceeding with any solutions. The first thing to note is that $(\partial v/\partial r - v/r)$ is zero for solid body rotation so that this term in equation (7-33) does not contribute to $\partial T/\partial r$ at $r = r_i$. It is also noted that a factor of two appears before the v^2/r term in equation (7-33) while a factor of unity appears in equation (7-14). There is thus a discontinuity in the temperature gradient at $r = r_i$ due to the different heat transfer laws for laminar and turbulent flow. To alleviate this difficulty requires a buffer region between the laminar and turbulent region which has not been introduced into the theory. However, this simplification of the theory should not interfere with obtaining some interesting approximate solutions.

For the assumption of a potential vortex external to the eye of the vortex, a particularly simple solution can be obtained. In this case the tangential velocity is given by

$$v = \frac{\Gamma_o}{2\pi r} \tag{7-34}$$

The term proportional to $C_3 C_4$ in equation (7-33) must be zero since it will produce a $\log r$ term which is not regular as $r \to \infty$. Thus we obtain

$$\frac{\partial}{\partial r}\left(c_p T + \frac{v^2}{2}\right) = \frac{\Gamma}{2\pi^2 r^3} \tag{7-35}$$

If we take as a boundary condition

$$T = T_\infty^* \qquad r = \infty$$

then

$$c_p T + \frac{3}{2} v^2 = c_p T_\infty^* \tag{7-36}$$

The temperature of the eye is then given by

$$T_i = T_\infty^* - \frac{3v_i^2}{2c_p} \tag{7-37}$$

The eye will be colder than the free stream. This result should give an approximate idea of how cold the eye will be for the case of an equilibrium turbulent vortex.

7.3.3 <u>Improved solution based on logarithmic circulation distri-</u><u>bution.</u>- For an equilibrium vortex the circulation distribution given by the logarithmic law yields a good approximation even in the wake region even though it does not have the desired properties as $r \to \infty$. If we limit the solution to the region $r \le r_o$, we can use the logarithmic circulation distribution to obtain an improved solution. We can retain both terms in the right-hand side of equation (7-33) since the range of r is limited. At $r = r_o$ we can apply both temperature and temperature gradient boundary conditions assuming that the stagnation enthalpy is constant for $r > r_o$

$$c_p T + \frac{v^2}{2} = T_\infty^* ; \qquad r > r_o \tag{7-38}$$

$$\frac{\partial}{\partial r}\left(c_p T + \frac{v^2}{2}\right) = 0 ; \quad r > r_o \tag{7-39}$$

Subject to this outer condition, it is readily found from equation (7-33) that

$$\begin{aligned}
c_p T + \frac{v^2}{2} - c_p T_\infty^* = 2 \Big\{ &(0.928\ K_1)^2 \Big[F_1(r_o) - F_1(r)\Big] \\
&+ 0.928\ K_1^2 (1 - 0.928\ \ln r_1)\Big[F_2(r_o) - F_2(r)\Big] \\
&+ K_1^2 (1 - 0.928\ \ln r_1)^2 \Big[F_3(r_o) - F_3(r)\Big] \Big\} \\
&+ C_s \Big[0.928\ K_1 (\ln r - \ln r_o) - 0.928\ K_1 (\ln^2 r - \ln^2 r_o) \\
&- 2K_1 (1 - 0.928\ \ln r_1)(\ln r - \ln r_o)\Big] \tag{7-40}
\end{aligned}$$

84

where

$$C_5 = \frac{2v^2/r}{r\left(\frac{\partial v}{\partial r} - \frac{v}{r}\right)}\Bigg|_{r=r_o} \tag{7-41}$$

$$C_5 = 2\left\{(0.928\ K_1^2)\ \frac{\ln^2 r_o}{r_o^3} + 0.928\ K_1^2(1 - 0.928\ \ln\ r_1)\ \frac{\ln\ r_o}{r_o^3}\right.$$

$$\left. + \frac{K_1^2}{r_o^3}\ (1 - 0.928\ \ln\ r_1)^2\right\}\Bigg/\left[0.928\ \frac{K_1}{r_o} - 2(0.928)K_1\ \frac{\ln\ r_o}{r_o}\right.$$

$$\left. - \frac{2K_1}{r_o}\ (1 - 0.928\ \ln\ r_1)\right] \tag{7-42}$$

with

$$\left.\begin{aligned} F_1(r) &= \frac{2\ \ln^2 r + 2\ \ln\ r + 1}{4r^2} \\[2mm] \tilde{F}_2(r) &= \frac{2\ \ln\ r + 1}{4r^2} \\[2mm] F_3(r) &= \frac{1}{2r^2} \end{aligned}\right\} \tag{7-43}$$
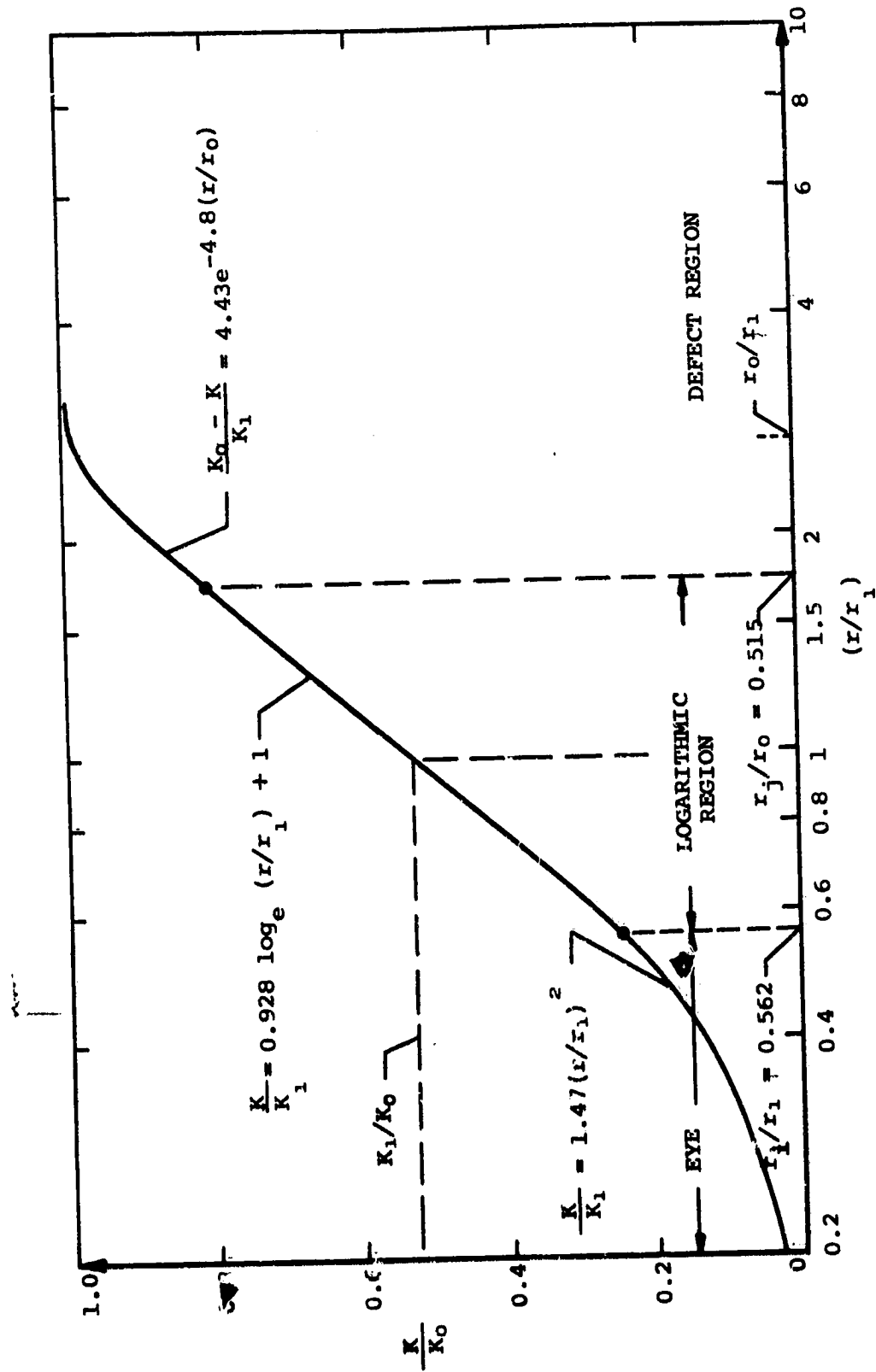
Figure 7-1.- Empirical circulation distribution for equilibrium turbulent vortex.

$$\frac{K_o - K}{K_1} = 4.43e^{-4.8(r/r_o)}$$

$$\frac{K}{K_1} = 0.928 \log_e (r/r_1) + 1$$

$$\frac{K}{K_1} = 1.47(r/r_1)^2$$

DEFECT REGION

LOGARITHMIC REGION

EYE

r_o/r_1

$r_j/r_o = 0.515$

$r_j/r_1 = 0.562$

(r/r_1)

K_1/K_o

$\frac{K}{K_o}$

8.0 ASYMPTOTIC BUOYANCY PHASE

8.1 Introduction

It is of interest to know the ultimate disposition of the exhaust gas products in the stratosphere. Several studies of this question are available, that of Overcamp and Fay (ref. 8-1). In reference 8-1 smoke-stack plume theory is applied to the hot wake of an aircraft. In reference 8-2, several dispersive mechanisms are discussed; namely, wake collapse, wind shear, buoyancy rise, and turbulent diffusion. Without discussing these results in detail, we note that they are not mutually exclusive, not linearly superposable, and certain ones are dependent on atmospheric turbulence and winds. There is noticeable difference between the buoyancy results of the two groups of authors.

In this section are set the tasks of finding the asymptotic solution for a quiescient atmosphere. We will address the problem of a hot region of recirculating flow associated with the pair of turbulent vortices. We will assume that at some distance behind the aircraft the axial flow in the recirculating region had died out, that the vortices are close to horizontal, and that the wake moves along with any horizontal wind.

The paper of Fay and Overcamp concerning the effects of buoyancy on the width of the recirculation region includes a correlation of the width of such regions obtained from contrail data. The paper also includes an interesting comparison between the data correlation and an approximate solution obtained from the stack plume theory of Hewett, Fay, and Hoult (ref. 8-4). In order to assess the theoretical basis of this comparison we now examine the theory of that reference.

Consider a hot plume emerging from a stack in a uniform cross wind so that the plume is stationary in stack coordinates. Let v be the
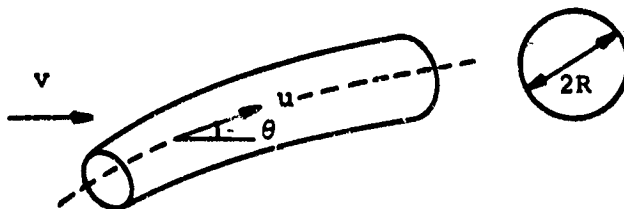
horizontal wind velocity and u the uniform axial velocity of the gas in the plume at angle θ to the horizontal. The rate of entrainment ϵ is taken proportional to the relative wind velocities parallel and perpendicular to the plume axis as follows

$$\epsilon = 2\pi R \left[\alpha |u - v \cos \theta| + \beta |v \sin \theta| \right] \qquad (8\text{-}1)$$

In this equation α and β are constants of the order of unity. Subject to the condition that $R = 0$ at $x = 0$ (at the stack) the following approximate solution is obtained from reference 8-4 for the plume radius

$$\frac{R}{\ell_b S^{2/3}} = \left[3\beta \left(1 - \cos \frac{x}{\ell_b S} \right) \right]^{1/} \quad ; \quad \frac{x}{\ell_b S} \leq \pi \qquad (8\text{-}2)$$

$$\ell_b = gH / \pi \rho_\infty c_p T_\infty^* (U_\infty^*)^3$$

$$S = U_\infty^* / \ell_b \omega$$

$$\omega = \frac{g}{\sqrt{c_p T_\infty^*}} = \text{Brunt-Väisällä frequency} \qquad (8\text{-}3)$$

Expansion of the above expression for small values of $x/\ell_b S$ yields

$$\frac{R}{\ell_b} = \left(\frac{3\beta}{2} \right)^{1/3} \left(\frac{x}{\ell_b} \right)^{2/3}$$

Consider a distance d_b such that the cumulative buoyancy force equals the lift

$$d_b = \frac{c_p T}{g} \frac{L U_\infty^*}{H} \qquad (8\text{-}4)$$

and introduce a new reference length ℓ such that

$$\ell = (\ell_b d_b^2)^{1/3} \qquad (8\text{-}5)$$

Then we obtain

$$\left(\frac{2R}{\ell} \right) = 2 \left(\frac{3\beta}{2} \right)^{1/3} \left(\frac{x}{d_b} \right)^{2/3} \qquad (8\text{-}6)$$

88

This power law is compared with the contrail data of reference 8-1 in figure 8-1 assuming $\beta = 1$. After an initial period, the contrail wake grows in size at a rate equal to or greater than that given by the above power law.

Examination of the limitations on x in equation (8-2) shows that the power law is valid only for very short times. We can write

$$\frac{x}{\ell_b S} = \frac{x\omega}{v} = \omega t \leq \pi$$

For $T = 392^{\circ}R$ we find that

$$\omega = 0.021 \text{ rad/sec}$$

and the maximum time corresponding to π radius is about 150 seconds. Since the power law is valid only for much lesser times than the maximum time, it should be valid only for periods less than a minute. What is of interest is that the power law is in fair agreement with the contrail data for much longer periods of time. However, we cannot conclude that buoyancy is the dominant mechanism since the buoyancy theory has been extended far beyond its range of validity. This observation is not necessarily true for a supersonic airplane.

In this section we carry out a detailed derivation using the above entrainment model for a hot wake which is initially horizontal and which possesses no axial nor vertical velocity. Kinetic energy effects are initially included, and the case of stratification associated with a uniform atmospheric temperature is treated. An analytic solution in closed form is found. The complete mathematical-solution is not carried out, but numerical results obtained on a computer are presented for an initial value of R not equal to zero. These are compared with the data correlations and theory of Fay and Overcamp.

8.2 Horizontal Wake Analysis

It is to be expected that the axial flow in the recirculation region will damp out some distance behind the aircraft, but that the vorticity and heat content of the recirculating flow will still be substantially unchanged. We assume that the wake is nearly horizontal with small vertical velocity at some point in its equilibrium vortex phase. Consider a cross section of this wake at time $t = t_i$

89
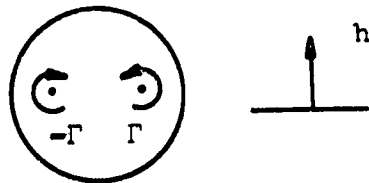
Let the average density in the wake be $\overline{\rho}$. Let h be distance measured vertically from the $t = t_i$ altitude. The atmospheric density is ρ_∞ and at $t = t_i$ is designated $\rho_{\infty i}$. Let the vertical rate of rise of the wake be w. We will assume the wake is circular of radius R for simplicity. Let m_i be the mass of air in a section of wake of thickness Δx at $t = t_i$

$$m_i = \pi R_i^2 \, \overline{\rho}_i \, \Delta x \qquad (8\text{-}7)$$

Let $\dot{m}_e$ be the time rate of mass entrainment into the wake section due to its rate of rise w. Thus we have

$$\dot{m}_e = 2\pi R \, \Delta x \, \alpha \, |w| \rho_\infty \qquad (8\text{-}8)$$

where α is a dimensionless entrainment coefficient. The total mass in the wake section at time t is then

$$m = m_i + 2\pi \, \Delta x \, \alpha \int_{t_i}^{t} R w \rho_\infty dt \qquad (8\text{-}9)$$

Since we will be dealing only with positive values of w, we remove the magnitude sign.

The vertical momentum equation can be obtained by equating the buoyant force equal to the rate of change of vertical momentum. The buoyant force F_B is

$$F_B = \pi R^2 \Delta x (\rho_\infty - \overline{\rho}) g \qquad (8\text{-}10)$$

With

$$F_B = \frac{d}{dt} (mw) \qquad (8\text{-}11)$$

90

we find that

$$\frac{dw}{dt} = \frac{g(R^2\rho_\infty - R_i^2\overline{\rho}_i) - 2\alpha\left[Rw^2\rho_\infty + g\int_{t_i}^{t} Rw\rho_\infty dt\right]}{\overline{\rho}_i R_i^2 + 2\alpha\int_{t_i}^{t} Rw\rho_\infty dt} \qquad (8\text{-}12)$$

with the initial condition

$$\left.\frac{dw}{dt}\right|_{t_i} = \frac{g(\rho_{\infty_i} - \overline{\rho}_i) - 2\alpha w_i^2 \rho_\infty / R_i}{\overline{\rho}_i} \qquad (8\text{-}13)$$

The application of the law of the conservation of energy to the problem is of particular interest because it yields a closed solution for the size of the wake cross section as a function of altitude. The change in total enthalpy of the recirculation fluid between time "t" and "t_i" is equal to the sum of the work done on the wake by the buoyant force during this time, the energy added to it by the entrained mass, and the work done by the fluid against atmospheric pressure.

$$m\left(c_p\overline{T} + \frac{w^2}{2}\right) - m_i\left(c_p\overline{T}_i + \frac{w_i^2}{2}\right) = \int_{t_i}^{t} F_B w\ dt + m_e c_p T_\infty^* + \int_{p_{\infty_i}}^{r} \frac{m}{\rho}\ dp \qquad (8\text{-}14)$$

In this equation it is not necessary to include potential energy terms if we use the net buoyant force in calculating the work done on the wake. This is true because the increase in potential energy between two points a short distance apart, $d(mgh)$, is equal to work done on the wake $(mg)dh$ plus potential energy $(gh)dm$ added to wake.

Here we assume that the external air temperature is constant with altitude at T_∞^*. The temperature $\overline{T}$ is the mass averaged temperature of the recirculating flow and is given by

$$\overline{T} = \frac{P_\infty}{R_g\overline{\rho}} \qquad (8\text{-}15)$$

91

where R_g is the gas constant for the recirculating flow. Since

$$\bar{\rho} = \frac{m}{\pi R^2 \Delta x} \tag{8-16}$$

$$\bar{T} = \frac{p_\infty \pi R^2 \Delta x}{m R_g} \tag{8-17}$$

we have

$$m c_p \bar{T} = \frac{c_p}{R_g} \left(p_\infty \pi R^2 \Delta x \right) \tag{8-18}$$

Also

$$\frac{m}{\rho} dp = -\frac{m}{\rho} \rho_\infty g \, dh = -(\pi \Delta x) R^2 \rho_\infty g \, dh \tag{8-19}$$

In differential form equation (8-14) can be written

$$\frac{c_p}{R_g} (\pi \Delta x) \frac{d}{dt} (p_\infty R^2) = -\frac{1}{2} \frac{d(mw^2)}{dt} + w \frac{d}{dt} (mw) + c_p T_\infty^* \frac{dm}{dt} - (\pi \Delta x) R^2 \rho_\infty g w$$

or with the help of equation (8-8)

$$w \rho_\infty \left[2\alpha \frac{|w|}{w} \left(c_p T_\infty^* + \frac{w^2}{2} \right) + \left(\frac{c_p}{R_g} - 1 \right) gR \right] = \frac{2c_p}{R_g} p_\infty \frac{dR}{dt} \tag{8-20}$$

Neglecting w^2 compared to $c_p T_\infty^*$ and assuming w is positive yields

$$\left(2\alpha \, c_p T_\infty^* + \frac{gR}{\gamma - 1} \right) dh = 2c_p T_\infty^* dR \tag{8-21}$$

The solution of the equation subject to the initial condition $R = R_i$ when $h = 0$ is

$$\alpha + \frac{gR}{2\gamma R_g T_\infty^*} = \left(\alpha + \frac{gR_i}{2\alpha R_g T_\infty^*} \right) e^{hg/2\gamma R_g T_\infty^*} \tag{8-22}$$

For small values of $hg/2\gamma R_g T_\infty^*$, the approximate solution is

92

$$R = R_i + \alpha h \qquad (8\text{-}23)$$

We have assumed in the derivation that the average pressure of the recirculating flow is equal to the atmospheric pressure at the height of its center.

8.3 Solution of Vertical Momentum Equation

We can write equation (8-12) in the form

$$2\frac{dw}{dt} + \frac{w^2(4\alpha R\rho_\infty)}{\overline{\rho}_i R_i^2 + 2\alpha \int_{t_i}^{t} Rw\rho_\infty dt} = -2g + \frac{2gR^2\rho_\infty}{\overline{\rho}_i R_i^2 + 2\alpha \int_{t_i}^{t} Rw\rho_\infty dt} \qquad (8\text{-}24)$$

or

$$\frac{dw^2}{dh} + w^2 F = G \qquad (8\text{-}25)$$

$$F = \frac{4\alpha R\rho_\infty}{\overline{\rho}_i R_i^2 + 2\alpha \int_{t_i}^{t} Rw\rho_\infty dt} \qquad (8\text{-}26)$$

$$G = \frac{2gR^2\rho_\infty}{\overline{\rho}_i R_i^2 + 2\alpha \int_{t_i}^{t} Rw\rho_\infty dt} - 2g \qquad (8\text{-}27)$$

We will determine the explicit functions $F(h)$ and $G(h)$ and thus show that equation (8-25) is a linear equation for w^2.

Starting with the integral, we have

$$\int_{t_i}^{t} Rw\rho_\infty dt = \int_{0}^{h} R\rho_\infty dz \qquad (8\text{-}28)$$

93

For an isothermal atmosphere of temperature T_∞^*, we have

$$\frac{\rho_{\infty_i}}{\rho_\infty} = e^{hg/R_g T_\infty^*} \tag{8-29}$$

$$\rho_\infty = \rho_{\infty_i} e^{-hg/R_g T_\infty^*} \tag{8-30}$$

Thus

$$\int_0^h R\rho_\infty dh = 2\gamma \left(\frac{R_g T_\infty^*}{g}\right)^2 \rho_{\infty_i} \int_0^\xi \left[\left(\alpha + \frac{gR_i}{2\gamma R_g T_\infty^*}\right) e^{\xi/2\gamma} - \alpha\right] e^{-\xi} d\xi \tag{8-31}$$

where

$$\xi = \frac{hg}{R_g T_\infty^*} \tag{8-32}$$

Carrying out the integration yields

$$\int_0^h R\rho_\infty dh = 2\gamma \rho_{\infty_i}\left(\frac{R_g T_\infty^*}{g}\right)^2 \left[2\left(\alpha + \frac{gR_i}{2\gamma R_g T_\infty^*}\right)\left(\frac{2\gamma}{2\gamma - 1}\right)\left[1 - e^{-\xi(2\gamma-1)/2\gamma}\right] - \alpha\left(1 - e^{-\xi}\right)\right]$$

Thus

$$F(h) = 8\alpha\gamma \left(\frac{R_g T_\infty^*}{g}\right)\rho_{\infty_i}\left[\left(\alpha + \frac{gR_i}{2\gamma R_g T_\infty^*}\right) e^{\xi/2\gamma} - \alpha\right]\frac{e^{-\xi}}{D} \tag{8-33}$$

$$D = \overline{\rho}_i R_i^2 + 4\alpha\gamma\left(\frac{R_g T_\infty^*}{g}\right)^2 \rho_{\infty_i}\left[2\left(\alpha + \frac{gR_i}{2\gamma R_g T_\infty^*}\right)\left(\frac{2\gamma}{2\gamma - 1}\right)\left[1 - e^{-\xi(2\gamma-1)/2\gamma}\right] - \alpha\left(1 - e^{-\xi}\right)\right]$$

$$G(h) = \frac{2g\left(\frac{2\gamma R_g T_\infty^*}{g}\right)^2 \rho_{\infty_i}\left[\left(\alpha + \frac{gR_i}{2\gamma R_g T_\infty^*}\right) e^{\xi/2\gamma} - \alpha\right]^2 e^{-\xi}}{D} - 2g \tag{8-34}$$

94

A formal mathematical solution can be obtained in the form

$$w^2 = e^{-\int F(h)\,dh}\left[\int G(\eta)\,(e^{\int F(h)\,dh})\,d\eta_i + C\right] \qquad (8-35)$$

subject to the initial condition

$$w = 0 \qquad \text{at} \qquad t = t_i$$

We have chosen to do the solution numerically for our case.

8.4 Calculative Example for a Supersonic Airplane and Comparisons with Data and Theory

Once the wake is a short distance behind a supersonic airplane, it has subsonic velocity with respect to an observer on the ground. It is thus expected that a subsonic buoyant wake theory should be applicable to the supersonic airplane case. For the purpose of illustration, we now present two example calculations for an example supersonic airplane using the following parameters:

Initial altitude: 70,000 ft (21.3 km.)

Flight speed: 2,670 ft/sec (815 m./sec)

Wake temperature rise: $9.3^{\circ}F$ $(5.16^{\circ}C)$

Free-stream temperature: $T_{\infty}^{*} = 392.3^{\circ}R$ $(217.9^{\circ}K)$

Entrainment coefficients: $\alpha = 0.3$ and $\alpha = 0.9$

Initial radius: $R_i = 42.7$ ft (13.0 m.)

Initial density: $\rho_{\infty_i} = 0.0001389$ slug/ft^3

Ratio of specific heats: $\gamma = 1.4$

The various characteristic lengths used in the Fay-Overcamp theory of reference 8-1 are estimated to be

$\ell_b = 1.90 \times 10^{-4}$ ft

$d_b = 163,500$ ft

$\ell = 172.5$ ft

The calculations have been made by determining R as a function of h from equation (8-22). The vertical velocity w was determined as a function of h by integrating equation (8-25) numerically. The time scale has been established by the equation

$$t = \int_0^t \frac{dh}{w}$$

The radius R has been nondimensionlized in the form $2R/\ell$ and the
distance x in the form x/d_b so that the results can be presented
on figure 8-1 for comparison on the data and the Fay-Overcamp theory.

First the comparison of the present calculations with the theory of
Fay and Overcamp, equation (8-6), shows generally fair agreement within the
middle of the range. The slope of the Fay and Overcamp theory is slightly
larger in the mid-range. At small values of x/d_b there is a divergence
between the theories because of the difference in initial conditions. For
large values of x/d_b the present calculations show a peak at approximately
$x/d_b = 2.5$. The Brunt-Väisällä frequency for the present case of 0.021
radians/second yields a value of $x/d_b = 2.45$ for π radius. The theo-
retical solution thus peaks at just about this value. However, the power
law, equation (8-6), does not exhibit a peak value of R. It is noted
that the final radius of the wake is about 50 percent greater for $\alpha = 0.9$
than for $\alpha = 0.3$.

With regard to comparison between the present calculations and the
correlated data, several points are significant. In the intermediate
range the slope of the data points is about twice that of the theory.
One point of interest is that the values of x/d_b corresponding to π
radians for the data of figure 8-1 varies between 0.62 to 0.84. Yet no
maximum value of R occurs experimentally for values of x/d_b much
greater than these values. It thus appears that there are significant
physical factors not accounted for in the present buoyancy model. It is
also of interest that the value of x/d_b for π radius is 3 to 4 times
larger for the supersonic case considered here than for the subsonic
cases shown.

The results for $\alpha = 0.3$ and $\alpha = 0.9$ show about a four-fold and a
six-fold overall increase in wake radius at the peaks, respectively,
due to wake entrainment. The value of $\alpha = 0.3$ corresponds to a com-
pletely quiescent atmosphere. This value was obtained from the work of
Tsang on line thermals described in reference 8-5. By placing a cylinder
containing heavier fluid horizontally in a tank of lighter fluid and
suddenly withdrawing the cylinder horizontally he created an initial

condition of a cylindrical mass of fluid of higher density in a surrounding fluid of lower density without disturbing the fluid. His mean value of α obtained from his figure 10 yields $\alpha = 0.33$. Richards, reference 8-6, performed similar tests but did not take sufficient care to minimize initial disturbances. His values of α range from 0.316 to 0.67. It is thus apparent that the value of α can be doubled by moderate initial disturbances. We have used $\alpha = 0.9$ as an approximation for the real stratosphere.

There is evidence, as pointed out above, of serious shortcomings in present buoyant wake models. One factor which has received scant attention is the role of changing vortex strength during the buoyant rise. During entrainment circulation is induced in the recirculation region of opposite sign to that existing just behind the aircraft. Account should be taken of this phenomenon in the fluid mechanical model and possibly in the energy equation.

Overcamp and Fay (ref. 8-1) on the basis of their theoretical analysis and contrail and towing tank experiments concluded that, far downstream from the aircraft, buoyancy is the dominant mechanism affecting the growth of the wake. They compared their calculations and towing tank data with flight data of the visible horizontal width of persistent contrails from three different subsonic aircraft. Conti, et al., in reference 8-2, considered the possible influences of wind shear, wake collapse, turbulent diffusion and buoyancy on dispersion of the wake. For purposes of modeling they treated each mechanism separately and by linear superposition they concluded that the relative significance of each of the mechanisms was as follows: collapse, 0.33; shear, 0.43; buoyancy, 0.08 and turbulence, 0.16. These calculations were based upon the B-52 wake width measurements, and they postulated that the effect of buoyancy would be relatively insignificant when compared to the other dispersion mechanisms. The information which is presently available on wake dimensions in the final dispersion phase is so scant that it becomes a matter of conjecture as to which mechanism, if any, is the most significant.

It is clear from the above discussion that further experiments are required to resolve the problems of buoyant wakes. Flight data of wake dimensions together with local stratospheric turbulence and wind conditions should help clarify the issue but until these are obtained, we must rely on laboratory and wind-tunnel experiments to clarify the problem.
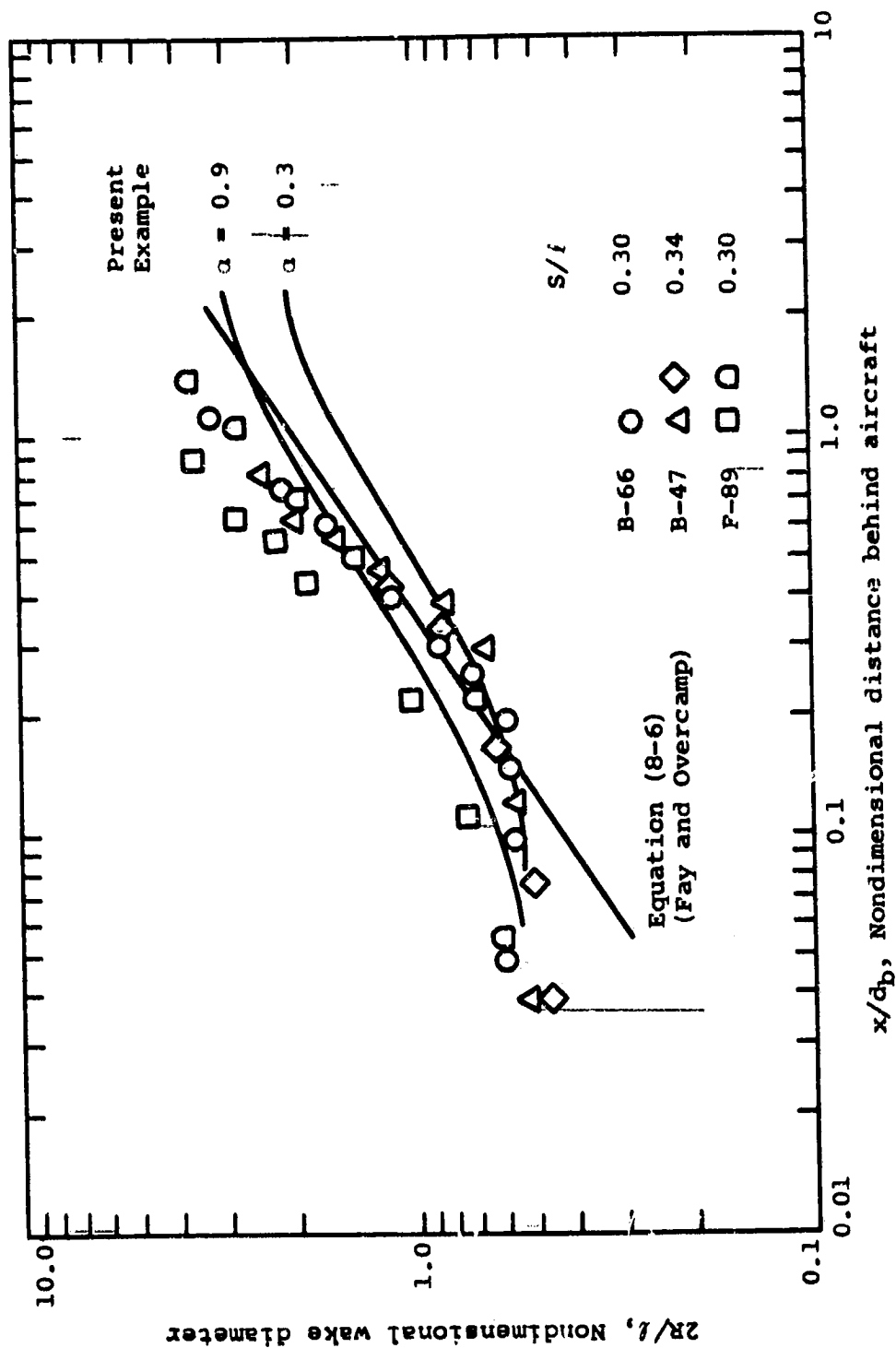
Figure 8-1. Comparison of buoyancy theories with subsonic contrail data.

98

9.0 CALCULATIVE EXAMPLE

9.1 Introduction

In order to show the application of the foregoing theoretical work, it will now be applied to an illustrative example of a supersonic aircraft flying in the stratosphere. For illustrative purposes, we will assume an airplane of wing span 59 feet flying at an altitude of 70,000 feet at a Mach number of 2.75. It will be assumed that the wing is elliptically loaded and the airplane weight is 100,000 pounds. With regard to the propulsion system, it is assumed that the engine exits are located on the wings with their centerlines at the middle of the semispans.

In the ensuing example, we will calculate the wake characteristics at the various stages using the theories developed in Sections 4 to 8. It is assumed that the atmospheric properties are given by the standard atmosphere as listed in reference 9-1.

9.2 Pure Jet Phase

A calculative example for supersonic flight has been carried out using the theory and correlation curve given in figure 4-2. The following initial jet conditions have been assumed:

$$M_\infty = 2.75 \qquad M_j = 2.53 \qquad T_{O_\infty} = 0.308 \qquad U_\infty = 0.575$$

For future reference the calculated results have been tabulated in Table 9-I in nondimensional form. This table shows that the length of the potential core is about 66.4 nozzle-exit radii. The calculations have been carried to a distance farther downstream than the point where entrainment of jets by the vortices has become complete. The column headed E_m/E_z shows how well the law of the conservation of energy has been fulfilled by its closeness to unity. The terms U_{ave}/U_∞ and T_{ave}/T_∞ give the mass average jet velocity and temperature at the various axial positions. The ratio V_r/U_∞ shows the magnitude of the radial velocity at the edge of the jet.

For illustrative purposes we show the variations in centerline temperature and mass average cross-sectional temperature in figure 9-1 as taken from Table 9-I. The centerline temperature is constant until the end of the potential core and decreases fairly rapidly thereafter. The

99

average temperature starts to fall immediately because of the high density free-stream air being entrained initially. The average temperature is much lower than the centerline temperature and decreases fairly slowly after the end of the potential core.

It is possible to determine the local relative concentration of the exhaust gases as a fraction of their concentrations at the engine exit (i.e., its mass fraction). If we assume that the various gas components of the engine exhaust remain in the same relative proportions, then the relative concentration or mass fraction, c, of the exhaust gases is given by equation (4-77). The mass fraction, c, has been determined with the help of Table 9-I to obtain concentration profiles at two axial stations. These profiles of relative concentration are shown in figure 9-2 for an axial station at the end of the potential core and an axial station at 138 exit radii downstream of the exit.

9.3 Initial Interaction

The initial interaction equations (5-18) through (5-21) have been integrated downstream to the point of strong interaction between vortex and jet using the above initial jet conditions and the following aircraft parameters and geometry:

Jet downward inclination: 4.9°

Circulation parameter: K_o = 935 ft^2/sec = 87 meters^2/sec

Span: b = 59 ft = 18 meters

Nozzle radius: r_n^* = 3 ft = 0.915 meter

with the jet nozzle assumed to be located at half the semispan of the wing. The results of these integrations are shown in figures 9-3 and 9-4. Figure 9-3 is a side view of the vertical positions of the jet and right-wing panel vortex centroid, as they proceed downstream, observed from an inertial coordinate system attached to the trailing edge of the aircraft. The jet closely follows its initial downward slope of 4.9° for approximately 12 meters (40 ft) and then, due to both the entrainment of free-stream air and the action of crossflow drag, rapidly begins to align itself in the free-stream direction. The vortex centroid proceeds downward at an initially slow and uniform rate, but begins to move much faster at approximately $z^* = z \cdot r_n^*$ = 60 meters (200 ft), indicating that the vortex

100

and jet are interacting strongly at this location. This interaction is most clearly observed in figure 9-4 which shows the crossflow plane view of the motions. The effect of crossflow drag and ingested free-stream air in slowing the initial downward motion of the jet is also evident from the relative spacing of the jet trajectory points. While the calculation has been carried to $z^* = 73$ meters (240 ft), it is clear that the jet and concentrated vortex have begun to interact strongly somewhat upstream of this location, at approximately $z^* = 60$ meters (200 ft). Consequently, the process of jet break-up and ingestion into the vortex recirculation region should be started at or upstream of $z^* = 60$ meters for this particular example.

9.4 Jet Disintegration

The differential equations (6-1) through (6-4) describing the jet disintegration process have been applied to the present example at various longitudinal positions at and upstream of the location where the initial interaction calculations indicate strong interaction. In these results, shown in figures 9-5(a) through 9-5(c), the jet has been subdivided into five equal-area segments, with initial crossflow plane locations and velocities provided by the initial interaction results. In order to facilitate visualization of the ingestion process, the results are presented in vortex coordinates. Figure 9-5(a) shows the crossflow plane trajectories of the hot gas segments when the break-up process is initiated at $z^* = 59.6$ meters (195 ft). The trajectory points correspond to Δz^* increments of 9.1 meters (30 ft), and the calculations for a particular segment are terminated when that segment approaches within 0.3 meter (1 ft) of the vortex centerline. These results indicate that all of the hot gas segments are captured by the vortex at approximately $z^* \sim 120$ meters (400 ft).

In order to illustrate the sensitivity of the break-up process to the assumed point of its initiation, figures 9-5(b) and 9-5(c) have been prepared showing the hot gas trajectories when the break-up process is initiated at $z_i^* = 46$ meters (150 ft) and 23 meters (75 ft), respectively. Figure 9-5(b) shows that when $z_i^* = 46$ meters, a point clearly upstream of the strong interaction location, all of the hot gas is still captured by the vortex, with all the hot gas spiralling in toward the core. Figure 9-5(c) displays the analogous results for $z_i^* = 23$ meters, a point

101

slightly more than one wing span of the trailing edge. These results indicate that even if the break-up process is started at this very early stage, 60 percent of the gas will be ingested into the vortex recirculation region. Consequently, for the parameters and initial conditions of this example, the present theory indicates that the vortex pair will capture all of the hot jet exhaust within essentially 120 meters (6-7 wing spans) downstream of the trailing edge.

9.5 Equilibrium Vortex Phase

It is of interest first to look at the characteristics of the trailing-vortices-before ingestion of the hot-jet into its center as a guide to evaluating the effects of such ingestion. First let us determine its tangential velocity profile and its temperature distribution. In determining its tangential velocity distribution it is necessary to obtain an approximate idea of its core diameter and its maximum tangential velocity. It has been found in such papers as references 9-2 and 9-3 that the core diameters are relatively insensitive to angle of attack. It has also been found that for a Convair-990 wing model, the core diameter is about twice as large as that for a rectangular wing. The loading on the wing of the Convair 990 model is probably fairly representative of an elliptical span loading. From a measurement of $r_1 = 1.1$ inches (2.8 cms) for a rectangular wing of 8 feet (2.44 m) span, the scaling by a factor of 2 to a 59-foot span wing yields

$$r_1 = 1.4 \text{ feet } (0.43 \text{ m.})$$

With regard to maximum tangential velocity, Orloff and Grant (ref.9-2) find that the maximum tangential velocity as a fraction of V_∞ scales linearly with angle of attack for a rectangular wing. This agrees with the finding of constant core diameter and a constant nondimensional velocity field in planes perpendicular to the vortex axis with V_∞ as the nondimensionalizing quantity. Also, the work of Corsiglia, Schwind and Chigier (ref. 9-3) show that there is little decay of the peak tangential velocity with axial distance up to 31 span lengths behind the wing. An estimate of the maximum tangential velocity for both the rectangular wing and the Convair 990 model is given by

$$\frac{v_1}{c_L V_\infty} = 0.8 \tag{9-1}$$

This yields a value of v_1 for the present cases of

$$v_1 = 271 \text{ ft/sec } (83 \text{ m/sec})$$

Thus

$$K_1 = (1.4)(271) = 379 \text{ ft}^2/\text{sec } (35.2 \text{ m}^2/\text{sec})$$

Based on these values and equations (7-1) to (7-3) the nondimensional tangential velocity distribution shown in figure 9-6 has been calculated. In the wake region, the extension of the law of the logarithmic region is shown since this approximation has been used in the theory of Section 7.

We now apply equation (7-40) to determine the temperature distribution in the trailing vortex before hot gas ingestion. The results are shown in figure 9-7. The theory shows that the static temperature reaches a minimum at the eye, and is constant in the eye.

Consider now the effect of hot gas ingestion into the vortex. The hot gas is completely ingested at 133 exit radii assuming the break-up starts at 65 exit radii at the end of the potential core. Between these limits we have the following approximate quantites for the pure jet

z	T_{ave}^*/T_∞^*	r_e^*/r_n^*	c_{ave}	r_e^*	$(T_{ave}^* - T_\infty^*)$	r_e^*
66	1.53	1.784	0.205	5.23 ft	208°F (116°C)	1.6 m.
138	1.34	2.10	0.133	6.3 ft	134°F (75°C)	1.93 m.

We now use these values to estimate the temperatures and concentrations at the end of ingestion. During ingestion the question arises whether the rate of mixing with free-stream air is increased or decreased with respect to the mixing rate of the free jet. During ingestion the air tends to move into the center and displace the air in the inner region of the vortex. The free-jet calculations show a decrease in average mass fraction from 0.205 to 0.133 over the length of the ingestion process. The effect of the vortex is generally to inhibit entrainment of air into the center of the vortex. Accordingly, it is thought that the average mass fraction in the vortex center at the end of jet ingestion will be between the two values quoted above.

Several other points now need to be made. First the radius of the ingested hot gas is now 6.3 feet (1.93 m.) versus a core radius without ingestion of about 1.4 feet (0.43 m.). It is clear that the whole structure of the cold vertex can be changed as a result of ingestion. The possibility of vortex bursting cannot be dismissed. Additional analysis of the vortex with the hot gas core has not been made. However, at $r = 6.3$ feet the temperature drop associated with the turbulent vortex solution will yield a very small drop in temperature (fig. 9-7) so that no substantial cooling of the gas from $134^{\circ}F$ above the free-stream temperature should occur. Accordingly, the center of the vortex out to a radius of 6.3 feet should have an average temperature approximately $149^{\circ}F$ above the free stream at the end of ingestion, and all the exhaust gas should be trapped in this radius with an average concentration equal to or greater than 0.133 of its value at the jet exit.

One can now ask the question of how fast the hot gas core will cool off as the equilibrium vortex phase continues. In order to answer this question precisely, we must know how the vortex structure was changed as a result of hot gas ingestion. (What changes occur in r_1 and K_1?) Unsteady momentum and heat transfer analyses of the vortex are necessary to answer this question. Whether unsteady heat transfer effects would be significant before the buoyancy phase starts within ten seconds is not known. Thereafter the vorticity distribution will be altered by the mass entrainment associated with buoyant rise of the recirculating fluid.

We expect a slow approach of the vortex with a hot core to the thermal equilibrium temperature distribution derived in Section 7 through analogy with the slow diffusion of vorticity from an equilibrium turbulent vortex. The diffusion of heat and of vorticity should have comparable time scales for a turbulent vortex. Diffusion of vorticity has been studied in reference 9-4, and a numerical example has been carried out. The vorticity in the recirculation region can diffuse outward across the enclosing streamline or it can diffuse to the vertical plane of symmetry where it is annihilated by symmetry. For the particular example considered in reference 9-4, it was found it took more than an hour for the vorticity in one half of the recirculation region to decrease by $1/e$. It is thus probable that the hot gas in the vortex center remains hot and concentrated until the onset of the buoyancy phase and possibly for some time thereafter.

9.6 Asymptotic Buoyant Phase

In connection with the question of when the asymptotic buoyancy phase starts, Fay and Overcamp, ref. 9-5, define a characteristic time t_c

$$t_c = \frac{2 \rho_\infty U_\infty^* b''}{L} \qquad (9-2)$$

ρ_∞ = air mass density b = airplane span

U_∞^* = airplane speed L = airplane lift

Their data from contrail measurements, figure 1 of their reference, shows that the buoyancy phase, measured by the onset of significant increase in contrail width, occurs at a time of about $2t_c$

For the supersonic example being considered herein the characteristic time t_c is only 4.8 seconds so that the onset of the buoyancy phase starts at about 9.6 seconds at a distance about 25,000 feet behind the aircraft. (This short elapsed time is another reason that the hot gas in the center of the vortex has little time to cool down during the equilibrium vortex phase.)

The initial conditions for the buoyancy calculations include the following:

Δt = average wake temperature rise due to engine heat

R_i = initial wake radius (assumed circular)

ρ_{∞_i} = initial atmospheric mass density

T_∞^* = atmospheric temperature (constant at $392.3^\circ R$) $(218^\circ K)$

α = entrainment coefficient

$$\bar{\rho}_i = \frac{\rho_{\infty_i} T_\infty^*}{T_\infty^* + \Delta t} = \text{initial average mass density of wake}$$

The value of Δt can be determined from the following formula based on the assumptions that all of the engine heat goes into the wake and the span loading is elliptical.

$$\Delta t = 0.288 \frac{C_D (U_\infty^*)^2}{\eta \; \cancel{R} \; c_p} \tag{9-3}$$

C_D = airplane drag coefficient

$\cancel{R}$ = b^2/wing reference area

η = efficiency of conversion of engine heat into propulsion

c_p = specific heat of air in mechanical work units per unit mass per degree

For our example case, the following numbers were used:

$\Delta t = 9.3^\circ F \; (5.16^\circ C)$

$R_i = 43$ feet (13.1 m)

$\rho_{\infty_i} = 0.0001389$ slugs/ft^3, (h $\approx$ 70,000 ft)

$T_\infty^* = 392.3^\circ R$

$\alpha = 0.3$ and 0.9

Equation (8-24) was integrated using the above input quantities for the two entrainment coefficients, and the calculated results are tabulated in Table 9-II up to the time the wake reaches its maximum rise. It is noted that the static temperature rise for the present example is much larger than the fractional part of a degree usually found for subsonic aircraft. This result is a consequence of the greater speed and lower aspect ratio as shown by the above formula. Table 9-II shows, however, that the average temperature of the wake is almost equal to that of the atmosphere at the end of the buoyant rise.

Inspection of Table 9-II shows that the increase in radius of the wake due to entrainment is given closely by αh for the entire range of the tables. The rate of entrainment is greater for the larger entrainment coefficient as shown in figure 9-8(a), but the increase is not proportional to α. The vertical rise shown in figure 9-8(b) is slower for the large entrainment coefficient as would be expected because the same initial buoyant force must now act on more fluid. The decreased vertical velocity

tends to make the rate of entrainment less than proportional to α. The results for $\alpha = 0.3$ are believed to be representative of a quiescient stratosphere, and thus only represent an idealized extreme of the real stratosphere. The results for $\alpha = 0.9$ are considered more representative of real stratospheric effects until better data on entrainment coefficients for line thermals in the stratosphere are available.

The question of what the concentration of the exhaust gases is during the buoyancy phase cannot be answered at this point. Since the buoyancy phase starts after about 10 seconds, it is probable that no significant decay of the trailing vorticity[1] has occurred; and that the hot gases at the center of the vortices have not diffused significantly. With the onset of the buoyant rise, a new induced circulation pattern is imposed on the recirculating fluid which tends to oppose the trailing vortices. At least this is the deduction one would make from the results of Tsarg (ref. 8-5) which show that a horizontal cylinder of denser fluid initially with no circulation develops a vortex pair of the opposite sense of the trailing vortices as they move under the influence of buoyancy. This generated vorticity varies theoretically as $t^{1/3}$ for constant density external to the region (ref. 8-5). A detailed analysis of the buoyant wake considering the initial trailing vortex circulation should be made to study the details of the turbulent mixing process. An experimental study of this problem would also be extremely valuable.

It is of interest for chemical studies to know the actual distribution of temperatures to which the exhaust gases are subject during the buoyant phase. No attempt to determine this distribution was made in the present work. Upper and lower bounds on the temperature of the exhaust gases can however be given. A lower bound on the temperature and mass fraction of the exhaust gas can be calculated on the basis of the assumption of homogeneous gases in the recirculation region. An upper bound would be given by assuming that the exhaust gases are frozen in the vortex cores at the temperature and mass fraction corresponding to the end of hot gas ingestion.

---

[1] Vortex bursting would probably not diffuse vorticity from the recirculation region although the Crow instability could break up the recirculating region.

TABLE 9-I.- JET MIXING RESULTS

$M_j = 2.53$, $M_\infty = 2.75$, $T_{o_\infty} = 0.308$, $U_\infty = 0.575$

η	r_e	r_d	r_i	$\dfrac{U_c}{U_\infty}$	$\dfrac{T_c}{T_\infty}$	M_c	$\dfrac{E_m}{E_z}$	$\dfrac{U_{ave}}{U_\infty}$	$\dfrac{T_{ave}}{T_\infty}$	$\dot{m}_a$	$\dfrac{V_r}{U_\infty}$
0.00	1.000	1.000	1.000	1.740	3.578	2.53	1.000	1.740	3.578	0.00	.00124
5.00	1.058	0.994	0.937	1.740	3.578	2.53	0.981	1.607	3.115	0.220	.00113
10.00	1.117	0.989	0.870	1.740	3.578	2.53	0.977	1.508	2.769	0.457	.00108
15.00	1.176	0.982	0.802	1.740	3.578	2.53	0.980	1.433	2.509	0.710	.00100
20.00	1.235	0.977	0.730	1.740	3.578	2.53	0.977	1.375	2.305	0.975	.00097
25.00	1.294	0.970	0.658	1.740	3.578	2.53	0.979	1.328	2.143	1.257	.00092
30.00	1.353	0.963	0.582	1.740	3.578	2.53	0.980	1.290	2.012	1.554	.00089
35.00	1.411	0.960	0.505	1.740	3.578	2.53	0.976	1.259	1.904	1.851	.00088
40.00	1.469	0.953	0.426	1.740	3.578	2.53	0.976	1.234	1.814	2.166	.00087
45.00	1.525	0.948	0.346	1.740	3.578	2.53	0.976	1.212	1.739	2.487	.00087
50.00	1.580	0.942	0.265	1.740	3.578	2.53	0.975	1.194	1.676	2.810	.00087
55.00	1.633	0.939	0.183	1.740	3.578	2.53	0.973	1.179	1.623	3.133	.00088
60.00	1.684	0.928	0.101	1.740	3.578	2.53	0.978	1.166	1.577	3.474	.00089
66.42	1.744	0.927	0.000	1.740	3.578	2.53	0.973	1.152	1.530	3.860	.00165
70.78	1.767	0.924		1.714	3.488	2.525	0.976	1.147	1.513	4.016	.00164
75.20	1.790	0.921		1.689	3.401	2.520	0.976	1.143	1.497	4.179	.00154
79.68	1.814	0.918		1.666	3.319	2.515	0.976	1.138	1.482	4.340	.00150
84.21	1.837	0.916		1.643	3.241	2.510	0.976	1.134	1.468	4.506	.00145
88.81	1.861	0.913		1.622	3.167	2.507	0.976	1.130	1.454	4.674	.00141
93.46	1.884	0.910		1.602	3.096	2.505	0.976	1.126	1.441	4.845	.00137
98.17	1.907	0.907		1.582	3.028	2.500	0.976	1.123	1.428	5.019	.00133
117.60	2.003	0.896		1.512	2.783	2.492	0.976	1.109	1.381	5.754	.00119

TABLE 9-I. - CONTINUED.

z	r_e	r_d	r_i	$\dfrac{U_c}{U_\infty}$	$\dfrac{T_c}{T_\infty}$	M_c	$\dfrac{E_m}{E_z}$	$\dfrac{U_{ave}}{U_\infty}$	$\dfrac{T_{ave}}{T_\infty}$	$\dot{m}_a$	$\dfrac{V_r}{U_\infty}$
138.00	2.100	0.888		1.453	2.577	2.490	0.977	1.098	1.342	6.539	.00107
159.37	2.198	0.875		1.403	2.402	2.487	0.978	1.088	1.307	7.382	.00097
181.73	2.299	0.864		1.359	2.251	2.492	0.979	1.080	1.277	8.288	.00088
199.16	2.377	0.857		1.331	2.152	2.495	0.980	1.074	1.257	9.015	.00082
217.18	2.455	0.850		1.305	2.063	2.502	0.980	1.069	1.239	9.777	.00077
242.12	2.561	0.841		1.275	1.957	2.482	0.981	1.062	1.217	10.855	.00071
261.57	2.643	0.834		1.255	1.886	2.512	0.982	1.058	1.203	11.715	.00066
281.57	2.726	0.828		1.236	1.822	2.517	0.983	1.054	1.189	12.618	.00062
302.22	2.810	0.822		1.219	1.764	2.525	0.984	1.051	1.177	13.569	.00059
323.51	2.896	0.861		1.204	1.711	2.532	0.984	1.047	1.166	14.568	.00056
338.06	2.955	0.813		1.195	1.679	2.536	0.985	1.045	1.158	15.262	.00054
360.44	3.043	0.807		1.182	1.633	2.543	0.986	1.043	1.149	16.346	.00051
383.49	3.133	0.802		1.170	1.591	2.552	0.986	1.140	1.139	17.484	.00048
407.15	3.226	0.797		1.159	1.553	2.557	0.987	1.137	1.130	18.688	.00046
456.49	3.416	0.788		1.139	1.484	2.571	0.988	1.033	1.116	21.263	.00041
508.71	3.613	0.780		1.122	1.426	2.589	0.989	1.029	1.103	24.102	.00037
545.17	3.748	0.775		1.113	1.393	2.593	0.990	1.027	1.095	26.137	.00035
602.43	3.956	0.768		1.100	1.348	2.606	0.991	1.024	1.085	29.412	.00032
642.33	4.097	0.764		1.093	1.322	2.613	0.991	1.023	1.079	31.750	.00030
704.87	4.314	0.758		1.083	1.288	2.624	0.992	1.020	1.071	35.492	.00027
748.38	4.461	0.755		1.077	1.267	2.631	0.993	1.019	1.066	38.148	.00025
793.36	4.611	0.751		1.071	1.249	2.636	0.993	1.018	1.062	40.938	.00024

TABLE 9-I.- CONCLUDED.

z	r_e	r_d	r_i	$\dfrac{U_c}{U_\infty}$	$\dfrac{T_c}{T_\infty}$	M_c	$\dfrac{E_m}{E_z}$	$\dfrac{U_{ave}}{U_\infty}$	$\dfrac{T_{ave}}{T_\infty}$	$\dot{m}_a$	$\dfrac{v_r}{U_\infty}$
838.86	4.763	0.748		1.067	1.232	2.641	0.994	1.016	1.057	43.864	.00023
912.46	4.995	0.744		1.060	1.210	2.651	0.994	1.015	1.052	48.510	.00021
962.80	5.152	0.742		1.056	1.196	2.656	0.994	1.014	1.049	51.782	.00020
1014.72	5.311	0.739		1.053	1.184	2.662	0.995	1.013	1.046	55.193	.00019

110

TABLE 9-II.- BUOYANT PHASE CALCULATIONS FOR EXAMPLE CASE.

$$\alpha = 0.3$$

t	h		w		R		R/R_i	T̄
Min.	Feet	Meters	Feet/Sec	Meters/Sec	Feet	Meters		°R
0.00	0.00	0.00	0.00	0.000	42.7	13.0	1.00	401.83
0.10	12.50	3.81	3.88	1.184	46.5	14.2	1.09	400.26
0.15	25.00	7.62	4.88	1.488	50.2	15.3	1.18	399.03
0.22	50.00	15.24	5.62	1.712	57.7	17.6	1.35	397.21
0.37	100.00	30.48	5.68	1.732	72.8	22.2	1.70	395.20
0.52	150.00	45.72	5.30	1.615	87.9	26.8	2.06	394.07
0.69	200.00	60.96	4.81	1.466	103.0	31.4	2.41	393.35
0.87	250.00	76.20	4.28	1.305	118.0	36.0	2.76	392.83
1.08	300.00	91.44	3.70	1.129	133.2	40.6	3.12	392.52
1.33	350.00	106.68	3.05	0.929	148.3	45.2	3.47	392.24
1.64	400.00	121.92	2.22	0.677	163.4	49.8	3.83	391.99
1.86	425.00	129.54	1.66	0.507	171.0	52.1	4.00	391.88
2.20	450.00	137.16	0.77	0.236	178.6	54.4	4.18	391.82
2.41	456.25	139.07	0.23	0.071	180.4	55.0	4.23	391.76

Table 9-II.- Concluded.

$\alpha = 0.9$

| t	h		w		R		R/R$_i$	$\overline{T}$
Min.	Feet	Meters	Feet/Sec	Meters/Sec	Feet	Meters		°R
0.00	0.00	0.00	0.00	0.000	42.7	13.0	1.00	401.83
0.11	12.50	3.81	3.11	0.949	54.0	16.5	1.26	397.88
0.17	25.00	7.62	3.36	1.025	65.2	19.9	1.53	396.20
0.23	37.50	11.43	3.31	1.008	76.5	23.3	1.79	395.11
0.30	50.00	15.24	3.17	0.967	87.8	26.8	2.06	394.41
0.37	62.50	19.05	3.02	0.919	99.0	30.2	2.32	393.89
0.44	75.00	22.86	2.86	0.872	110.3	33.6	2.58	393.51
0.51	87.50	25.67	2.71	0.825	121.6	37.1	2.85	393.19
0.59	100.00	30.48	2.56	0.779	132.9	40.5	3.11	393.01
0.67	112.50	34.29	2.41	0.734	144.1	43.9	3.38	392.83
0.76	125.00	38.10	2.26	0.690	155.4	47.4	3.64	392.68
0.86	137.50	41.91	2.12	0.646	166.7	50.8	3.90	392.59
0.96	150.00	45.72	1.97	0.601	178.0	54.3	4.17	392.46
1.07	162.50	49.53	1.82	0.554	189.3	57.7	4.43	392.39
1.19	175.00	53.34	1.66	0.505	200.6	61.1	4.70	392.31
1.32	187.50	57.15	1.48	0.452	211.9	64.6	4.96	392.26
1.47	200.00	60.96	1.29	0.393	223.2	68.0	5.23	392.18
1.65	212.50	64.77	1.05	0.324	234.5	71.5	5.49	392.12
1.88	225.00	68.58	0.78	0.237	245.8	74.9	5.76	392.07
2 27	237.50	72.39	0.29	0.088	257.1	78.4	6.02	392.04

112
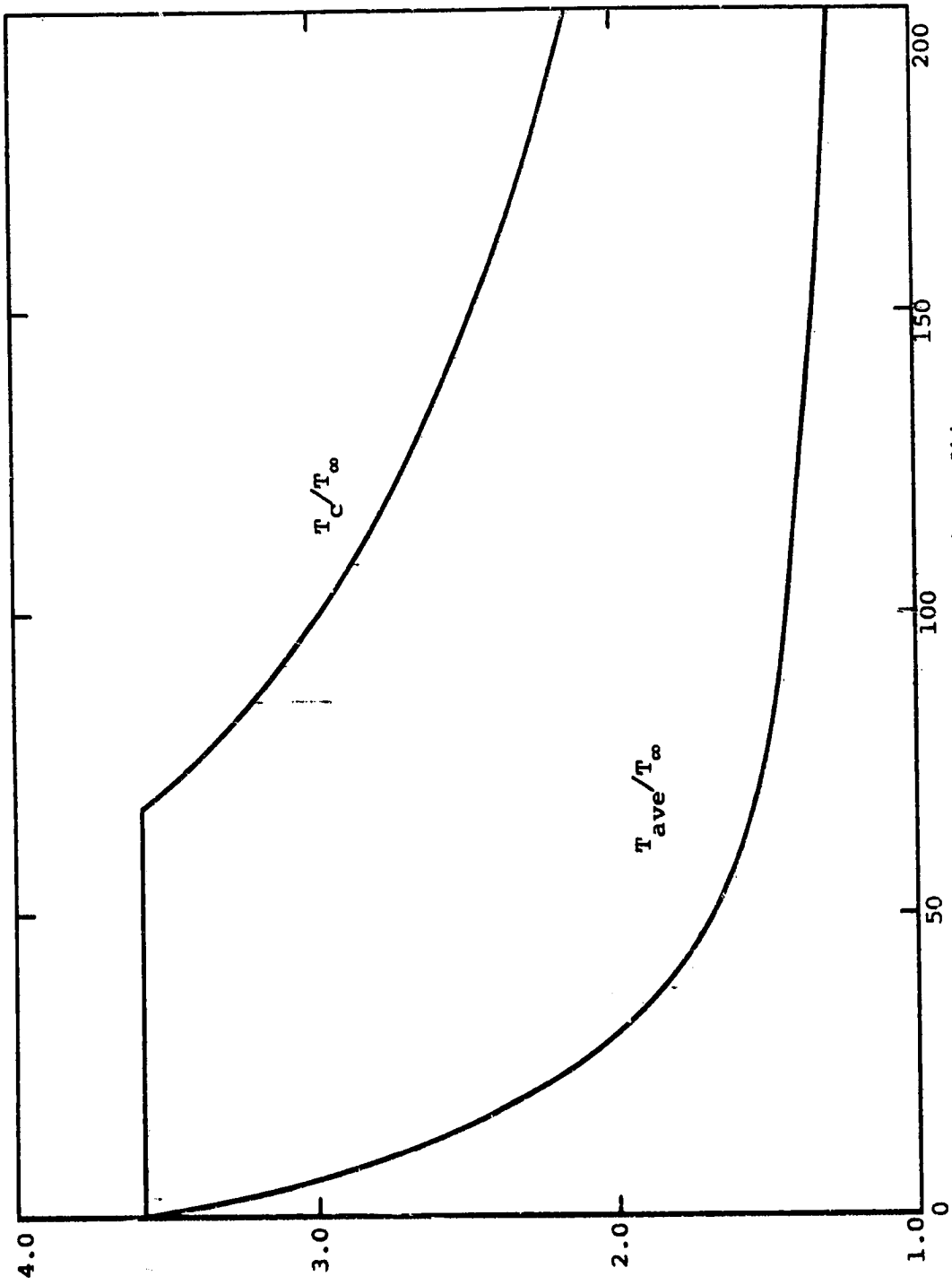
Figure 9-1.- Axial distributions of centerline and average temperature.

113
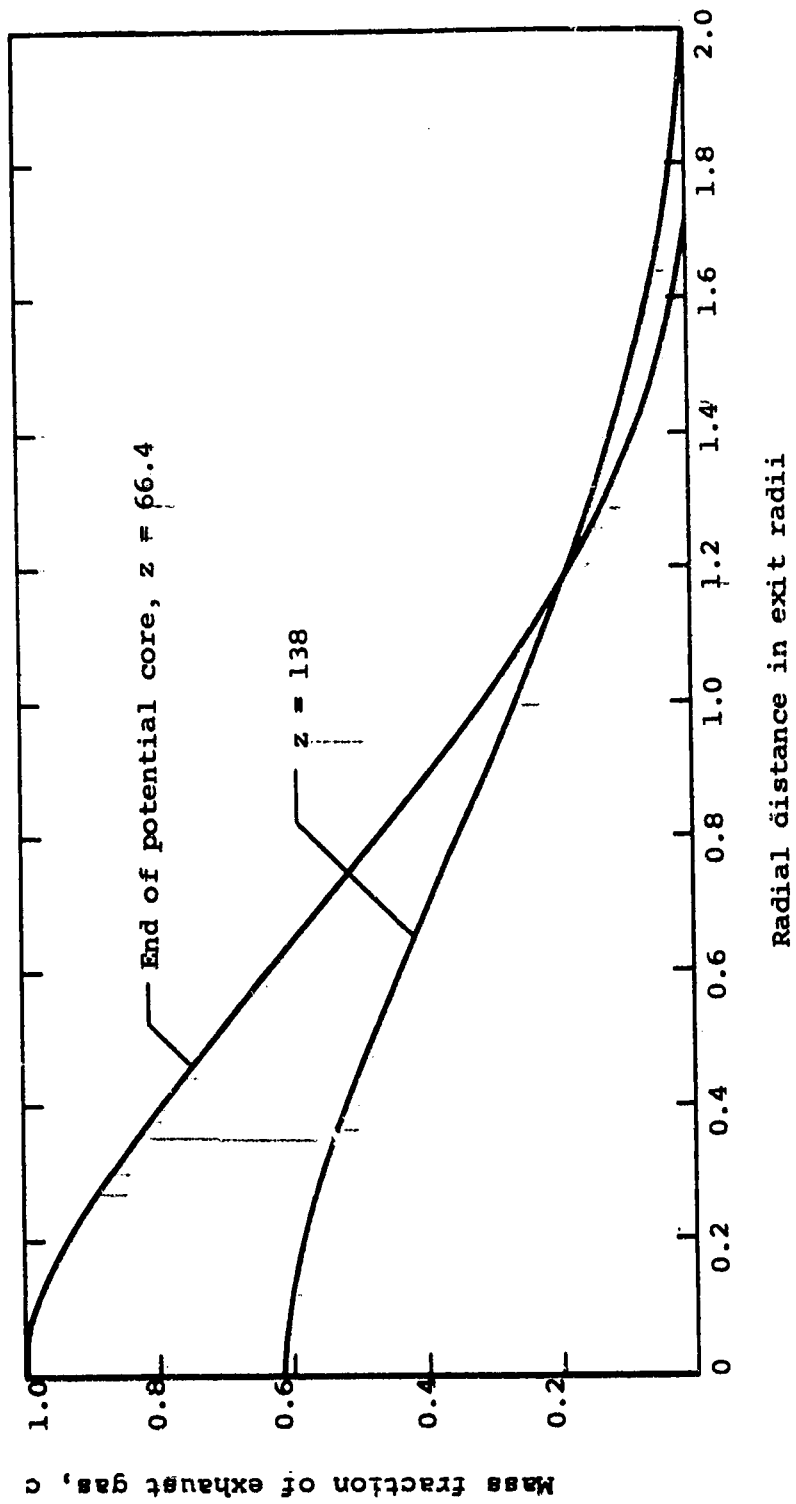
Figure 9-2.- Representative profiles of relative concentration
in pure jet stage.

114
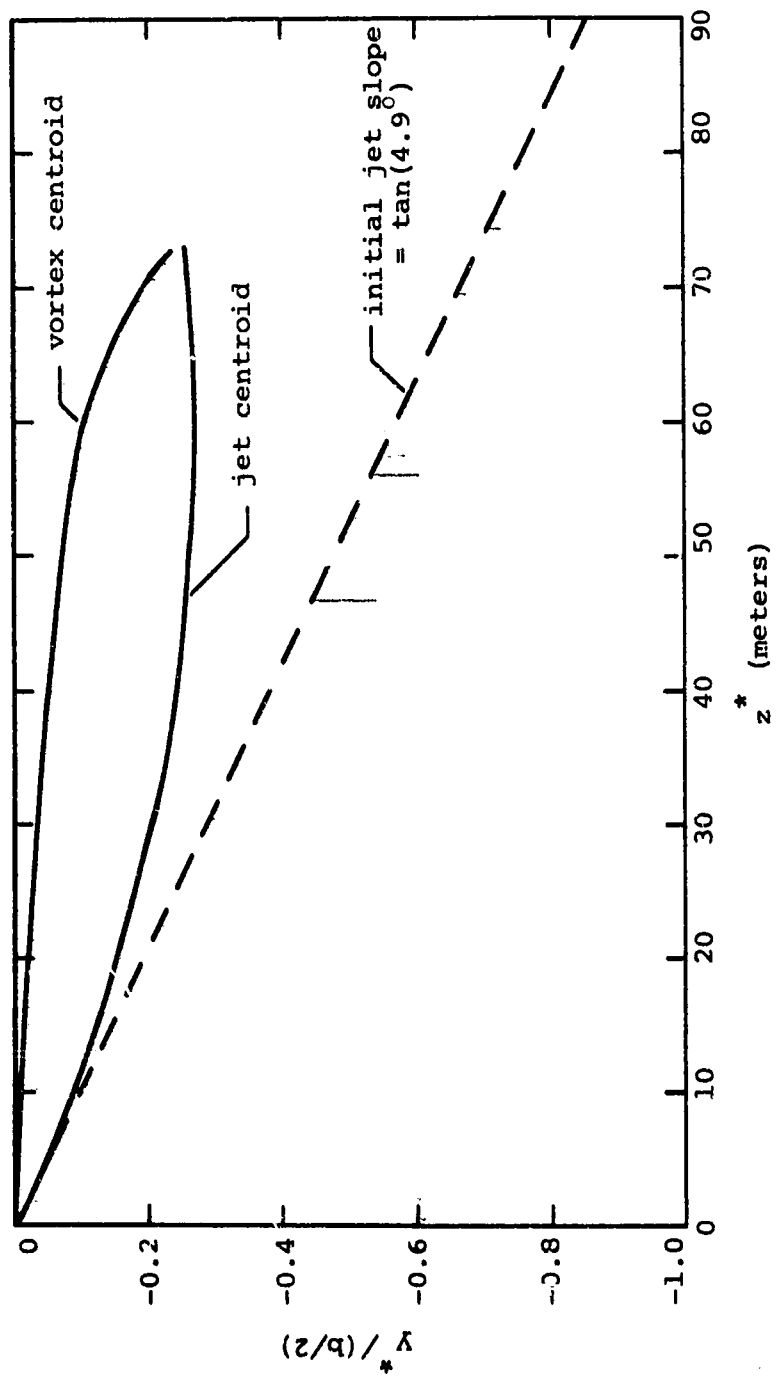
Figure 9-3.- Trajectories of hot jet exhaust and right panel vortex centroid ~ in inertial coordinates.
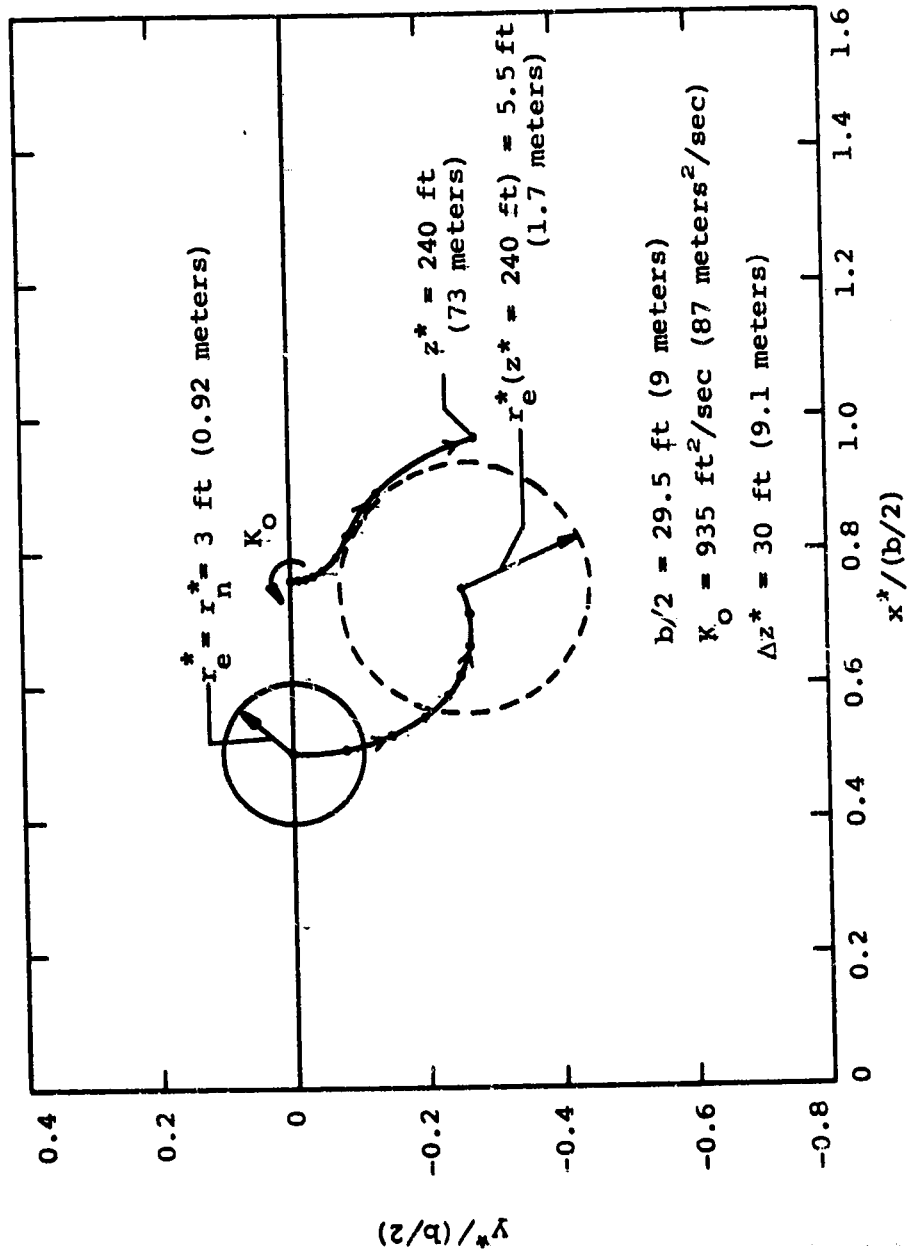
Figure 9-4.- Trajectories of hot jet exhaust and right panel vortex centroid in inertial coordinates.

$K_O = 935 \ ft^2/sec$

$(87 \ meters^2/sec)$

$z_i^* = 195 \ ft \ (59.6 \ meters)$

$\Delta z^* = 30 \ ft \ (9.1 \ meters)$
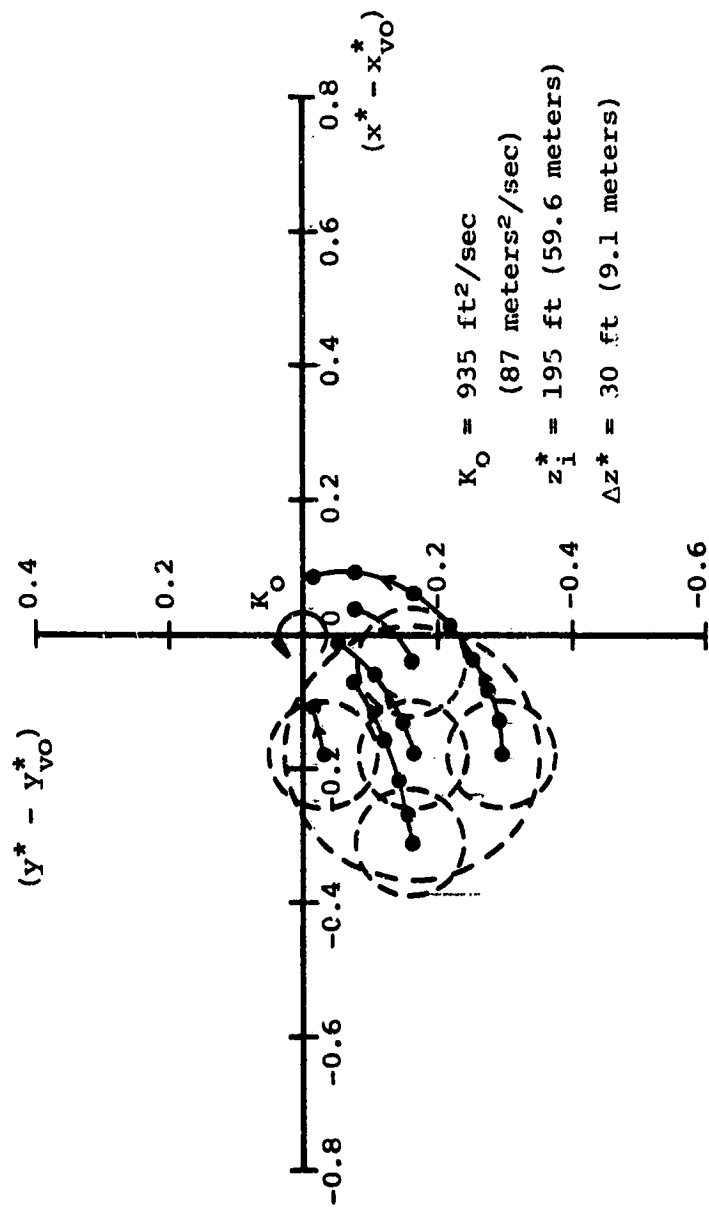
(a) $z_i^* = 195$ feet.

Figure 9-5.- Trajectories of hot gas exhaust segments during break-up process in vortex coordinates.

117

$(y^* - y_{vo}^*)$

$(x^* - x_{vo}^*)$

$K_o = 935$ ft^2/sec
(87 meters^2/sec)

$z_i^* = 150$ ft (46 meters)

$\Delta z^* = 30$ ft (9.1 meters)
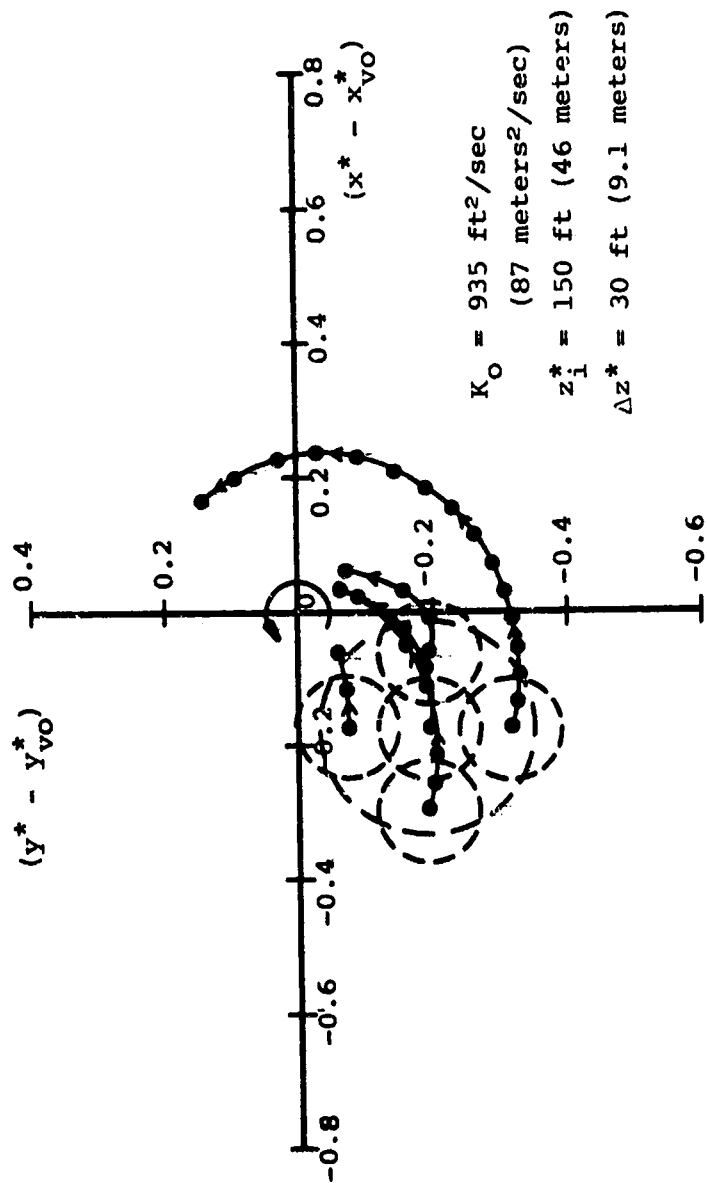
(b) $z_i^* = 150$ feet.

Figure 9-5.- Continued.

118

$K_O = 935 \text{ ft}^2/\text{sec}$
$(87 \text{ meters}^2/\text{sec})$

$z_i^* = 75 \text{ ft } (23 \text{ meters})$

$\Delta z^* = 30 \text{ ft } (9.1 \text{ meters})$
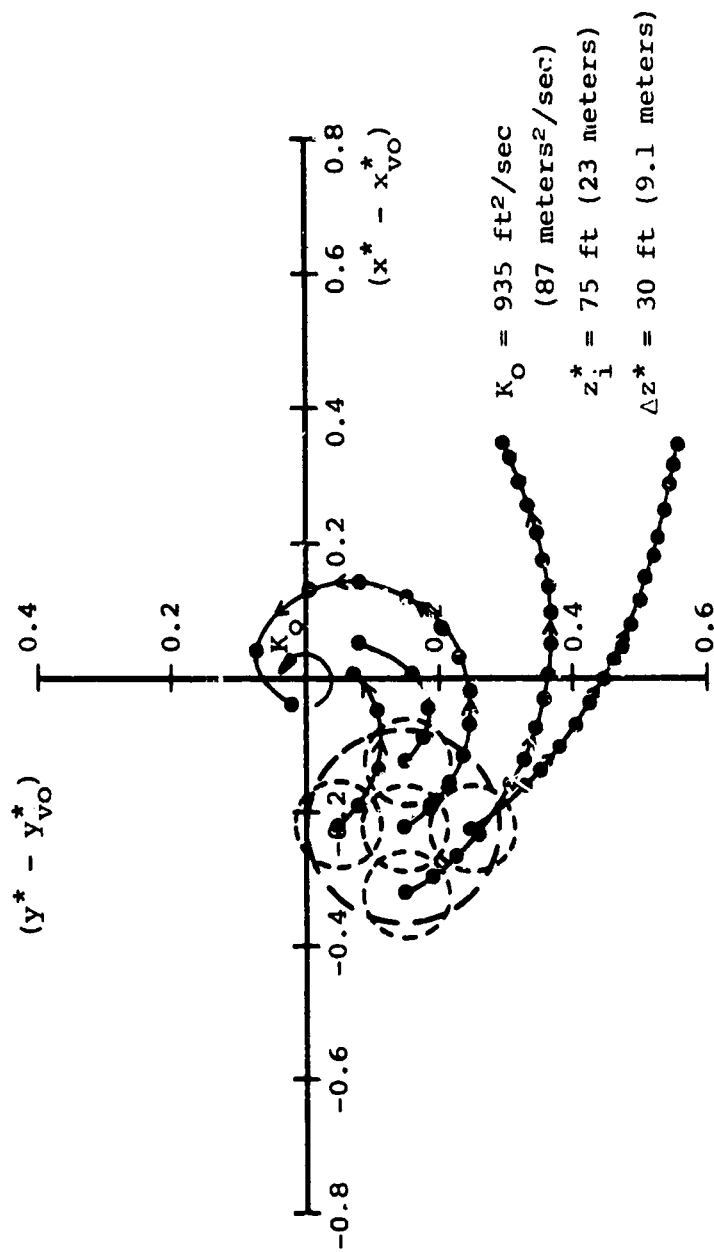
(c) $z_i^* = 75$ feet.

Figure 9-5.- Concluded.

119
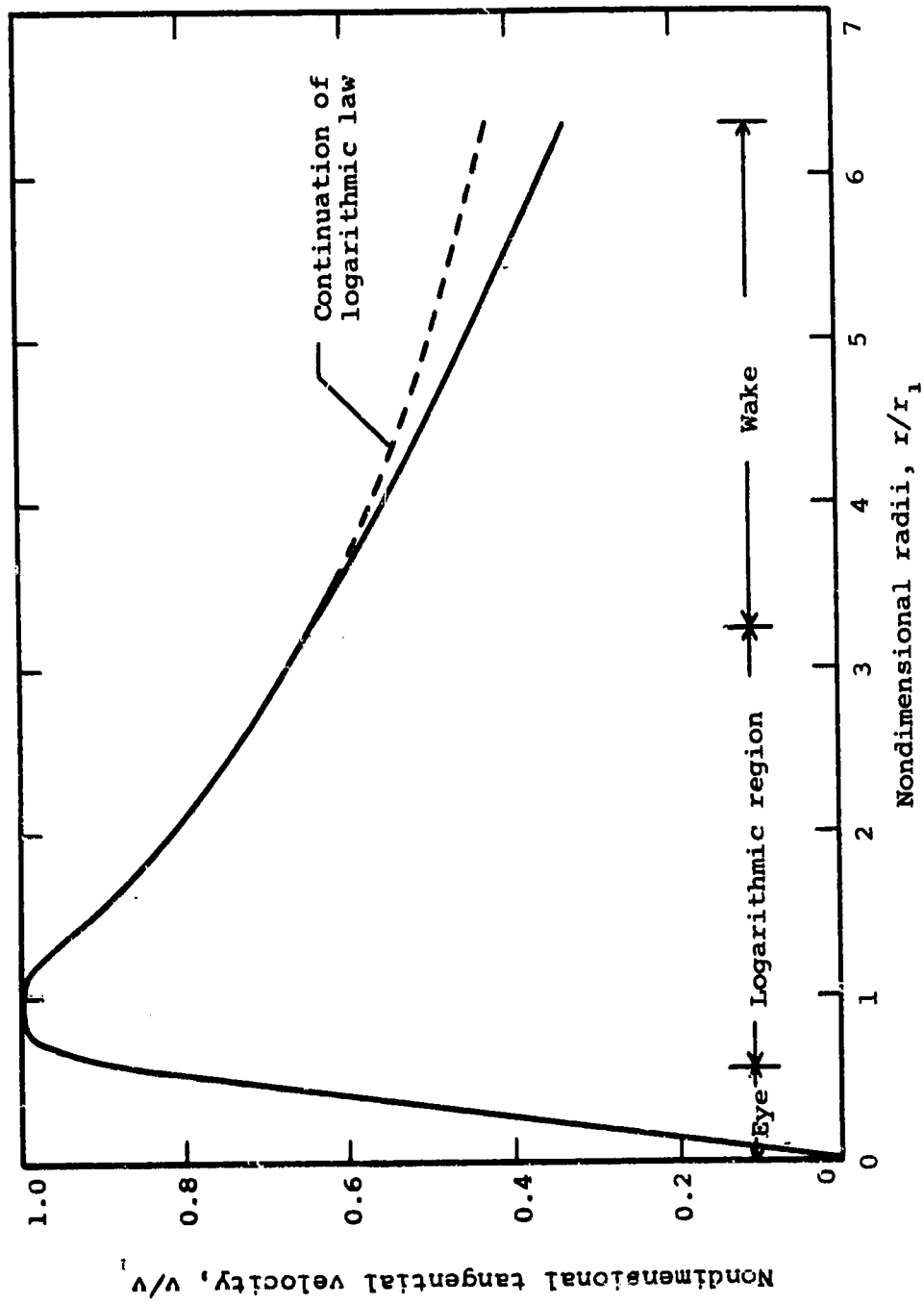
Figure 9-6.— Nondimensional tangential velocity distribution for vortex; no hot gas ingestion.
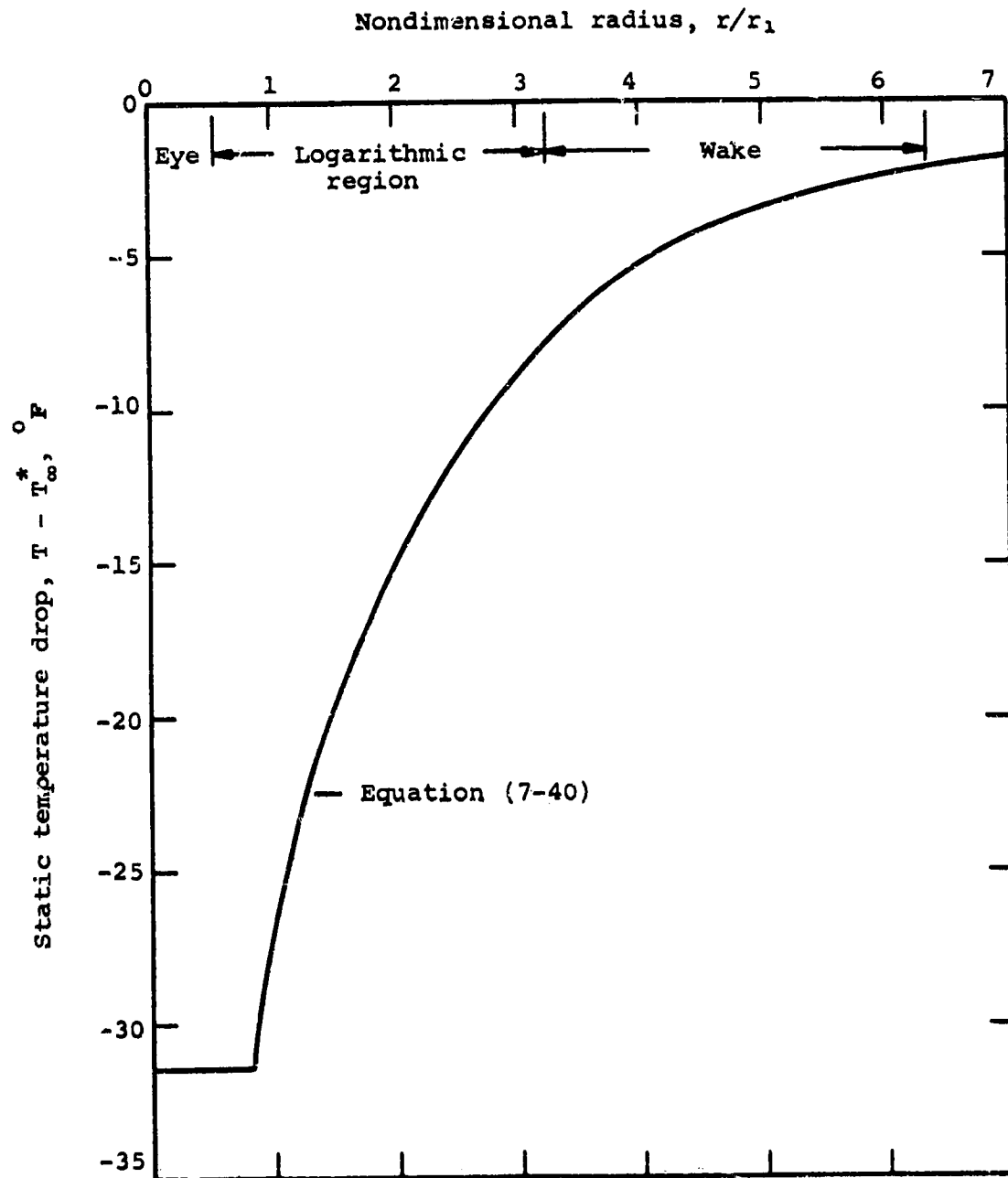
Figure 9-7.- Static temperature drop in vortex; no hot gas ingestion.
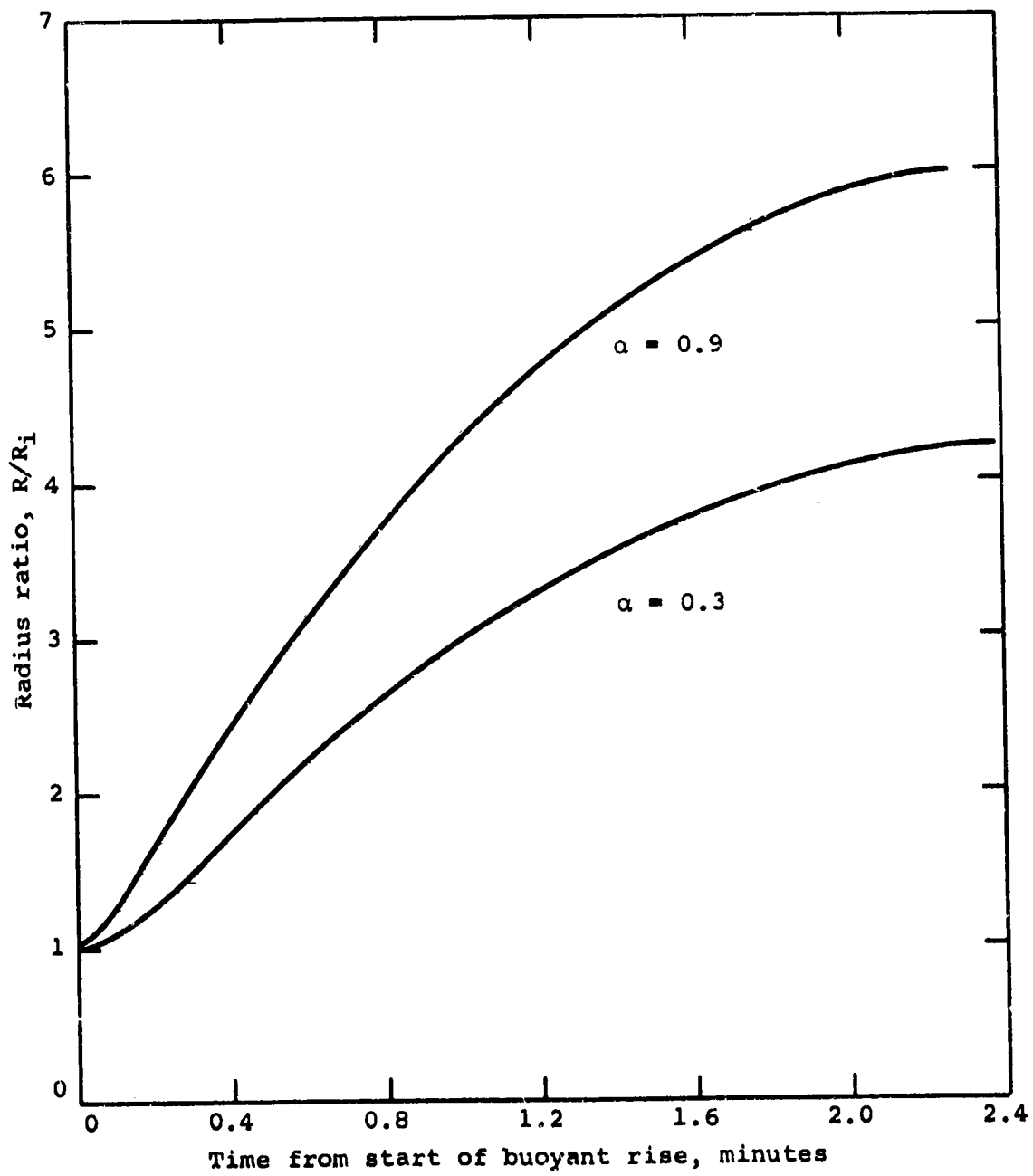
(a) Wake equivalent radius.

Figure 9-8.- Characteristics of wake in asymptotic
buoyant phase.
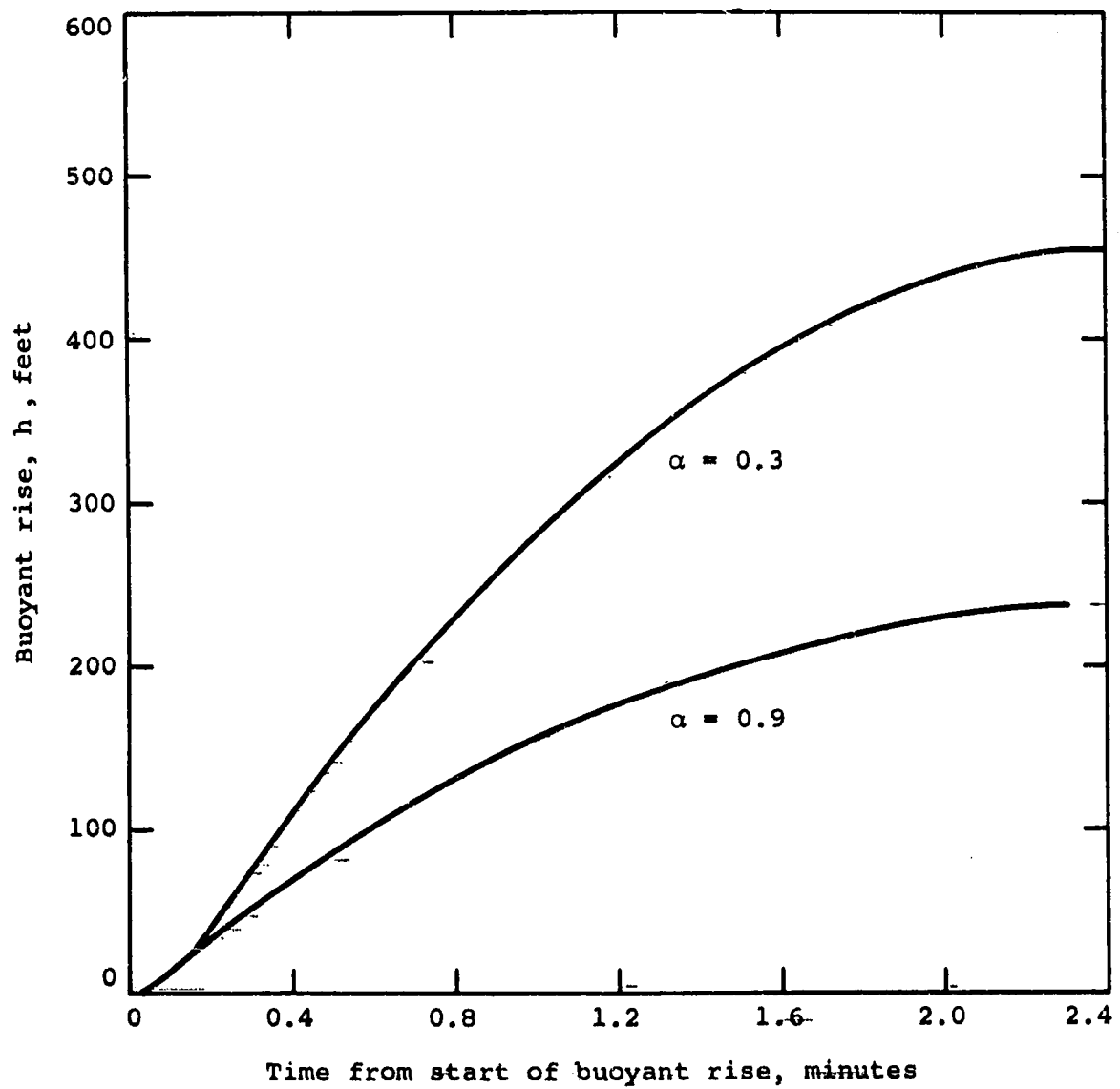
(b)   Vertical rise.

Figure 9-8.- Concluded.

10.0 CONCLUDING REMARKS

Detailed analysis has been made of the ingestion and dispersion of engine exhaust products in the trailing vortex system of a supersonic aircraft. While the analysis is not limited to supersonic flight, the following concluding remarks are directed principally to this speed regime.

1. An analysis has been made of the mixing between the hot supersonic jets of the supersonic aircraft and the co-flowing supersonic stream. One set of experimental data was found covering this case, and the eddy-viscosity coefficients necessary to carry out supersonic jet calculations were determined from an empirical correlation of these data. It was found that the rate of mixing between the supersonic jet and the co-flowing supersonic stream was an order of magnitude less than would be expected on the basis of the subsonic eddy-viscosity results. As a result, the potential core of the supersonic jet is much longer than expected and the exhaust gases are subjected to elevated temperatures and concentrations over much longer distances than previously expected.

2. A new theory has been developed for the break-up of the engine jets and their ingestion into the center of the trailing vortices from the wing. It was found that ingestion started at the end of the potential core and that all of the hot gas from the engines was ingested into the trailing vortices within two core lengths. On the basis of the free-jet calculations the mass fraction of the exhaust gases changed only a small amount over the ingestion distance. It is thought that it changed even less during ingestion because of the effect of the vortex in inhibiting entrainment.

3. It was found that the volume of hot gas ingested into the core of the trailing vortices was much greater than the volume of the core of the trailing vortices alone. It is probably therefore that the tangential velocity distribution of the trailing vortices is substantially changed by hot gas ingestion. The vortex thermally insulates the hot gases from the stratosphere and prevents further mixing. An analysis of the hot trailing vortices was not made nor was the possibility of inducing vortex bursting by hot gas entrainment investigated.

4. It was found that the final buoyancy phase of the trailing vortices started only ten seconds after leaving the trailing edge. As a consequency, the equilibrium vortex phase was of short duration.

124

5. Buoyancy calculations were carried out based on the assumptions
that the wake is essentially horizontal with no axial flow. It was found
that the temperature rise in the wake of the supersonic aircraft is much
greater than that for a subsonic transport since temperature rise was
found to vary directly as speed squared and inversely as aspect ratio.
It was found that the calculated results depend on entrainment coefficient
which is expected to be dependent for its value on such factors as atmos-
pheric turbulence, atmospheric winds, and wake turbulence. Comparison
between the calculated results for the present supersonic example and the
correlation of Fay and Overcamp of contrail data for the width of the
wakes of subsonic aircraft shows good agreement.

6. In the buoyant model it was assumed that the recirculation region
remains intact during the buoyant entrainment process. Asymptotically the
solution yields a buoyant mass which rises to a maximum height and closely
approaches atmospheric temperature.

7. The buoyancy theory was developed on the basis of constant entrain-
ment coefficient measured in water tank tests. The value of the actual
entrainment coefficient for a buoyant wake in the stratosphere needs to be
determined by careful flight tests.

8. One assumption of the theory is that the initial vorticity at the
beginning of the buoyant phase does not have any significant effect on its
vertical motion. As a result of entrainment, vorticity is developed which
tends to destroy the circulation of the trailing vortices. It is probable
that the theory should be extended to include these vorticity effects, and
that experiments in tanks on line thermals with initial circulation should
be carried out to see how the entrainment coefficient is affected. -

9. For subsonic speeds it is probably important to develop the
equilibrium vortex theory with hot gas ingestion since the times involved
for this phase are significant. For the supersonic case this matter may
also be important so that proper initial conditions for the buoyancy phase
can be determined.

10. Velocity and temperature profiles have been specified at various
stages of the wake. If no chemical reaction is assumed to take place,
concentration distributions of individual checmical species can be deter-
mined simply from the knowledge of species concentrations at the engine
exhaust by using the analogy between heat and mass transfer. On the other

125

hand, since the rates of reaction of chemical species are dependent upon local temperature and species concentration, the analysis presented in this report could be used to predict variations of concentration of species under conditions of chemical reaction. In particular, if ambient concentrations of ozone and exit concentrations of NO are measured or assumed, local mixture ratios of NO and ozone can be determined on the basis that ozone is being entrained into the exhaust jet.

Nielsen Engineering & Research, Inc.
        Mountain View, California
                November 1973

126

11.0 REFERENCES

Section 1.0

1-1 Johnston, H. S. and Whitten, G.: Reaction of Ozone with Nitrogen Oxides at High Altitudes. AGARD-CPP-125.

1-2 Goldsmith, P., Tuck, A. F., Foot, J. S., Simmons, E. L., and Newson, R. L.: Nitrogen Oxides, Nuclear Weapons Testing, Concorde and Stratospheric Ozone. Paper presented at the 41st Meeting of AGARD Propulsion and Energetics Panel, London, 9-17, April 1973.

Section 3.0

3-1 Brockman, P., and Seals, R. K.: Laser Measurements of High Altitude Aircraft Emissions. AIAA 6th Fluid and Plasma Dynamics Conference, Palm Springs, California, July 16-18, 1973.

3-2 Wilder, J. G. and Hindersinn, K.: Final Report on Phase II of the Study of Air Exchange Problems in Supersonic Tunnels. Cornell Aero. Lab. Rept. No. AD-570-A7, Jan. 1953.

3-3 Abramovich, G. N.: The Theory of Turbulent Jets. Published by M.I.T. Press, Cambridge, Mass., 1963.

3-4 Wooler, P. T.: Development of an Analytical Model for the Flow of a Jet into a Subsonic Crosswind in "Analysis of a Jet in a Subsonic Crosswind." NASA SP-218, pp. 101-118.

3-5 Nielsen, J. N. and Schwind, R. G.: Decay of a Vortex Pair Behind an Aircraft, pp. 413-454 in "Aircraft Wake Turbulence and Its Detection." Edited by John H. Olson, Arnold Goldburg, and Milton Rogers. Published by Plenum Press, 1971.

3-6 Conti, R. J., Hoshizaki, H., and Redler, K. O., and Cassady, P. E.: Atmospheric Dispersion of Aircraft Exhaust. AIAA Paper No. 73-100, Presented at AIAA 11th Aerospace Sciences Meeting. Washington, D.C., Jan. 10-12, 1973.

3-7 Lockheed Missiles and Space Co., Inc.: Study of High-Altitude Wake Dynamics. Final Report: Task I, Problem Definition. LMSC-D309045. August 1972.

3-8 Overcamp, T. J. and Fay, J. A.: Dispersion of SST Trails in the Stratosphere. AIAA Paper No. 72-650, Presented at AIAA 5th Fluid and Plasma Dynamics Conference, Boston, Mass., June 26-28, 1972.

Section 4.0

4-1   Wilder, J. G. and Hindersinn, K.: Final Report on Phase II of the Study of Air Exchange Problems in Supersonic Tunnels. Cornell Aero. Lab. Rept. No. AD-570-A7, Jan. 1953.

4-2   Crocco, L.: Su di un valor massimo del coefficiente di transmissione del calore da una lamina piana a un fluido acorente. L'Aerotecnica, vol. 12, pp. 181-197, 1932.

4-3   Woolley, J. P.: Theoretical and Experimental Study of Supersonic Mixing of Turbulent Dissimilar Streams. NASA CR-66893, 1970.

4-4   Schlichting, H.: Boundary Layer Theory. 4th Ed., McGraw-Hill, Chap. XXIII, 1960.

4-5   Abramovich, G. N.: The Theory of Turbulent Jets. MIT Press, Cambridge, Mass., 1963.

4-6   Crane, L. J.: The Laminar and Turbulent Mixing of Jets of Compressible Fluid. Jour. of Fluid Mech., vol. 3, Part I, Oct. 1957.

4-7   Maydew, R. C. and Reed, J. F.: Turbulent Mixing of Axisymmetric Compressible Jets (in the Half-Jet Region) With Quiescent Air. Sandia Corp., Report SC-4764 (RR) Aerothermodynamics, March 1963.

4-8   Sabin, C. M.: An Analytical and Experimental Study of the Plane, Incompressible, Turbulent Free Shear Layer with Arbitrary Velocity Ratio and Pressure Gradient. Rept. MD-9, Thermosciences Div., Dept of Mech. Engr., Stanford Univ., Oct. 1963.

4-9   Ricou, F. P. and Spalding, D. B.: Measurement of Entrainment by Axisymmetrical Turbulent Jets. Jour. of Fluid Mech., vol. 11, part 1, Aug. 1961.

4-10   Corrsin, S. and Uberoi, M. S.: Further Experiments on the Flow and Heat Transfer in a Heated Turbulent Air Jet. NACA Rep. 998, 1950.

4-11   Warren, W. R.: An Analytical and Experimental Study of Compressible Free Jets: Doctoral Dissertation Series Publication No. 23,885, Univ. Microfilms, Ann Arbor, Mich., 1957.

4-12   Wilder, J. G. and Hindersinn, K.: Spreading of Supersonic Jets in Supersonic Streams: Aeronautical Engineering Review, pp. 54-68, Oct. 1953.

4-13   Eggers, J. M., and Torrence, M. G.: An Experimental Investigation of the Mixing of Compressible Air Jets in a Coaxial Configuration. NASA TN D-5315, 1969.

4-14   Liepmann, H. W. and Laufer, J.: Investigations of Free Turbulent Mixing. NACA TN 1257, 1947.

4-15 Albertson, M. L., Dai, Y. B., Jensen, R. A., and Rouse, H.:
       Diffusion of Submerged Jets. Proc. Am. Civil Engr., vol. 74,
       p. 1571, 1948.

4-16 Pabst, O.: Die Ausbreitung Heisser Gasstrahlen in Bewegter
       Luft. I. Teil, Versuche im Kerngebiet, Deutsche Luftfahrtforschung.
       Untersuch-Mitteilungen No. 8004; II Teil, U.-M. No. 8007, 1944.

4-17 Baker, R. L., and Weinstein, H.: Experimental Investigation of
       the Mixing of Two Parallel Streams of Dissimilar Fluids,
       NASA CR-957, 1968.

4-18 Tollmein, W.: Berechnung der Turbulenten Ausbreitungs Vörgange
       ZAMM 4, pp. 468-475, also NACA TM 1085, 1945.

4-19 Görtler, H.: Berechnung von Aufgaben den Freien Turbulenz
       auf Grund eines neuen Naherungsansatzes. ZAMM 22, p. 244, 1942.

4-20 Hinze, J. O.: "Turbulence". McGraw-Hill, N. Y., p.426, 1959.

Section 5.0

5-1   Wooler, P. T.: Development of an Analytical Model for the Flow
       of a Jet into a Subsonic Crosswind in "Analysis of a Jet in a
       Subsonic Crosswind." NASA SP-218, pp. 101-118.

5-2   Lamb, H.: Hydrodynamics. Dover Publications, New York, Sixth
       Edition, 1945.

Section 7.0

7-1   Nielsen, J. N. and Schwind, Richard G.: Decay of a Vortex Pair
       Behind an Aircraft, pp. 412-454, in "Aircraft Wake Turbulence
       and its Detection". Edited by John H. Olson, Arnold Goldburg,
       and Milton Rogers. Published by Plenum Press, 1971.

7-2   Hoffmann, E. R. and Joubert, P. N.: Turbulent Live Vortices.
       Journal of Fluid Mechanics, vol. 16, part 3, pp. 395-411,
       July 1963.

7-3   Hall, M. G.: The Structure of Concentrated Vortex Cores.
       "Progress in Aeronautical Sciences." Vol. 7, Edited by
       D. Kuchemann, pp. 53-110, 1966.

7-4   Kassner, R. and Knoernschild, E.: Friction Laws and Energy
       Transfer in Circular Flow. Wright-Patterson Air Force Base
       Tech. Rept. No. F-TR-2198-ND (1947).

Section 8.0

8-1   Overcamp, T. J. and Fay, J. A.: Dispersion of SST Trails in the
       Stratosphere. AIAA Paper No. 72-650. AIAA 5th Fluid Dynamics
       Conference, Boston, Mass., June 26-28, 1972.

8-2   Conti, R. J., Hoshizaki, H., Redler, K. O., and Cassady, P. E.:
       Atmospheric Dispersion of Aircraft Exhaust. AIAA Paper No. 73-100,
       AIAA 11th Aerospace Sciences Meeting, Jan. 10-12, 1973.

8-3   Lockheed Missiles and Space Co.: Study of High-Altitude Aircraft
       Wake Dynamics. Final Report: Task I, Problem Definition.
       LMSC-D309045, Aug. 1972.

8-4   Hewett, T. A., Fay, J. A. and Hoult, D. P.: Laboratory Experiments
       of Smokestack Plumes in a Stable Atmosphere. "Atmospheric Environ-
       ment." Vol. 5, pp. 767-789, Pergamon Press, 1971.

8-5   Tsang, Gee: Laboratory Study of Line Thermals. "Atmospheric
       Environment", vol. 5, pp. 445-471, Pergamon Press, 1971.

8-6   Richards, J. M.: Experiments on the Motion of Isolated Cylindrical
       Thermals Through Unstratified Surroundings. Inter. Jour. Air Water
       Pollution, vol. 7, pp. 17-34, 1963.

Section 9.0

9-1   Staff of the Ames 1- by 3-Foot Supersonic Wind-Tunnel Section: Notes
       and Tables for Use in the Analysis of Supersonic Flow. NACA
       TN 1428, 1947.

9-2   Orloff, K. L. and Grant, G. R.: The Application of a Scanning Laser
       Doppler Velocimeter to Trailing Vortex Definition and Alleviation.
       AIAA Paper No. 73-680. AIAA 6th Fluid and Plasma Dynamics Conference,
       Palm Springs, CA, July 16-18, 1973.

9-3   Corsiglia, V. R., Schwind, R. G., and Chigier, N. A.: Rapid Scanning,
       Three-Dimensional Hot Wire Anemometer Surveys for Wing Tip Vortices
       in 40- by 80-Foot Wind Tunnel. AIAA Paper No. 73-681, AIAA 6th
       Fluid and Plasma Dynamics Conference, Palm Springs, CA, July 16-18,
       1973.

9-4   Nielsen, J. N. and Schwind, R. G.: Decay of a Vortex Behind an
       Aircraft, pp. 413-454 in "Aircraft Wake Turbulence and its Detection"
       edited by John H. Olson, Arnold Goldburg, and Milton Rogers.
       Published by Plenum Press, 1971.

9-5   Overcamp, T. J. and Fay, J. A.: Dispersion of SST Trails in the
       Stratosphere. AIAA Paper No. 72-650, presented at the AIAA 5th
       Fluid and Plasma Dynamics Conference, Boston, Mass., June 26-28,
       1972.